4-2017

Controls on Fracture Network Characteristics of the Middle Member of the Bakken Formation, Elm Coulee Field, Williston Basin, USA

Shashank Khatri
University of Nebraska-Lincoln, shashank.geo14@gmail.com

Controls on Fracture Network Characteristics of the Middle Member of the Bakken Formation, Elm Coulee Field, Williston Basin, USA

By

Shashank Khatri

A Thesis

Presented to the Faculty of

The Graduate College at the University of Nebraska

In Partial Fulfillment of Requirements

For the Degree of Master of Science

Major: Earth and Atmospheric Sciences

Under the Supervision of Professor Caroline M. Burberry

Lincoln, Nebraska

April, 2017

Controls on Fracture Network Characteristics of the Middle Member of the Bakken Formation, Elm Coulee Field, Williston Basin, USA

Shashank Khatri, M.S.

University of Nebraska, 2017

Advisor: Caroline Burberry

The Bakken formation in the Elm Coulee Field of the Williston Basin consists of three members: 1) upper shale member, 2) middle silty dolostone member, and 3) lower shale member. The upper and lower members act as excellent source rocks and the main reservoir is the middle member with an average porosity of 3 to 9% and average permeability of 0.04md. The Bakken oil play in this area is a stratigraphic trap with a pinch-out to the southwest and a diagenetic facies change in the northeast. The main production is interpreted to come from matrix permeability in the field area. However, the first year production trends from the Elm Coulee Field show areas of anomalously high production.

This study used 3D seismic data from Crane Field, which is located in the southeastern part of the Elm Coulee Field, to investigate structures which might be responsible for the anomalous production trends at the Elm Coulee Field. We used post stack seismic conditioning and seismic attributes to amplify the structure of the basement. Further investigation revealed the presence of a pop-up structure in the central portion overlying a zone of basement deformation. This zone of deformation was interpreted to be composed of a left lateral wrench faulting system based on a model-driven approach. This study goes on further to map the structure and faults in 3 dimensions using a model driven approach, which reveals that the pop-up structure evolved from an obtuse angle

left lateral step over system in the basement. In addition, the presence of this left lateral wrench fault network is interpreted to be related to a regional left lateral strike slip system – the Brockton Froid Fault Zone The fracture network characteristics in the middle member of the Bakken Formation are directly related to the local stresses generated by the interpreted left lateral wrench fault system in the study. There are two fracture sets- NE-SW and NW-SE. The structure and fracture network characteristics help explain the presence of regions of anomalously high EUR (Estimated Ultimate Recovery) values in the Elm Coulee Field. The regions of anomalously high EURs in the Elm Coulee Field may be regions where the middle member of the Bakken Formation has increased natural fracturing related to the local stresses induced by left-lateral oblique slip strike slip faults.

Dedicated to

My late loving Grandma and Mentor

Santosh

And My Parents

Anil and Sangeeta

ACKNOWLEDGEMENTS

First and foremost I would like to acknowledge my advisor, Dr. Caroline Burberry. I will always be grateful for your guidance and expertise. You provided invaluable assistance by helping to collect field data with me. Thank you for all your personal and academic advice. I would also like to acknowledge Dr. Chris Fielding and Dr. David Watkins for serving on my committee.

I would like to thank the UNL Department of Earth and Atmospheric Sciences for their financial support during the summer of 2016, and the GSA Foundation "Graduate Student Research Grant" for contribution toward my research goals. Lastly I want to thank all the students in the department and in the UNL AAPG Student Chapter for their support and friendship throughout this wonderful journey. Thank you.

Table of Contents

CHAPTER 1
INTRODUCTION

The Bakken Petroleum System is classified as a continuous, unconventional, tight-oil accumulation with pervasive hydrocarbon saturations over a large areal extent (Sonnenberg and Pramudito, 2009). The system has characteristics of being abnormally pressured in many locations within the basin, has low porosity and permeability, and contains areas of stress-induced fracturing which aid in hydrocarbon accumulation. The reservoir displays low recovery rates with low water production. The lithology and localized natural fractures are thought to control the EUR (Estimated Ultimate Recovery) "sweet spots" (Sonnenberg et al., 2011). The Bakken Petroleum System is composed of the upper 50 feet of the Three Forks Formation (Late Devonian), the Bakken Formation (Devonian-Mississippian), and the lower 50 feet of the lower Lodgepole Formation (Early Mississippian) (Price and LeFever, 1992). The Bakken Formation consists of three members: an upper shale member, a middle silty dolostone member, and a lower shale member (Sonnenberg et al., 2011). The source beds for the petroleum system are the upper and lower organic-rich Bakken Formation shales. The reservoirs of the Bakken Petroleum System are all the members of the Bakken Formation, the lower member of the Lodgepole Formation and the upper member of the Three Forks Formation.

The Elm Coulee Field of the Williston Basin is a giant oil discovery in the middle member of the Bakken Formation, discovered in 2000. Horizontal drilling began in the field in 2000, and to date, more than 600 wells have been drilled on this field. The estimated ultimate recovery for the Field is more than 200 million bbl of oil (Sonnenberg and Pramudito, 2009). The Elm Coulee Field forms a stratigraphic trap by onlap of the

middle Bakken strata onto the underlying Three Forks Formation to the northwest, north north east, and southwest; and diagenetic facies change towards the east north east (Sonnenberg and Pramudito, 2009; Almanza, 2011) (Figure 1.1).

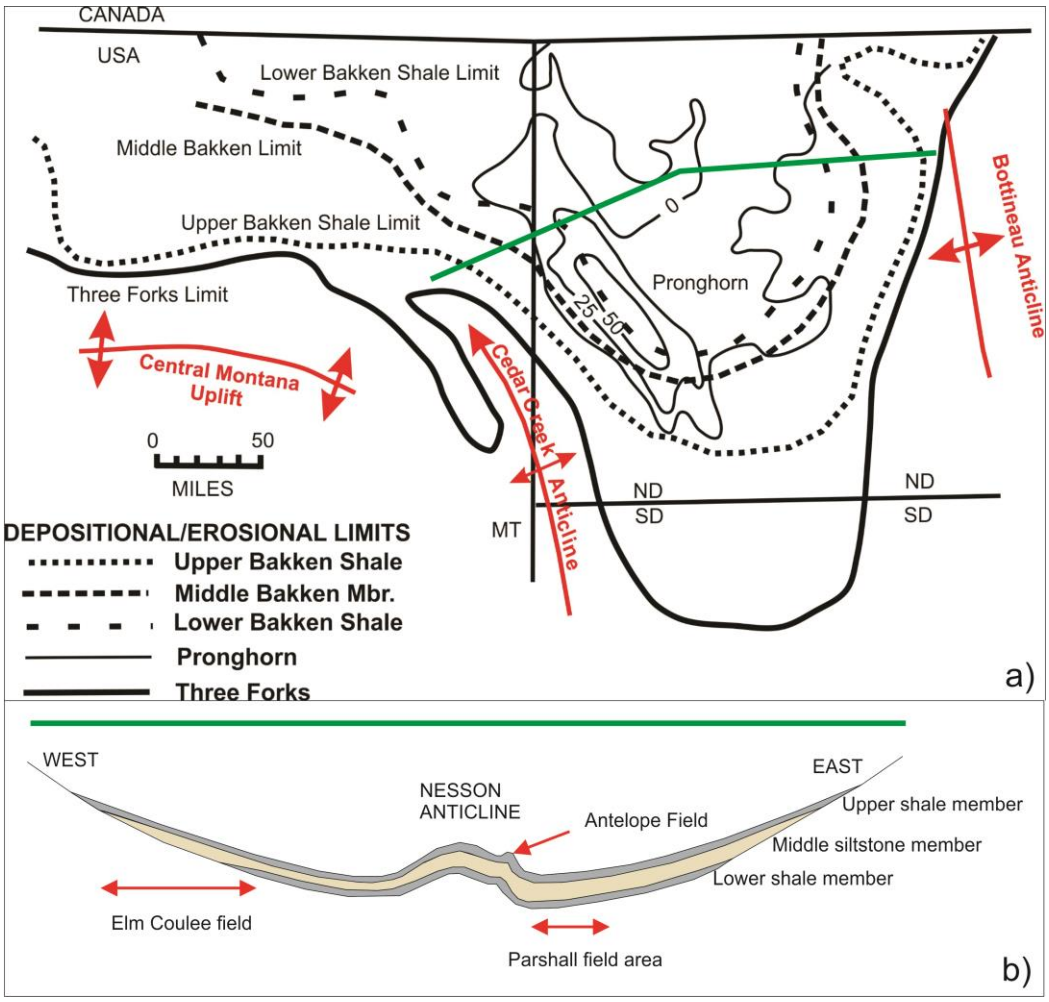

Figure 1.1 a) The depositional limits of the upper, middle and lower members of the Bakken Formation are shown. The green line shows the location of the cross section shown in b). b) Schematic cross section across the Williston Basin showing three members of the Bakken Formation and the onlapping relationships with underlying Three Forks Formation. Antelope field was the first Bakken production associated with a sharp anticlinal fold. The Elm Coulee Field is also shown on the cross section (modified from Sonnenberg and Pramudito, 2009).

The reservoirs in the Elm Coulee Field have low permeability. Productive areas or sweet spots are localized areas of improved reservoir permeability through natural fracturing, or

development of matrix permeability, or a combination of both. Evaluation of reservoir performance across the Elm Coulee Field using the EURs of the horizontal wells drilled in the Field indicated that the EURs cluster into regions of similar EUR (Honsberger, 2013) (Figure 1.2a). The sweet spots have an ovoid shape that roughly trends north and south (Almanza, 2011) (Figure 1.2b). Several recent studies have investigated the impact of natural fracture networks in the Elm Coulee Field on the reservoir performance to explain these anomalies in the production data from the Elm Coulee Field.

Almanza (2011) constructed a dual porosity model for the middle member of the Bakken Formation in the Elm Coulee Field. The study constructed a fracture model for Elm Coulee Field derived from production trends and seismic attributes. The model uses regional fracture trends to establish a fracture fabric. The regional fractures, which are a direct result of far field stresses, are oriented to the northeast and have a spacing of approximately 1250 feet. An orthogonal set of fractures is spaced 2,500 ft apart in the northwest direction. Production data was used for the detection of fracture swarms (Figure 1.3). The swarms were oriented in the maximum principal stress direction of N60E and have an approximate spacing of 25,000 ft. The fracture model was combined with the matrix model to develop a dual porosity model. It was concluded that the dual porosity model developed reflects the production in the study area, and that the best reservoir properties align with the best estimated ultimate recovery values (EURs) (Almanza, 2011).

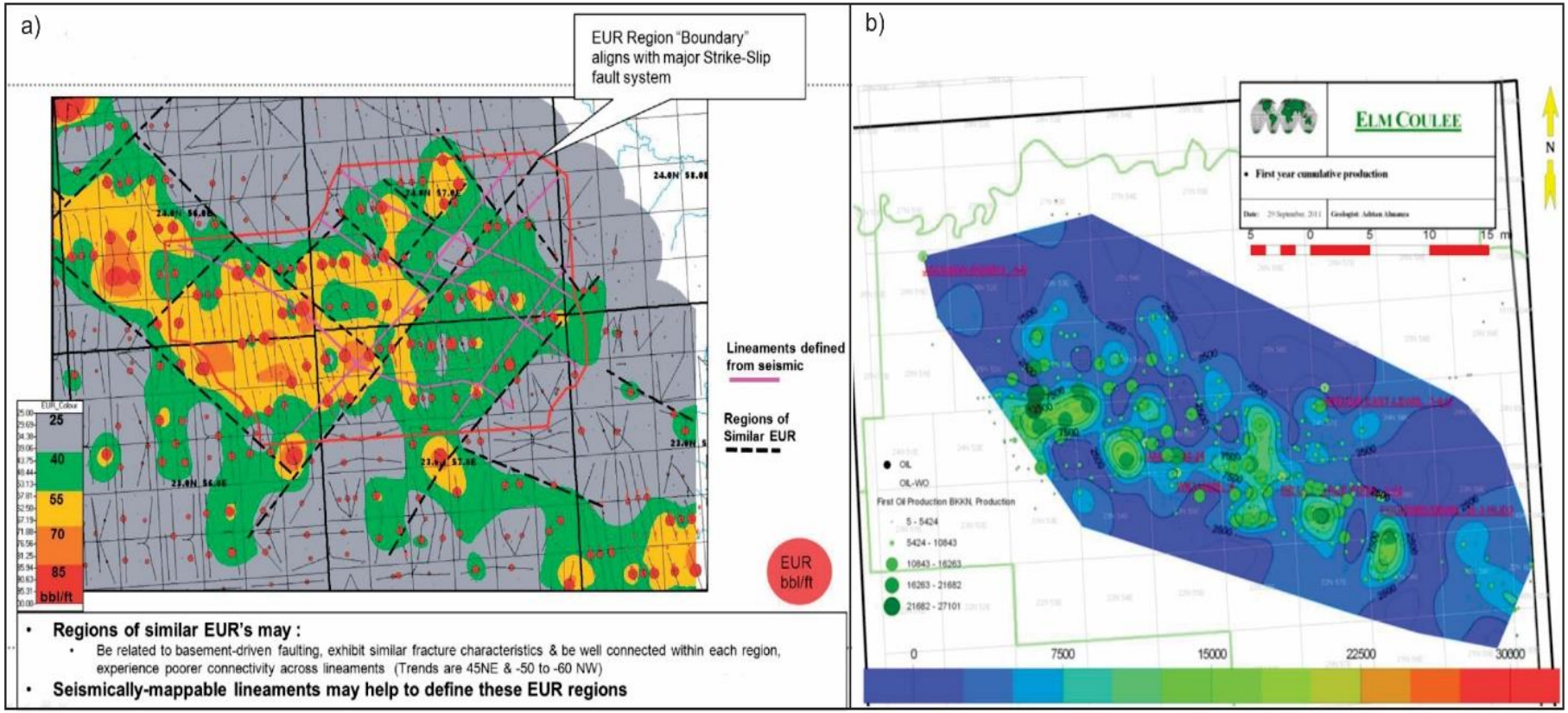

Figure 1.2 a) EUR data (normalized) - plotted at midpoint of horizontal path of the wells. The dotted lines show the interpreted boundaries of the compartments of similar EURs (Honsberger, 2013). b) First year cumulative production data showing ovoid shaped sweet spots in the Elm Coulee Field with anomalously high production (Almanza, 2011).

Honsberger (2013) investigated a 3D seismic data set from the Elm Coulee Field and interpreted lineaments at the Winnipeg Formation and Bakken Formation levels using seismic techniques and attributes. These lineaments showed two trends: a primary trend of 45^{0}NE and a secondary trend of approximately 60^{0}NW (Figure 1.4).

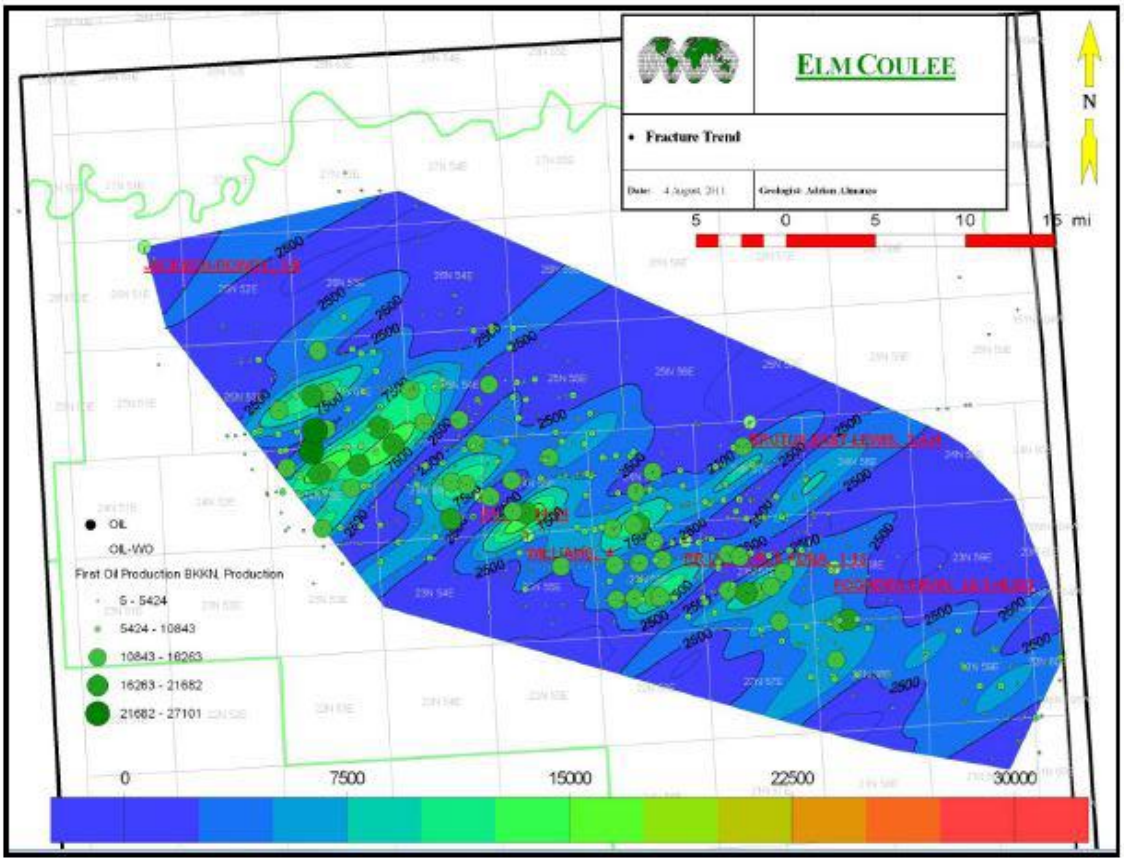

Figure 1.3 Initial production trends with a N60E Bias. This Bias trend, which is also the direction of the maximum principal stress in Williston Basin highlights the fracture swarms that were interpreted in the Elm Coulee field (Almanza, 2011).

It was interpreted that these lineaments appear to represent laterally extensive but small vertical-offset faults. Further, faults at the Winnipeg Formation appear related to subtle faults at the Bakken Formation, where both sets are part of a large-scale, basement-driven, regional strike-slip system that extends across the Williston basin with primary

fracture directions of ~45^0 NE, and secondary fracture directions of ~60^0 NW. The Elm Coulee Field is located on this major strike-slip system, with potential for other strike-slip faults elsewhere in the field.

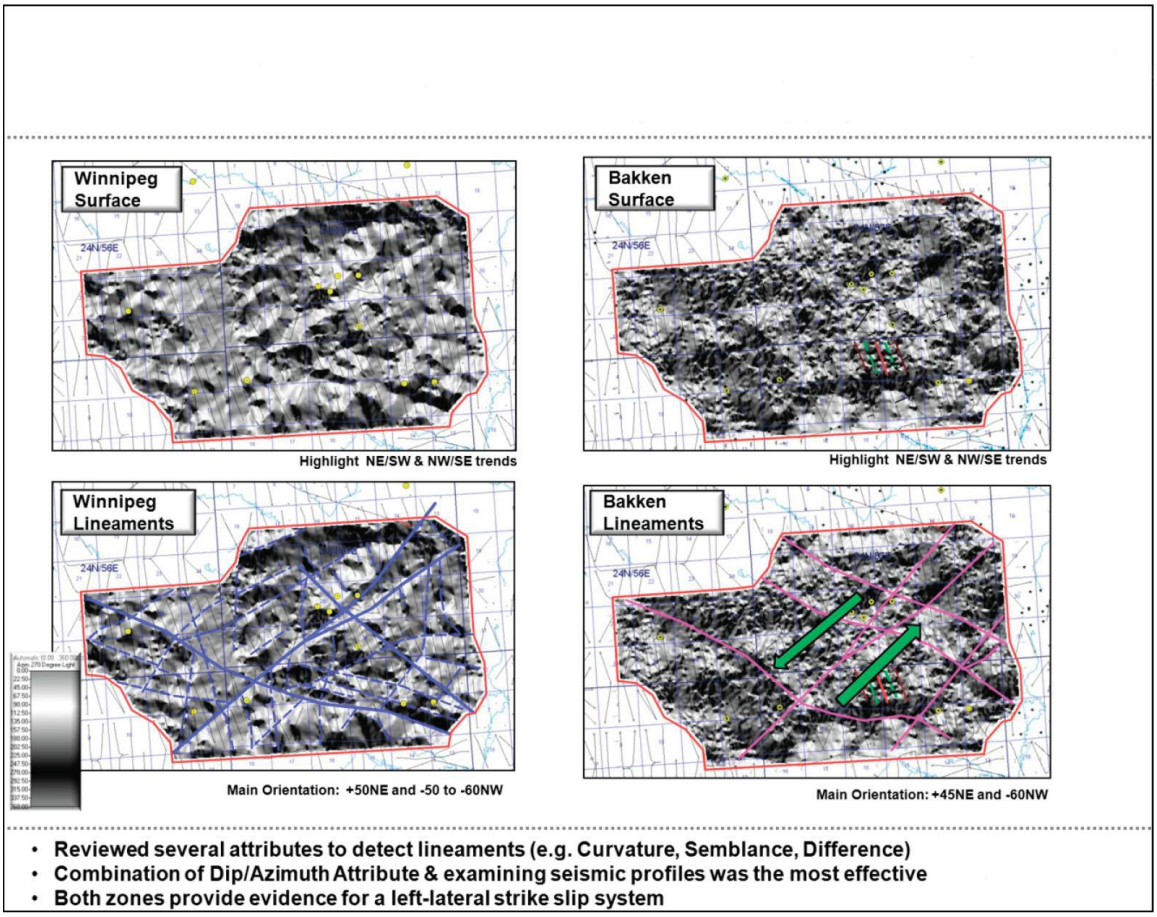

Figure 1.4 The Faulting/lineaments interpreted from seismic. Left: Winnipeg surface and lineaments; Right: Bakken surface and lineaments (Honsberger, 2013).

The study concluded that there are regions or compartments within the Elm Coulee Field that produce similarly, where distinct NE/SW and NW/SE – oriented faults may act as baffles and possibly fracture propagation barriers between compartments.

Eidsnes (2014) investigated the structural and stratigraphic factors influencing the hydrocarbon accumulations in the Bakken Petroleum System at the Elm Coulee Field,

using three seismic surveys that overlapped one another, the Vaux (19.66 mi^2), Intake II (9.69 mi^2), and South Fork (21.77 mi^2), and core analysis on six Elm Coulee wells. Eidsnes (2014) used Schlumberger's Ant Tracking attribute to pick faults in the seismic data. The Ant Tracked volume showed northwest-southeast trending fracture networks. However, the study could not establish a correlation between the results obtained from the Ant Tracking attribute and producing wells' EUR maps from the Elm Coulee Field (Eidsnes, 2014).

The purpose of the present study was to investigate the structure in a portion of the Elm Coulee Field area in greater detail, to study the controls on the natural fracture network characteristics of the middle member of the Bakken Formation, and to investigate the possible impact of the structure on the production from the middle member of the Bakken Formation, which is the main reservoir in the Elm Coulee Field. This study used a 3D Seismic data set from the Crane Field, which is located at the south eastern corner of the Elm Coulee Field (Figure 1.5) to investigate the structure in the area. The study area lies in the Western part of the Williston Basin. The generalized stratigraphic chart showing the stratigraphic architecture of the study area is shown in in Figure 1.6. In addition, an analog outcrop (Cottonwood Canyon Formation, Shell Canyon in Bighorn Mountains, Wyoming, USA) was used to simulate the behavior of the Bakken Formation under stress.

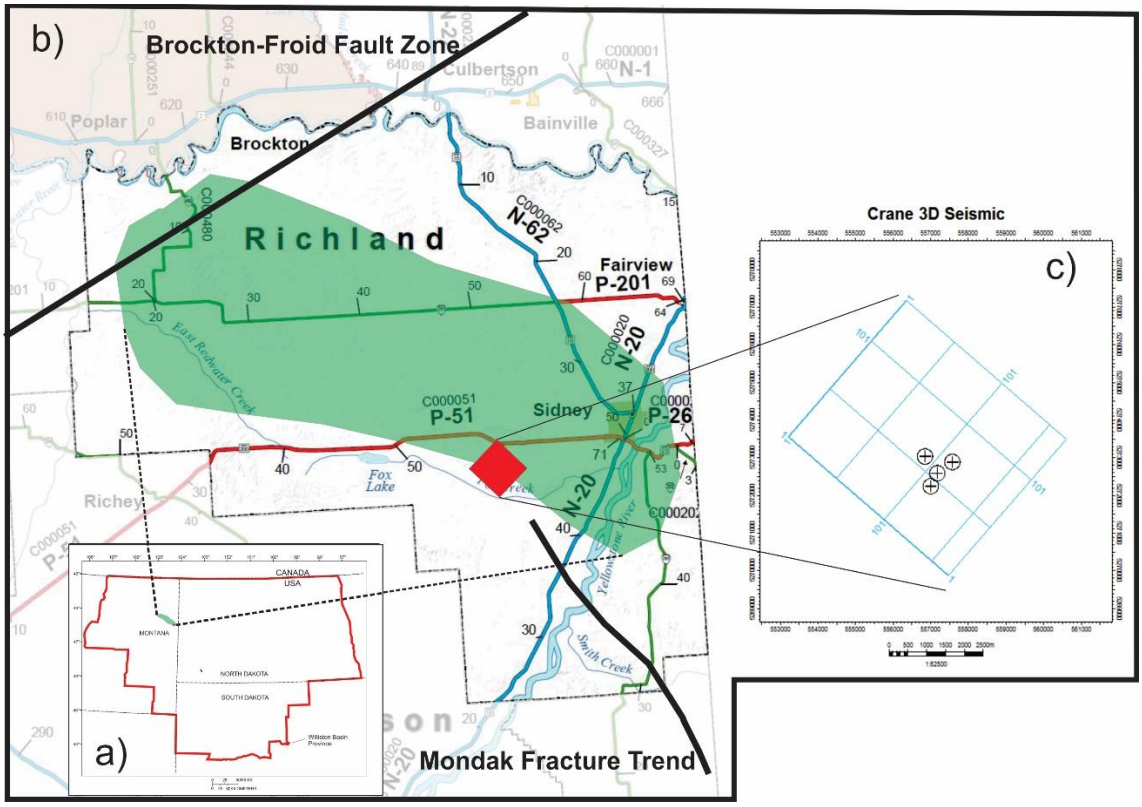

Figure 1.5 a) The US portion of the Williston Basin (here called as the Williston Basin province) is shown with red outline with the location of Elm Coulee shaded green. b) The Elm Coulee Field in the Richland County is shaded in green with the location of the Crane Field marked with a red square. The major structural trends: Brockton Froid Fault Zone and Mondak Fracture Trend are also shown. c) A 2D map showing the 3D seismic data used in this study with the 4 wells drilled along the seismic lines.

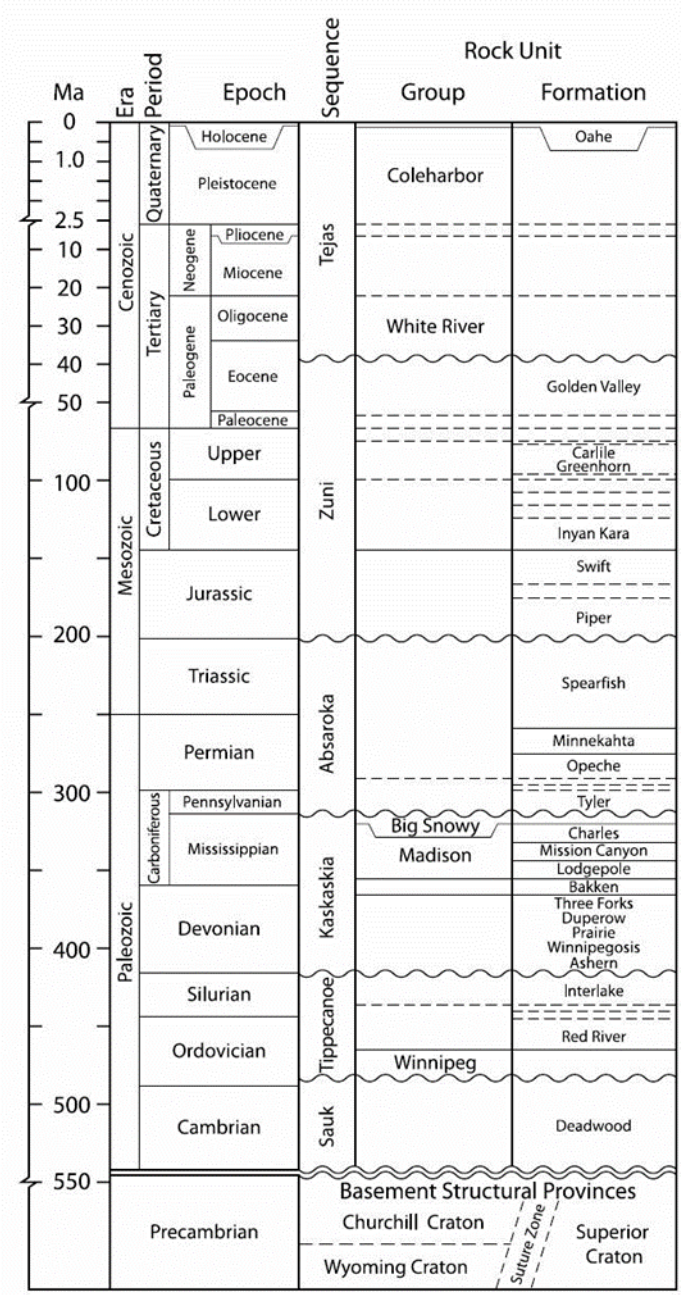

Figure 1.6 Generalized stratigraphic chart showing the major formations, groups and sequences in the Williston Basin (Kuhn et al., 2012).

CHAPTER 2
GEOLOGICAL BACKGROUND

2.1 Geological Setting

The Elm Coulee Field, which is the focus of this study, lies within the Williston Basin (Figure 2.1). The Williston Basin is an intracratonic sag basin that developed on the North American craton during the Ordovician and has undergone episodic subsidence through the Phanerozoic.

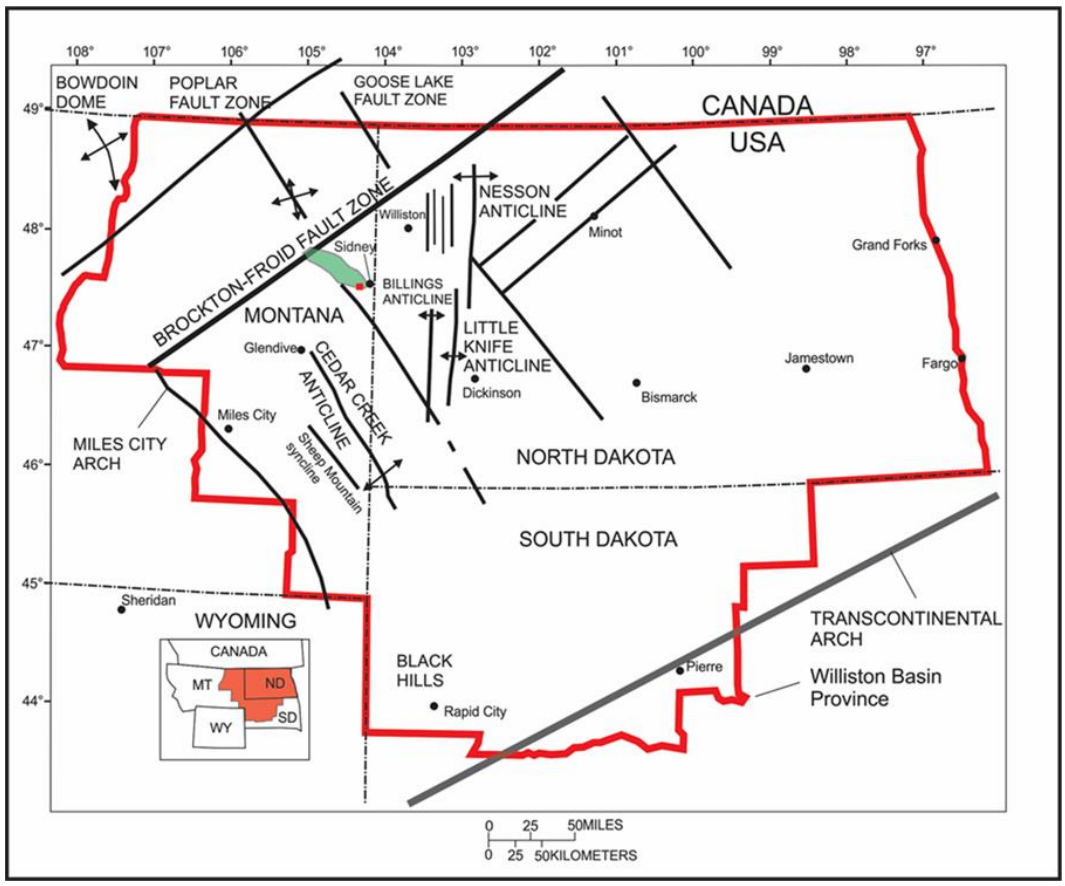

Figure 2.1 Williston Basin Province, showing major structural features. The province boundary is shown by red color. The Williston Basin Province boundary is delineated by State and county borders that are within the geologically defined Williston Basin in the United States. The location of the Elm Coulee Field is shaded in green color. Location of the Crane Field is shown by red square on the south eastern corner of the Elm Coulee Field. (Modified from Gaswirth, et al., 2013).

It is a roughly circular basin, deepest in the center, and covers approximately 300,000 km² over parts of eastern Montana, North Dakota, northwestern South Dakota, and the Saskatchewan and Manitoba Provinces of Canada (Gerhard, et al., 1990). The eastern and southern boundaries are geologically defined as the eastern and southernmost subcrops of Paleozoic and Mesozoic Formations; the western boundary in Montana and Wyoming follows the eastern edge of several Laramide structural uplifts that geologically define the basin (Gaswirth, et al., 2013).

2.1.1 Major Stratigraphic Sequences

The sediment infill in the Williston Basin is characterized by alternating deposition of clastic sedimentary rocks and carbonate sedimentary rocks that range in age from Cambrian to Quaternary. Subsidence and tectonic basin reconfiguration are the primary influences on sediment infill. Approximately 16,000 feet of sediment was deposited during the Phanerozoic in the Williston Basin (Gerhard et al., 1990) (Figure 1.6). Both Sloss (1963) and Gerhard et al. (1990) delineate several unconformity bounded sequences and their associated formations in the stratigraphic column shown in Figure 1.6. The Sauk sequence is the first major sequence of the group and consists of the Upper Cambrian Deadwood Formation. Sedimentation began over the low relief and variable Precambrian surface due to the transgression of the Sauk Sea. At the termination of the Sauk sequence, the Williston Basin began to subside as a result of the strike slip movement on the northeast-southwest trending basement propagating faults which triggered the onset of the Taconic orogeny. The Tippecanoe sequence unconformably overlies the Sauk sequence and is composed of Ordovician and Silurian sediments.

During this time depositional patterns suggest the subsidence at the present-day Williston Basin center which displays a connection to the Cordilleran Sea to the southwest (Gerhard et al., 1990). The initial transgression deposited the Winnipeg Group, which is composed of lower Ordovician shallow marine sandstone and shale, and Middle Ordovician through Silurian carbonates. The Tippecanoe sedimentation terminated due to a regression at the end of the Silurian which lead to erosion of previously deposited units. The Kaskaskia sequence formed following uplift of the Transcontinental Arch that shifted the basin center towards the northwest into the Canadian Shield resulting in a marine connection to the northwestern Elk-point. Gerhard et al. (1990) divides the Kaskaskia sequence into two regional sea level transgressions, the lower Kaskaskia and the upper Kaskaskia sequences. These sequences are divided at the Acadian unconformity, which occurs between the Three Forks and Bakken Formations and marks the beginning of uplift of the Transcontinental Arch and exposure prior to Bakken deposition. With the onset of the upper Kaskaskia sequence, the uplift also coincided with the a major change in basin configuration from a circular basin in northwestern North Dakota with a marine connection to the Cordilleran Sea, into the present-day depocenter and northwest-southeast trending Williston Basin. The Absaroka sequence began during the Early Pennsylvanian where North American tectonism was widespread creating erosion of the Ancestral Rocky Mountains, Hartville uplift, Sioux arch, and the Canadian Shield leading to deposition of clastic Pennsylvanian to Triassic strata. The Zuni sequence represents the Jurassic and Cretaceous deposits in the Williston Basin and successions of clastic sedimentary rocks and minor carbonate sedimentary rocks and salts. Subsidence of the Williston Basin as a structural depression halted during the Zuni

sequence, along with the basin subsidence. The last sequence described by Sloss (1963) and Gerhard et al. (1990) is the Tejas sequence, which continued sedimentary input from mid-Paleocene through Quaternary and consisted of mostly clastic input with some low grade coal.

2.1.2 Tectonics and Structural Setting

The geologic history of the Precambrian basement of the Williston Basin is critical to an understanding of the basin's evolution, structural configuration, sedimentation, and thermal patterns (Green, et al., 1985). The Precambrian basement is composed of three main geologic provinces; the Churchill hinterland, Trans-Hudson Orogen, and Superior Province (Figure 2.2). The Superior Province in the east and the Wyoming and Churchill Provinces in the west are separated by the Trans-Hudson orogenic belt, which is located between the east and west provinces and represents a continent-to-continent suture zone. The Trans-Hudson Orogenic belt is the result of the collision between the Superior and Churchill Provinces, occurring ~2.0 Ga (Williams et al., 1991). The boundaries between these provinces trend in a north/south orientation. The interaction of two Archean shear systems, the Brockton-Froid and the Transcontinental arch (here refers to the Colorado lineament) are believed to have created a depressed block between the shear systems, thus forming the basin and initiating sedimentation during the Late Ordovician (Gerhard and Anderson, 1988)(Fig 2.1 and Fig 2.4). The major structural features, including major faults, lineaments, fractures, and folds, of the Williston Basin are related to regional wrench-fault tectonism and movement along these two major shear systems (Fig 2.1) (Thomas, 1974; Brown and Brown, 1987).

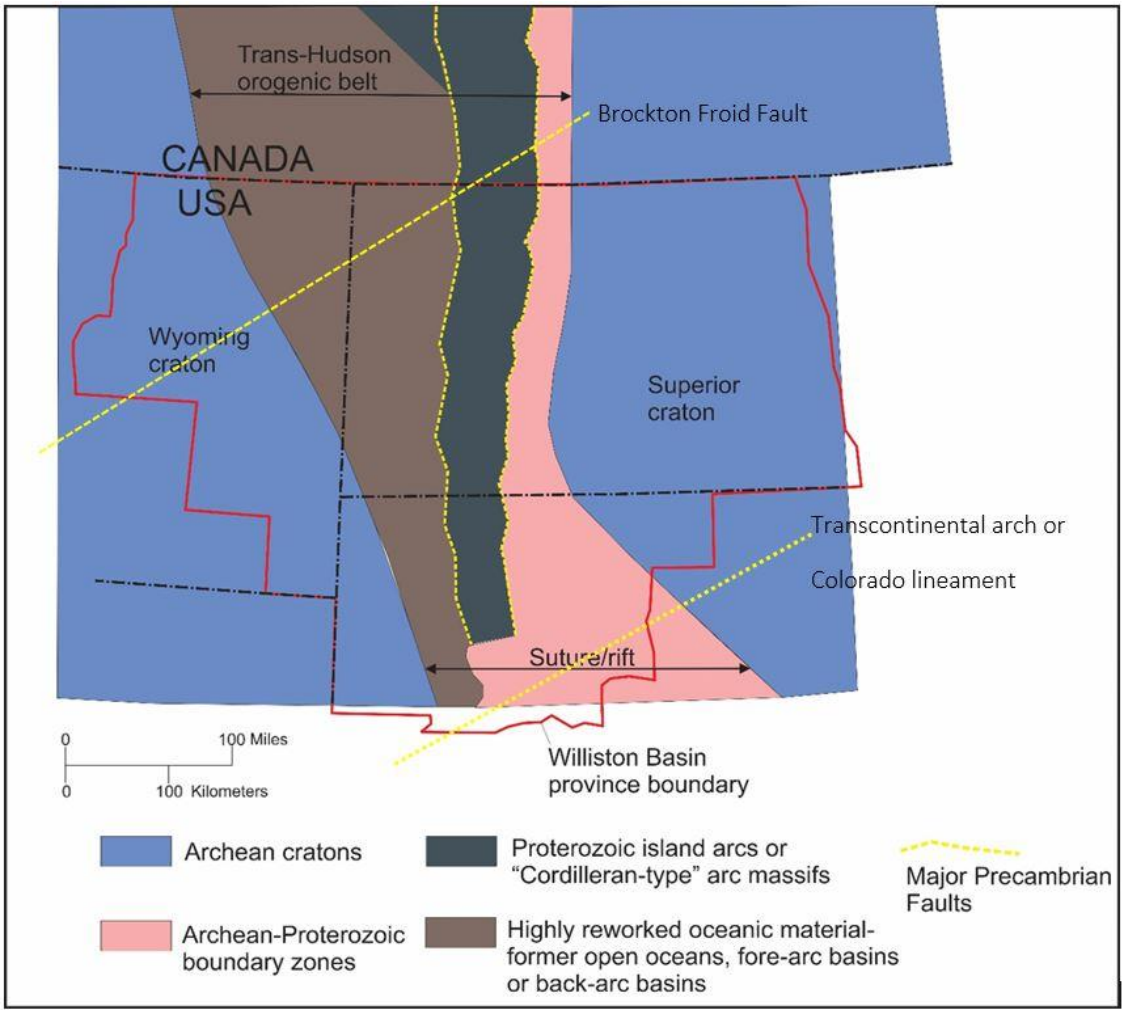

Figure 2.2 Map showing configuration of the Trans-Hudson orogenic belt and associated Precambrian faults of the Williston Basin (modified from Anna et al., 2013).

As is typical of most basins underlain by cratonic crust, episodes of strong folding did not occur in the Williston basin. Deformation that has taken place in Phanerozoic time has consisted mostly of fault displacements. Some of these are classic basement-involved structures resulting in anticlines; others are more subtly controlled, low-relief features affecting development of porosity during sedimentation or diagenesis. Most of the structural features in the Williston basin are controlled by the reactivation of the

Precambrian basement structures during the Phanerozoic. Most of this reactivation is believed to have occurred during the Late Cretaceous due to the Laramide Orogeny. Laramide was a thick skinned orogeny caused due to flat subduction of the Farallon plate under the North America craton. This has led to transfer of stresses farther inward into the craton. Some styles can be explained only by complicated or extraterrestrial processes. Several are accompanied by fractured reservoirs (Gerhard, et al., 1990).

Two of the largest anticlinal features of the Williston Basin, the Nesson and Cedar Creek anticlines are fault bounded anticlinal features. They share similar gross histories, but they differ in important features because of differing positions relative to the structural boundaries of the basin (Figure 2.1 and Figure 2.3).

Although the Nesson anticline is normally regarded as a relatively simple anticline with only one large bifurcation (Antelope anticline), detailed mapping has demonstrated several offsets, linear elements, and fault zones. Many of these fault zones and linear elements appear to have separate histories of motion and development. Some porosity variations occur within the major producing units, reflecting depositional or diagenetic differences (Gerhard, et al., 1990). The Nesson anticline is offset along its length by faults, including a major or master fault system on the west side of the main anticline. This fault system has been present and active since Precambrian time. These offsets are easily seen in the shape and location of producing oil Fields as well as in the development of linear elements over time along the crest of the main structure. Major movements along the master fault took place coeval with the sequence boundaries and at other times (Gerhard, et al., 1987).

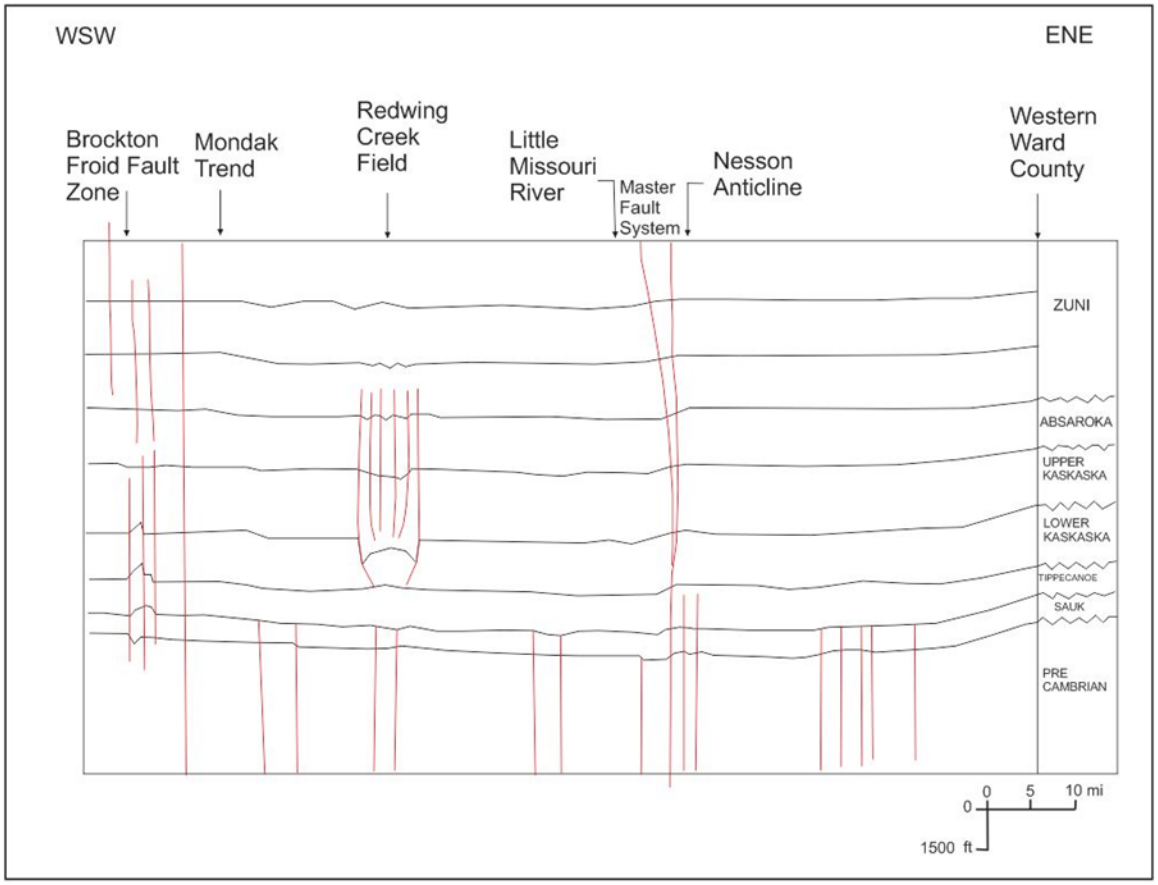

Figure 2.3 Cross-section across the Williston Basin showing major structural features with major stratigraphic sequences (Modified from Gerhard et al., 1990). There are several structures in the basin with complex evolution history.

As in the Nesson anticline, at least one episode of fault reversal occurred along the Cedar Creek anticline. A detailed tectonic history of the Cedar Creek anticline outlining several episodes of fault displacement is presented in Clement (1987). Post-Silurian to pre-Middle Devonian uplift and fault movement accompanied northward and eastward tilting of the Cedar Creek block. During latest Devonian time, fault movement occurred along the principal fault zone. The Cedar Creek block was uplifted and tilted northward and eastward. In the Late Mississippian-Early Pennsylvanian time, the central and northern part of the Cedar Creek area underwent gentle downwarping, and periods of subsidence

occurred with relative down-to-the-east faulting along most of the ancestral faults. Fault movement and subsidence continued during Permian and Triassic time. Relative tectonic stability was attained by Middle Jurassic time and maintained until post-Paleocene time. The Cedar Creek block underwent its greatest uplift during post-Paleocene time; younger Tertiary beds are not present in the area. The uplift was accompanied by major flexure and deep fault adjustment. The area was subsequently uplifted during middle Tertiary epeirogenic phases in the northern Rocky Mountain region, and thick Paleocene and Upper Cretaceous strata were eroded along the axis of the present structure (Clement, 1987).Within the North Dakota portion of the basin are two additional large-scale anticlinal structures that may have fault displacement in the underlying basement: the Billings and Little Knife anticlines (Figure 2.1). In addition, there are gentle folds or trends pervasive throughout the Williston Basin, which may be underlain by basement faults (Gerhard, et al., 1990). The major and minor pervasive structural features in the Williston Basin are controlled by the location of the basement faults (Figure 2.3). A regional left-lateral northeast-trending strike-slip system (Brockton-Froid Fault and Transcontinental Arch) is responsible for the generation of planes of basement faults in the Williston Basin (Gerhard et al., 1982)(Figure 2.4).It is indicated that wrench-fault motion generated by the these regional left-lateral shears is geometrically congruent with linear direction of basin structures (Figure 2.4b). A left lateral wrench faulting motion would create structural features in NNE-NE and NNW to NW direction, which is also the trend of the major structural features in the Williston Basin. The planes of basement faults became zones of weakness that controlled the later development of most basin structural elements, which have been talked about above.

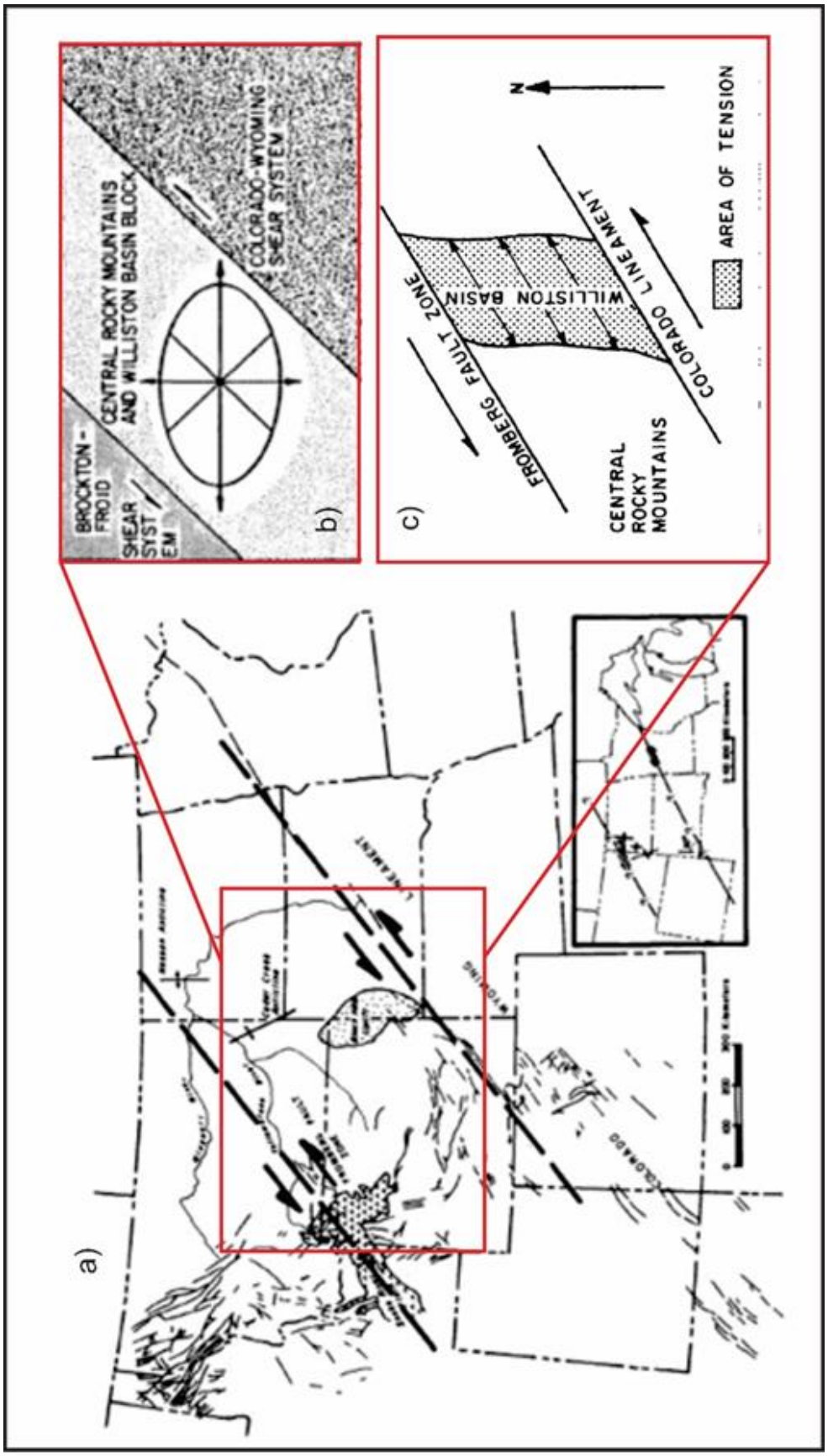

Figure 2.4 a) Map showing the regional left lateral northeast trending strike slip system (Brockton-Froid Fault or Fromberg Lineament and Transcontinental arch or Colorado lineament). b) Strain ellipse generated due to such a left lateral shear c) a possible model for the origin of subsidence in the Williston basin (Modified from Gerhard et al., 1990).

Thus, although basin structures may have originated with left-lateral shearing, absolute movement or sense of movement along these planes of mechanical weakness has varied over time as stress fields have varied in orientation (Gerhard, et al., 1990). This wrench faulting model has been used in establishing a theory for the origin of the Williston basin. Although thermal decay was suggested by Ahern and Mrkvicka (1984) as one mechanism for the origin of the Williston basin, data are inadequate to support that hypothesis. However, the wrench-fault model accounts for an early southwest-trending Paleozoic marine connection. This connection, bounded by left lateral shears, would be a depressed block of large regional extent. A "pull-apart" rift within this block (Figure 2.4c) was originally proposed by Gerhard et al. (1982) as a probable mode for initiation of the Williston Basin.

2.1.2.1 Wrench Faulting in the Bakken Formation

Wrench faulting is a common deformation mechanism in the Williston Basin. Faulting, sediment draping, and transpressional forces create subtle, low-relief features such as the Nesson Anticline and Cedar Creek Anticline. These features can be complex; the Nesson and Cedar Creek anticlines are both formed by faults with episodes of fault reversals in a relatively continuous history of deformation (Gerhard et al. 1990). The cross section of the Nesson Anticline is shown in Figure 2.5. Multiple faults compose this positive relief structure, and there are multiple changes in slip direction per-fault. Left-lateral motion along strike-slip faults in the Williston Basin should not be assumed, even when previous directionality of motion is indicated. Lateral movement reversal is common for structures in the Williston Basin, and the dominant sense of motion is uplift (Gerhard et al. 1990).

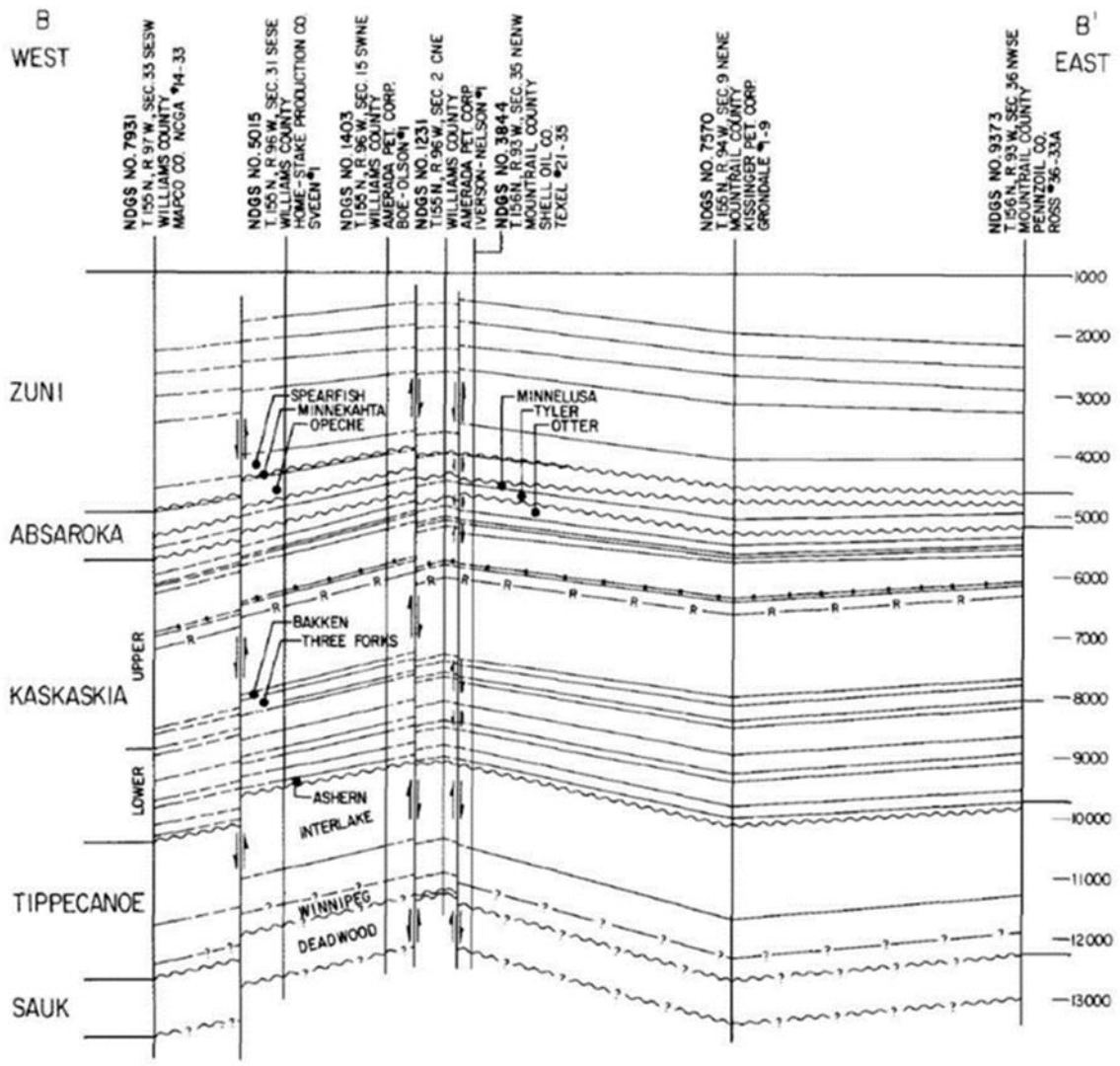

Figure 2.5 A west-east cross section of the Nesson anticline showing the major sub vertical faults associated with the structure (Gerhard et al., 1990).

Shephard (1990) associates wrench faulting with the creation of open mode fractures in an average of 4 mile-wide zones. These fractured regions have increased hydrocarbon recovery factors; they introduce permeability in an unconventional tight reservoir. Basement and wrench faulting also plays an important role in hydrocarbon migration. There has been a lot of speculation of Bakken sourced oil being leaked into the younger

reservoirs. Bakken-sourced oils in the Madison Group are not radially diffused, but travel along fracture sets introduced by basement faulting and connected shallower zones of weakness.

2.1.2.1 Bakken Petroleum System

The Bakken Petroleum System is composed of the upper 50 feet of the Three Forks Formation, the Bakken Formation, and the lower 50 feet of the lower Lodgepole Formation (Price and LeFever, 1992). The contact between the Three Forks Formation and overlying Bakken Formation in the basin center is conformable and transitions into an unconformable contact at the basin margins. According to Webster (1984), the unconformable contact displays evidence of subaerial exposure which has well developed diagenetic porosity. The Bakken Formation averages 140 feet thick in the central part of the basin. Each unit of the Bakken progressively onlaps each older member of the Bakken (Figure 1.1). The Bakken formation is subdivided into three members: lower and upper members both consisting of shelf black shale, and the sandy-silty middle member (Figure 2.6) (Angulo et al., 2008). The lower member and the lower interval of the middle member form an open-marine coarsening-upward parasequence. The parasequence consists of black shale deposited on a shelf; a lower to upper offshore siltstone interbedded with thin layers of silty, very fine grained sandstone; an offshore-transition of regularly interbedded siltstone and very fine-grained sandstone; and a lower shoreface very fine-grained sandstone. With the exception of the anoxic to dysaerobic shale, these open –marine deposits are intensely bioturbated, containing Phycosiphon, Nereites missouriensis, Planolites, Asterosoma, Chondrites, and Teichichnus. Both lower and upper members are considered world class mature source rocks with the lower

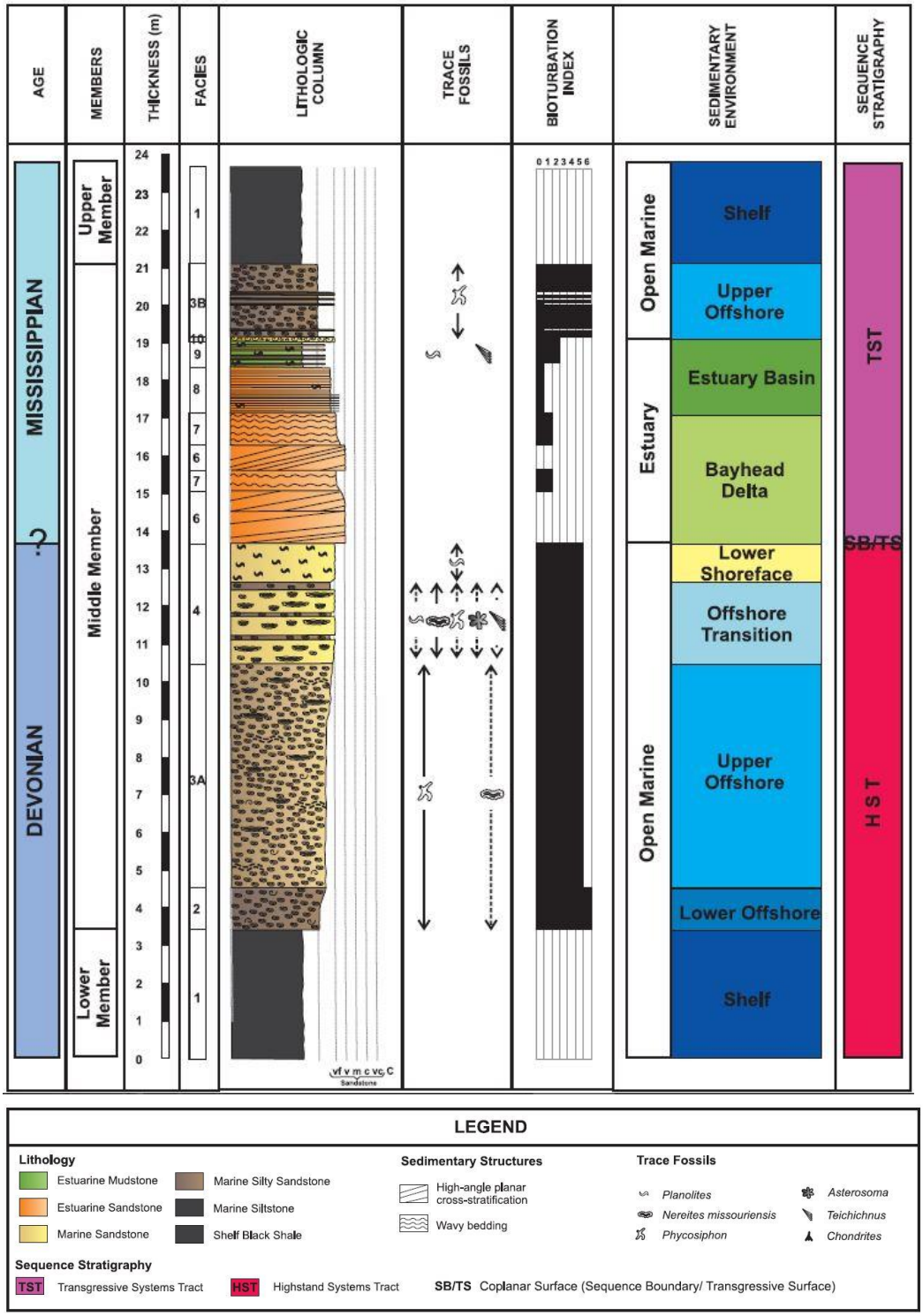

Figure 2.6 Idealized stratigraphic log of the Bakken Formation (Angulo et al., 2008)

member averaging a total organic content (TOC) of 11 weight percent (wt. %) and the upper having an average TOC of 11 wt. % (Meissner, 1991). Based on hydrogen and oxygen index characteristics the kerogen found in the Bakken Petroleum System is mainly type I and II (sapropelic), however type III kerogens are present along the shallow eastern flank of the basin (Sonnenberg et al., 2011). The Upper Bakken Shale is interpreted to have been deposited over a large flat area due to its relatively uniform thickness throughout the basin, while the Lower Bakken Shale displays localized thickness anomalies due to the Prairie salt dissolution that occurred prior to Bakken deposition (Webster, 1984). Due to this factor, lower member thicknesses can reach a maximum of 50 feet while the upper has a maximum thickness of only 23 feet (LeFever et al., 1991). The Middle Bakken Member is a complex and highly variable unit across the basin. It is a 20-30 foot thick unit that overlies the Lower Bakken Shale. Separating the two members is a sequence boundary that appears sharp to irregular in some places and as a gradational contact in others (Pitman et al., 2001). Where the sharp to irregular contact exists there is a thin lag deposit composed of pyrite nodules, pyritized shell fragments, and black mudstone intraclasts associated with it (LeFever et al., 1991).

Conformably overlying the Bakken Formation is the oldest unit within the Madison Group, the Lodgepole Formation. It is composed of argillaceous, shaly, silty, and cherty thin to medium bedded limestone. The lowermost member of the Lodgepole Formation is the Scallion member, which directly overlies the Bakken Formation and is a dense medium gray limestone containing abundant pelmatozoan material (Webster, 1984). Stratigraphically above the Scallion member is the False Bakken which is composed of black shales or marl and clay-rich limestones and a thickness range of zero to 250 feet

thick. The depositional environment for the lower Lodgepole members has been interpreted to be shallow marine environment on the slope and basin margin (Webster, 1984). The lower Lodgepole members are important to the Bakken Petroleum System because they act as the seal for the system. The Three Forks Formation averages 150 feet in thickness and is composed of green and tan to pink interbedded shales, and grey and to yellowish siltstones, carbonates, and evaporates (Gerhard et al., 1990). Sedimentary structures found within the Three Forks Formation include locally brecciated laminations and ripple laminations.

The source rocks were deposited in the Early Mississippian and Late Devonian. The reservoir rocks were deposited in the Late Devonian to the end of Early Mississippian. The structural traps were formed with the reactivation of the Precambrian basement faults by major orogenies(as described above in section 2.1.2). Laramide orogeny played a major role in the formation of structural traps in the basin. The oil generation started post Late Cretaceous (Gaswirth et al., 2013) (Figure 2.7).

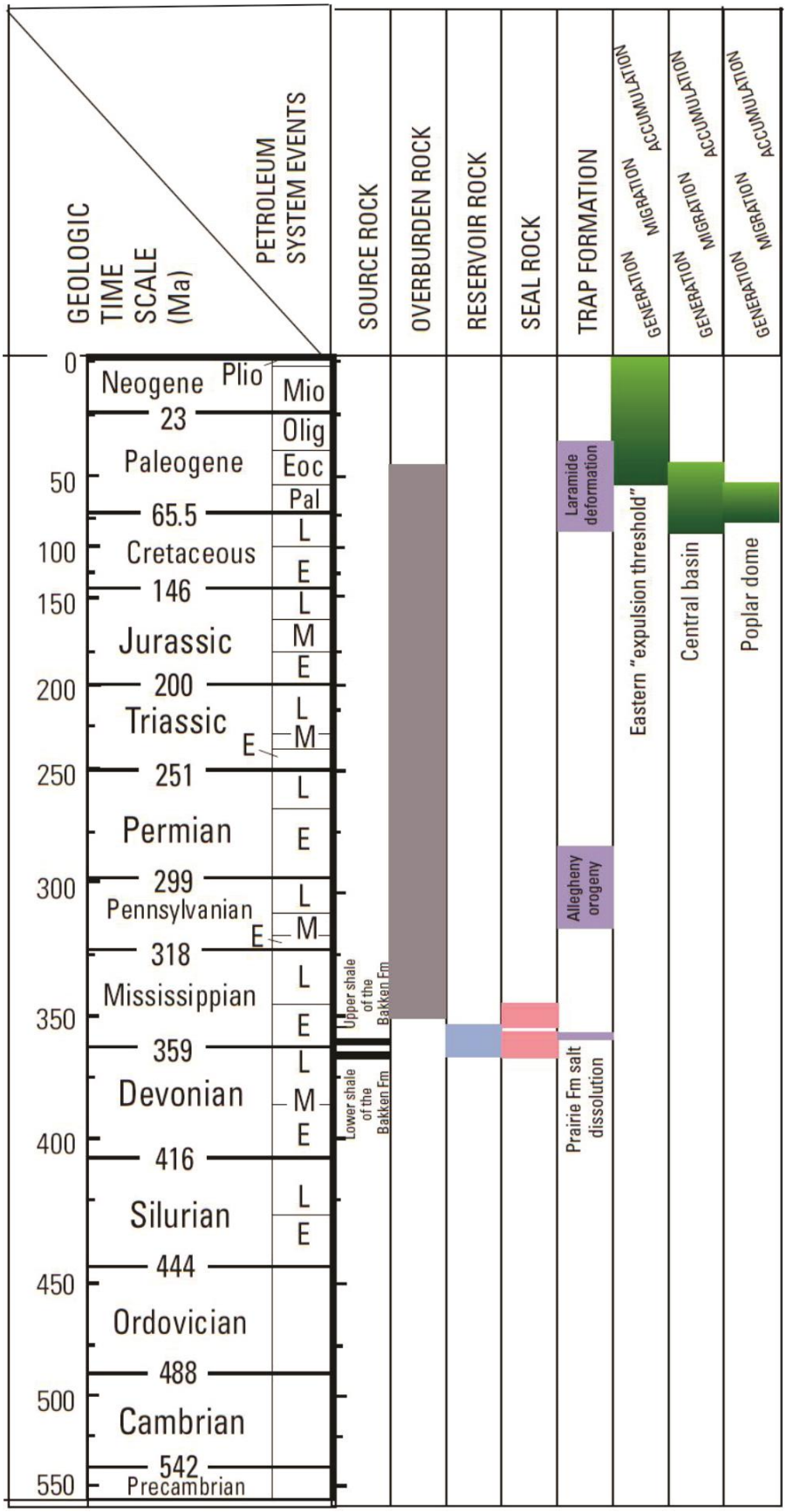

Figure 2.7 The petroleum systems chart for the Bakken Petroleum System showing the timing of source rock deposition and trap formation, and the age of overburden, reservoir, and seal rocks. The chart also depicts the timing of oil generation, migration, and accumulation as modeled for various wells in different parts of the Williston Basin. E, Early; M, Middle; L, Late; Pal, Paleocene; Eoc, Eocene; Olig, Oligocene; Mio, Miocene; Plio, Pliocene; Ma, Mega-annum. (Gaswirth et al., 2013).

CHAPTER 3
WRENCH FAULTING

Strike slip faulting accommodates the lateral and oblique movement of two adjacent crustal blocks with respect to each other. Oblique movement of crustal block introduces divergent or compressive stresses into the overall strike-slip regime (Christie-Blick & Biddle, 1985). In map view, the principal displacement zone is linear or curvilinear (Figure 3.1).

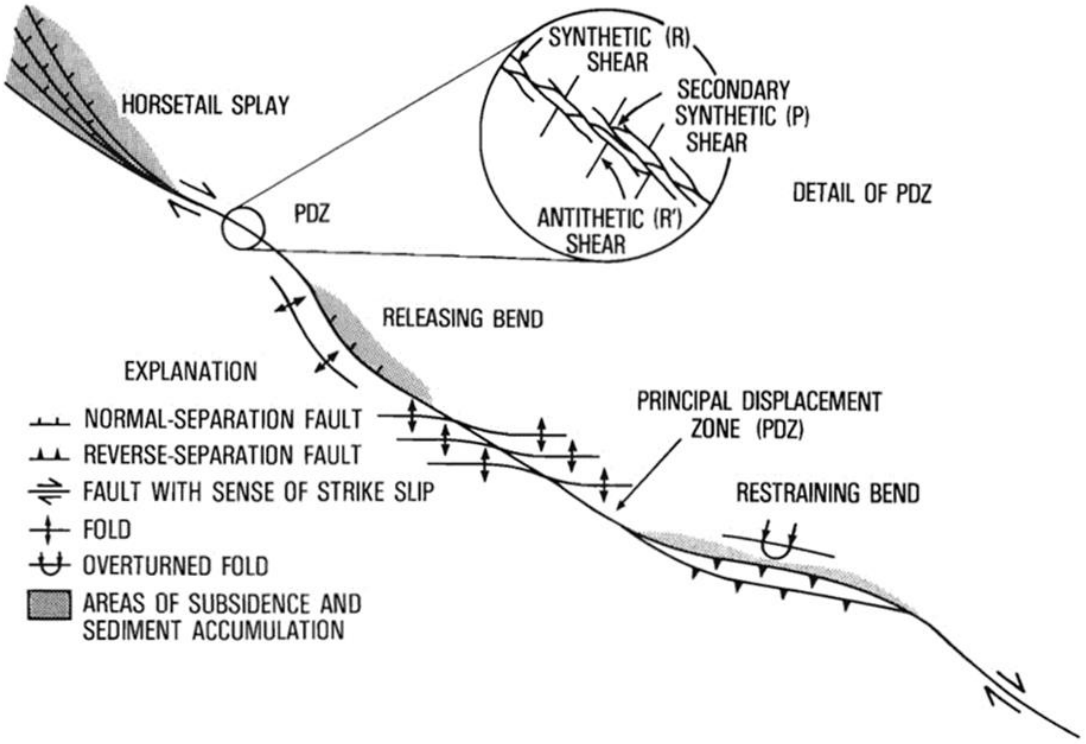

Figure 3.1 A map showing various structural features associated with a displacement zone of a dextral strike slip fault (Christie-Blick & Biddle, 1985).

Deviations as small as 3 degrees from the linear path of a strike slip fault introduce extensive deformation as is illustrated in Figure 3.1. This deformation includes synthetic and antithetic strike-slip faults, normal and reverse faults, and folding. These structures create oversteps, branching, and braiding features, and can also manifest as en echelon faulting (Jansen 2005). Synthetic faults form at angles of 10-20° or less to the direction of strike-slip, and antithetic faults form at angles of 70-80° to the system (Christie-Blick & Biddle, 1985). En echelon faulting, or step-overs, can connect the main strike-slip faults; these are parallel, short, overlapping or underlapping faults obliquely oriented to the direction of main displacement (Christie-Blick & Biddle 1985). En echelon faults sometimes have a displacement sense opposite of the main system; the step-overs may be right lateral strike-slip in a left-lateral strike slip system (Jansen 2005). These multi-oriented faults can create an extremely complex system of deformation in a narrow zone.

Wrench faults are prominent strike-slip faults that extend from a narrow, sub-vertical displacement zone at depth, usually as deep as igneous or metamorphic basement rocks, to a more laterally extensive, divergent zone of deformation in the sedimentary cover (Figure 3.2) (Christie-Blick & Biddle 1985). This upper divergent zone is composed of fault splays are created as isolated features in the more shallow zones that eventually join with the main wrench fault; these create “flower structures” or “palm tree structures” (Christie- Blick & Biddle 1985; Jansen 2005). The splays of a wrench fault can be composed of both normal and reverse faults in the same profile (Christie-Blick & Biddle 1985). The magnitude of slip and direction of slip can change for different horizons for

the same fault, i.e. one fault splay can change from a normal to a reverse fault up-section

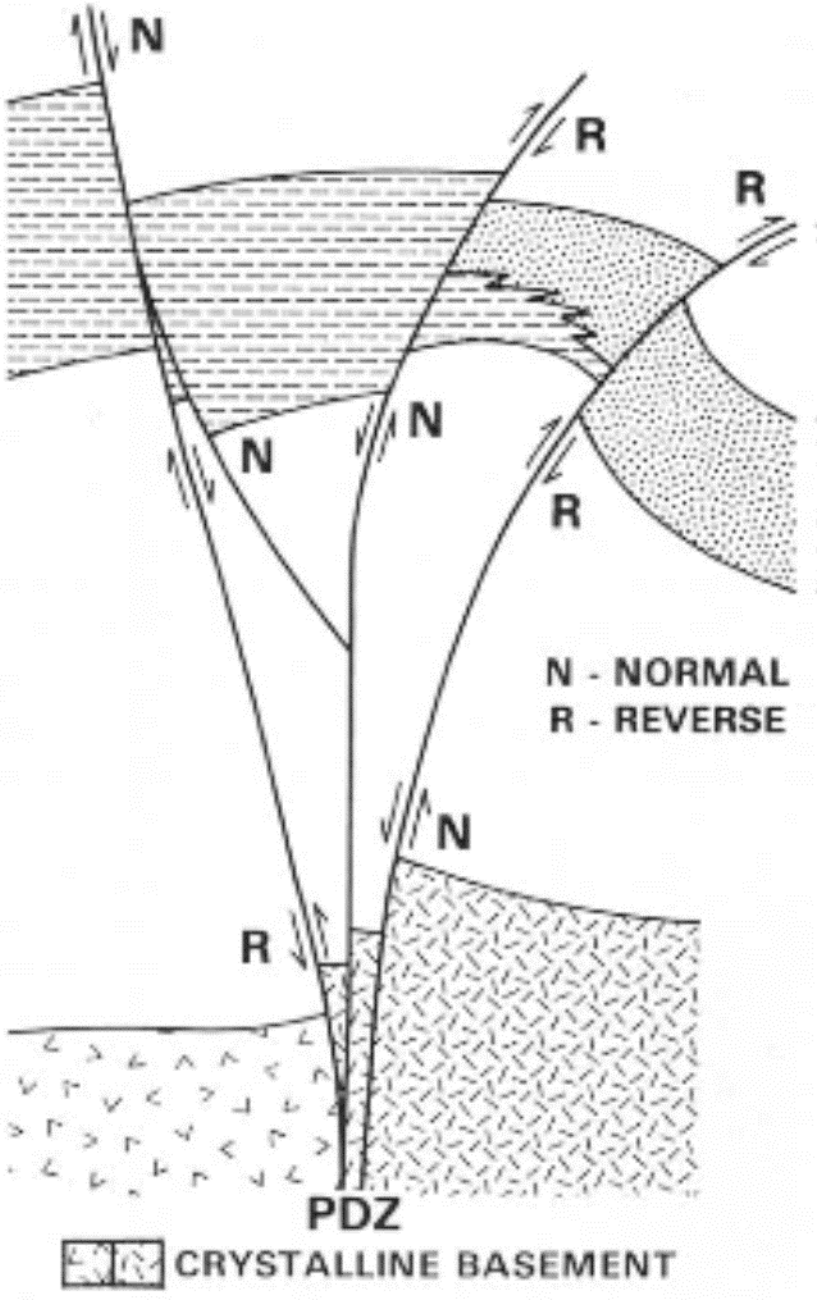

Figure 3.2 Idealized cross section of the displacement zone of a Wrench fault (Christie-Black & Biddle 1985).

(Christie- Blick & Biddle 1985). Alternatively, this change in fault direction can change laterally; a single horizon can be upthrown at one location of the fault and downthrown at a successive location (Christie- Blick & Biddle 1985). According to Christie-Blick and

Biddle (1985), there are five commonly observed sets of fractures: (1) synthetic strike-slip faults, (2) antithetic strike slip faults, (3) secondary synthetic faults, (4) extension or tension fractures, and (5) faults parallel to the principal displacement zones (Figure 3.3).

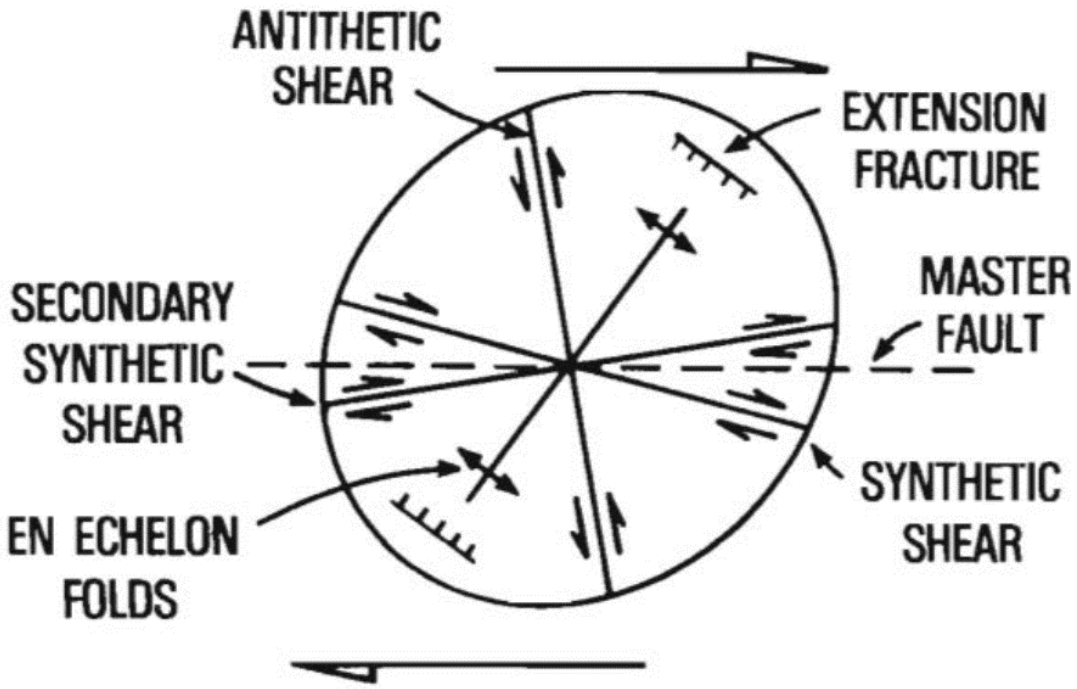

Figure 3.3 Strain ellipse showing the trends of structure features in the displacement zone of a dextral wrench fault (Christie-Blick & Biddle 1985).

The structural style of wrench fault system and resulting fracture types is influenced by the rotation of fault blocks, introducing convergent or divergent stresses to linear strike-slip faults. In addition, the rotation and resulting stress regime of one fault block may not translate to adjacent fault blocks (Christie-Blick & Biddle 1985). Deformation may be localized to a narrow range adjacent to the strike-slip fault. The simplest pull-apart basin is characterized by subsidence parallel to the strike of the main fault on the very edge of the fault. Fracturing tends to be most intense at fault intersections, where stress variations are high (Jansen 2005). Increased fracturing at fault intersections has been observed using

shear wave splitting analysis coupled with fault interpretation and production data (Jansen 2005).

3.1.1 Analog models for Wrench Fault Systems

Interpretation and analysis of complex three-dimensional (3-D) structures in the subsurface is one of the major challenges in hydrocarbon exploration. Seismic imaging of strike-slip structures is commonly very poor because of the steep stratal and fault dips as well as significant along-strike variations in structural geometries. In addition, subtle vertical offsets of these faults makes it increasingly difficult to map them in 3D seismic data. Hence, mapping such fault systems in 3D seismic data is incredibly complex and plagued by subjective interpretations such as shown in Figure 3.4. Such a fault system would be immensely difficult to trace in 3 dimensions.

Most conventional discontinuity detection seismic attributes are unsuccessful in precisely tracking these fault systems in 3Dseismic data due to subtle, in some cases sub-seismic, vertical offset generated by these fault systems. Hence, the analog models of wrench fault systems can be extremely useful in mapping such systems in 3D seismic data.

McClay and Banora (2001) used scaled sandbox models to simulate the geometries and progressive evolution of antiformal pop-up structures developed in a weak sedimentary cover above restraining stepovers in offset left lateral strike-slip fault systems in rigid basement (Figure 3.5). It was observed that the geometry and the evolution of the antiformal pop-up structure was dependent primarily on the basement fault geometry and stepover width (Figure 3.5).The vertical and horizontal sections of the completed models

permit the full three-dimensional (3-D) structure of the pop-ups to be analyzed in detail

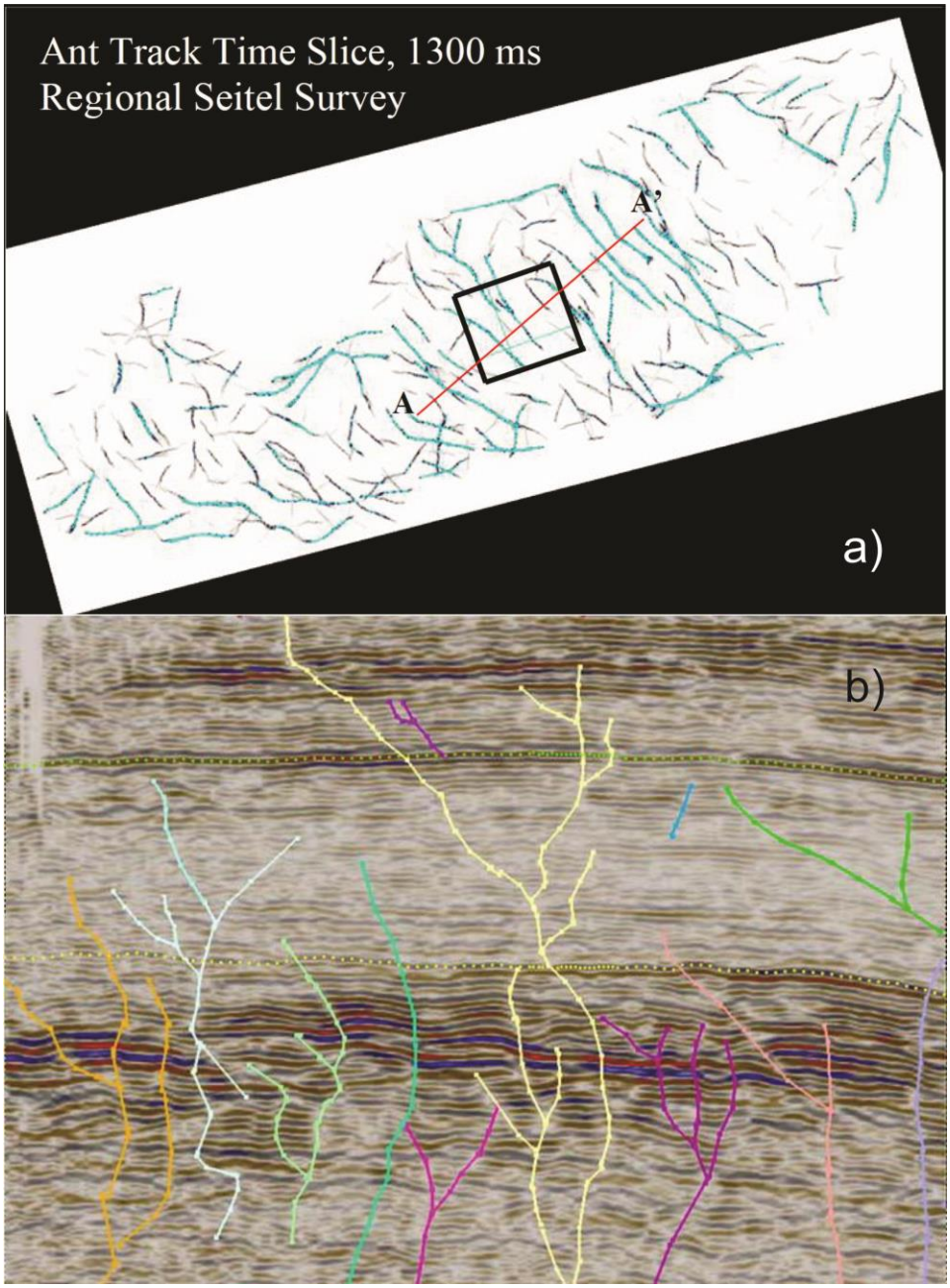

Figure 3.4 a) Time slice of entire Seitel survey (Rulison Field, Colorado) at 1300 ms TWT from computed ant track attribute volume. Blue lines indicate fault architecture at this depth. Red line A-A' indicates cross section shown in b). b) Manual interpretation of the fault network in the seismic section is shown (Jansen, 2005).

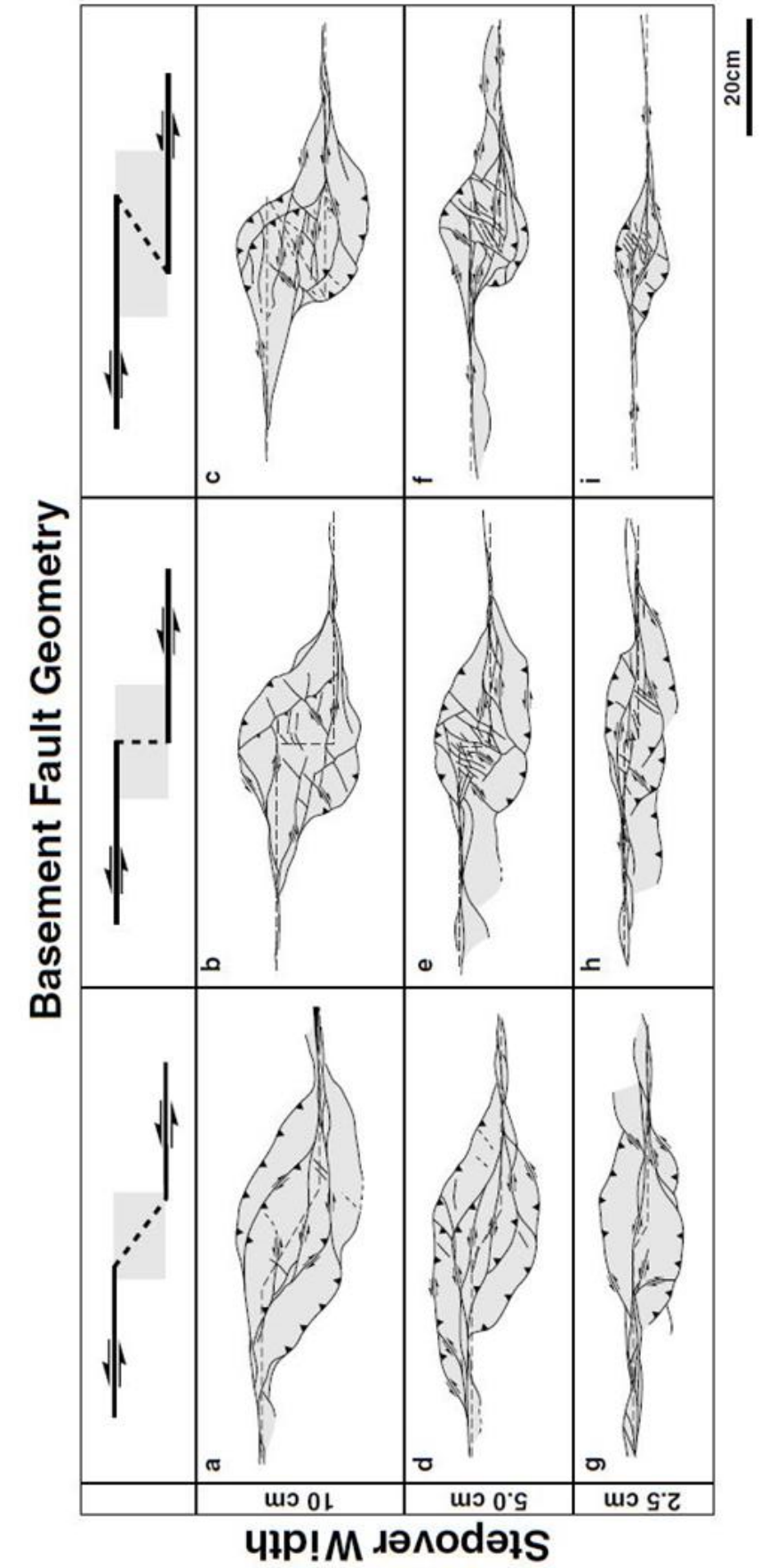

Figure 3.5 Summary of pop-up structures for restraining stepover spacing from 10 to 2.5 cm (McClay and Banora, 2001).

(Figure 3.6). Lozenge-shaped pop-ups are characteristic of underlapping stepovers, whereas rhomboidal and strongly sigmoidal pop-ups are characteristic of neutral and overlapping stepovers (Figure 3.5), respectively.

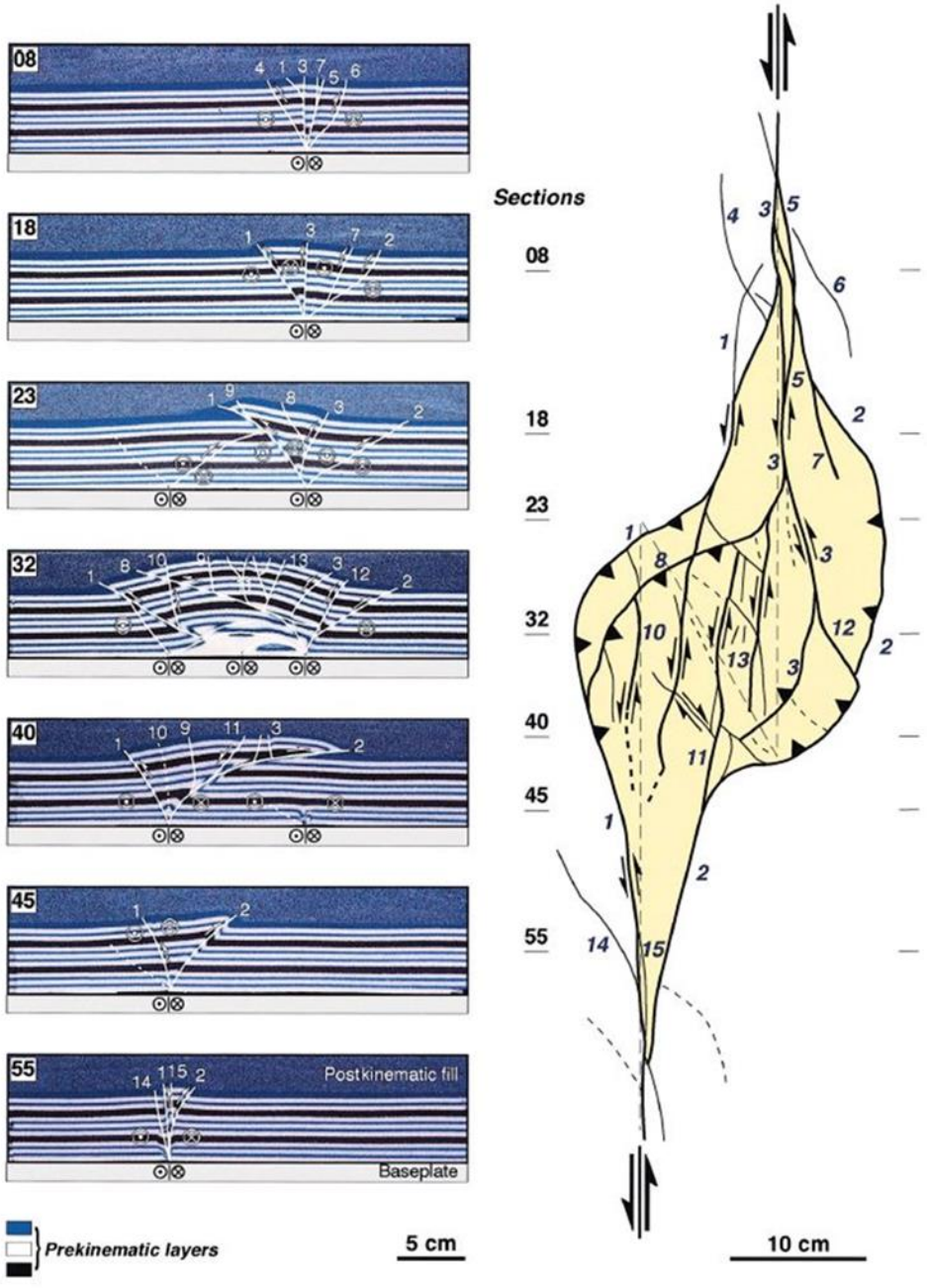

Figure 3.6 Serial vertical sections and a line diagram of the surface of experiment W309 after 10 cm left lateral strike-slip displacement on the basement fault system. Faults are numbered to permit correlation between the plan view diagram and the vertical sections (McClay and Banora, 2001).

In cross section the pop-ups are dominantly asymmetric with the bounding faults dipping inward into the basement fault systems. Symmetric pop-up geometries are only found above the central sections of the basement stepovers. All pop-ups produced in this study by Mcclay and Banora (2001) are doubly plunging anticlines that produced four-way dip closures. With increased stepover angle (neutral to overlapping) and increased displacement on the basement fault systems, crosscutting faults transect the central sections of the model pop-ups (McClay and Banora, 2001).

CHAPTER 4
METHODOLOGY

This study used a workflow for conditioning the 3D seismic data in order to increase the signal to noise ratio and amplify the structure of the basement. A model driven approach was used to aid in structural interpretations. In addition, an analog outcrop was used to derive the expected fracture density in the middle member of the Bakken Formation in the study area. A conceptual fracture model was developed based on the orientations of the fractures from the structural interpretations and density of the fractures from the analog field outcrop.

4.1 Seismic Investigation Methodology

This study used a 3D Seismic data set from the Crane Field, which is located at the south eastern corner of the Elm Coulee Field (Figure 1.5 and Figure 2.1). The data set was donated by Headington Oil Corporation. The data set has numerous wells drilled along the seismic lines; however, only four of these wells had density and sonic logs. The amplitude range of the data set is shown in Figure 4.1c. As shown by the red box in the Figure 4.1a, the deeper parts of the data set are plagued with noise. To amplify the structure of the basement to facilitate interpretation, it was necessary to condition the data set in order to amplify the signal to noise ratio. The workflow used to condition the data set is outlined in the Figure 4.2. A structural smoothing filter with dip guiding and edge enhancement (Structural smoothing DgEE) is applied to the original amplitude volume. Structural smoothing filter performs smoothing of the input signal guided by the

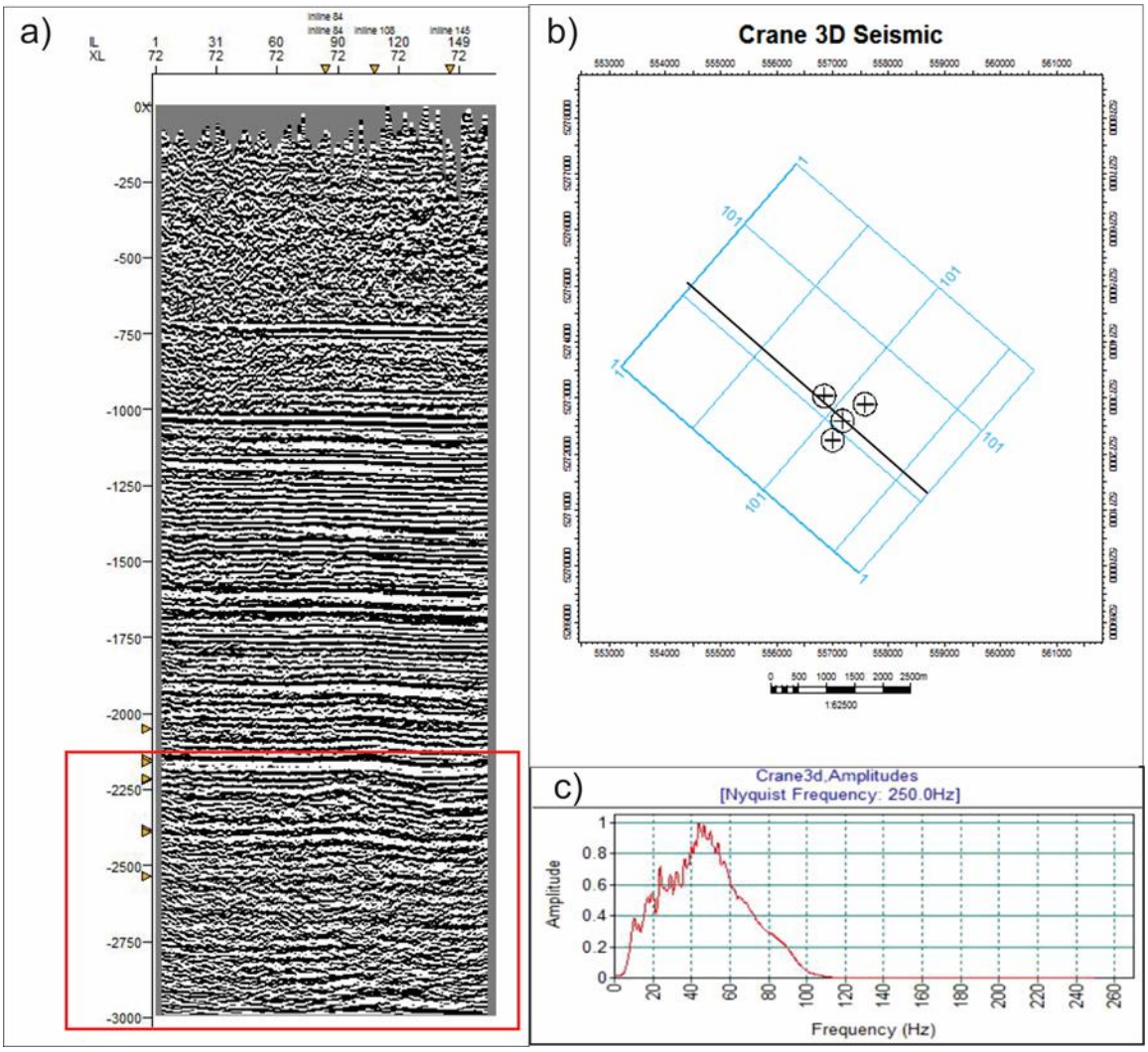

Figure 4.1a) The seismic section from the original Amplitude volume. The red box show the area of interest. The area of interest seems to have a low signal to noise ratio. b) Location of the seismic section. c) Amplitude spectrum of the 3D seismic data. Vertical Exaggeration =7.5

local structure to increase the continuity of the seismic reflectors (Randen et al., 2000). Principal component dip and azimuth computation are used to determine the local structure. Gaussian smoothing is then applied parallel to the orientation of this structure. Performing structural smoothing with dip guiding and edge enhancement performs structurally guided Gaussian smoothing and enhances detected edges (Figure 4.3). The second step was to extract an instantaneous phase attribute volume from structurally

smooth volume. Instantaneous phase attribute shows the continuity and discontinuity

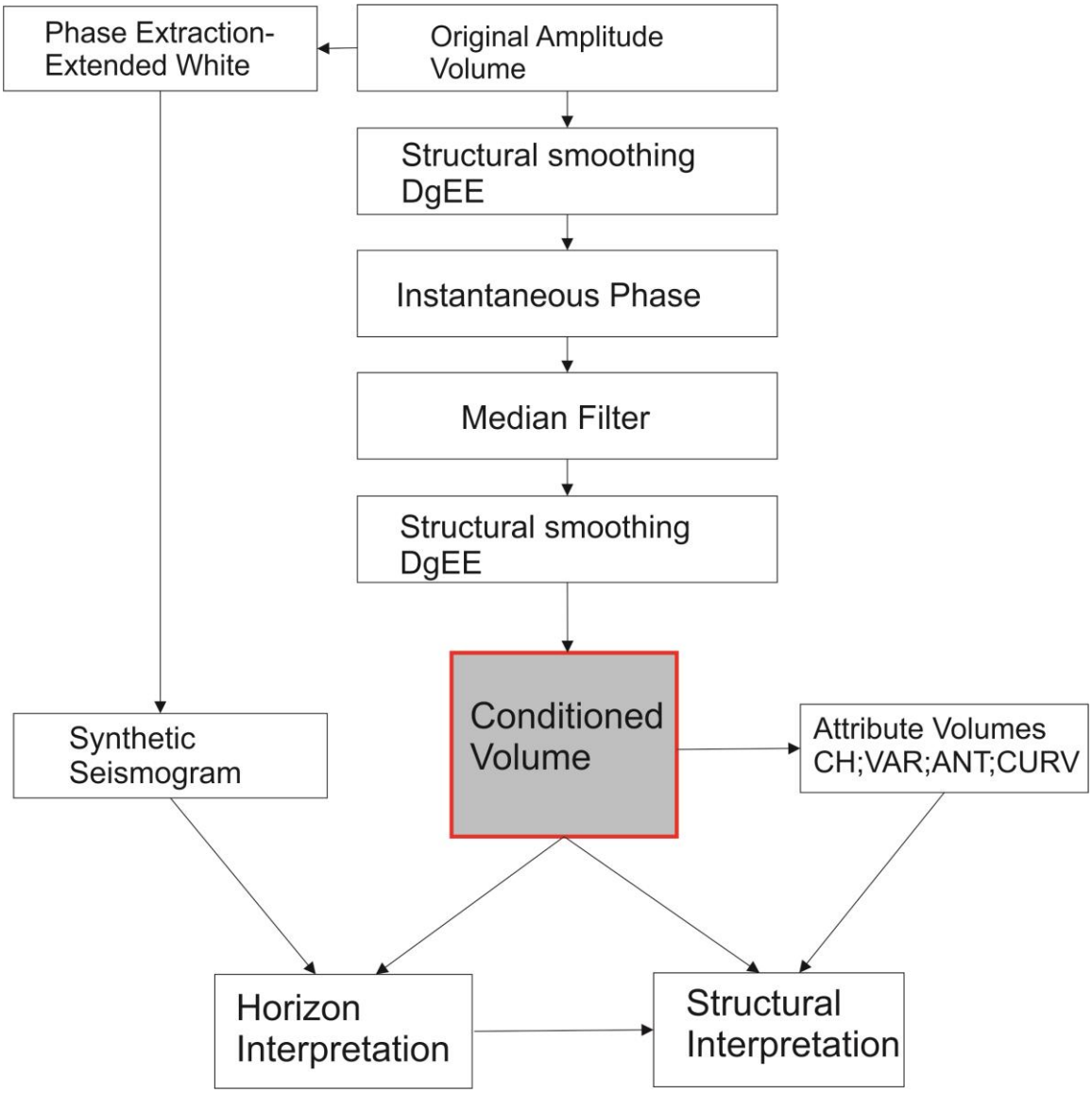

Figure 4.2 The workflow used for post stack conditioning of the 3D seismic data set. See text for discussion. DgEE: Dip guided with Edge Enhancement; CH: Chaos; VAR: Variance; ANT: Ant Track; CURV: Curvature. Parameters shown in the Appendix

of the reflection events, and shows bedding very well. This attribute is the best indicator of lateral continuity of a given horizon (Figure 4.4) (Subrahmanyam and Rao, 2008). It is

independent of the amplitude. Instantaneous phase is measured in degrees ($-\pi,\pi$). The phase along any

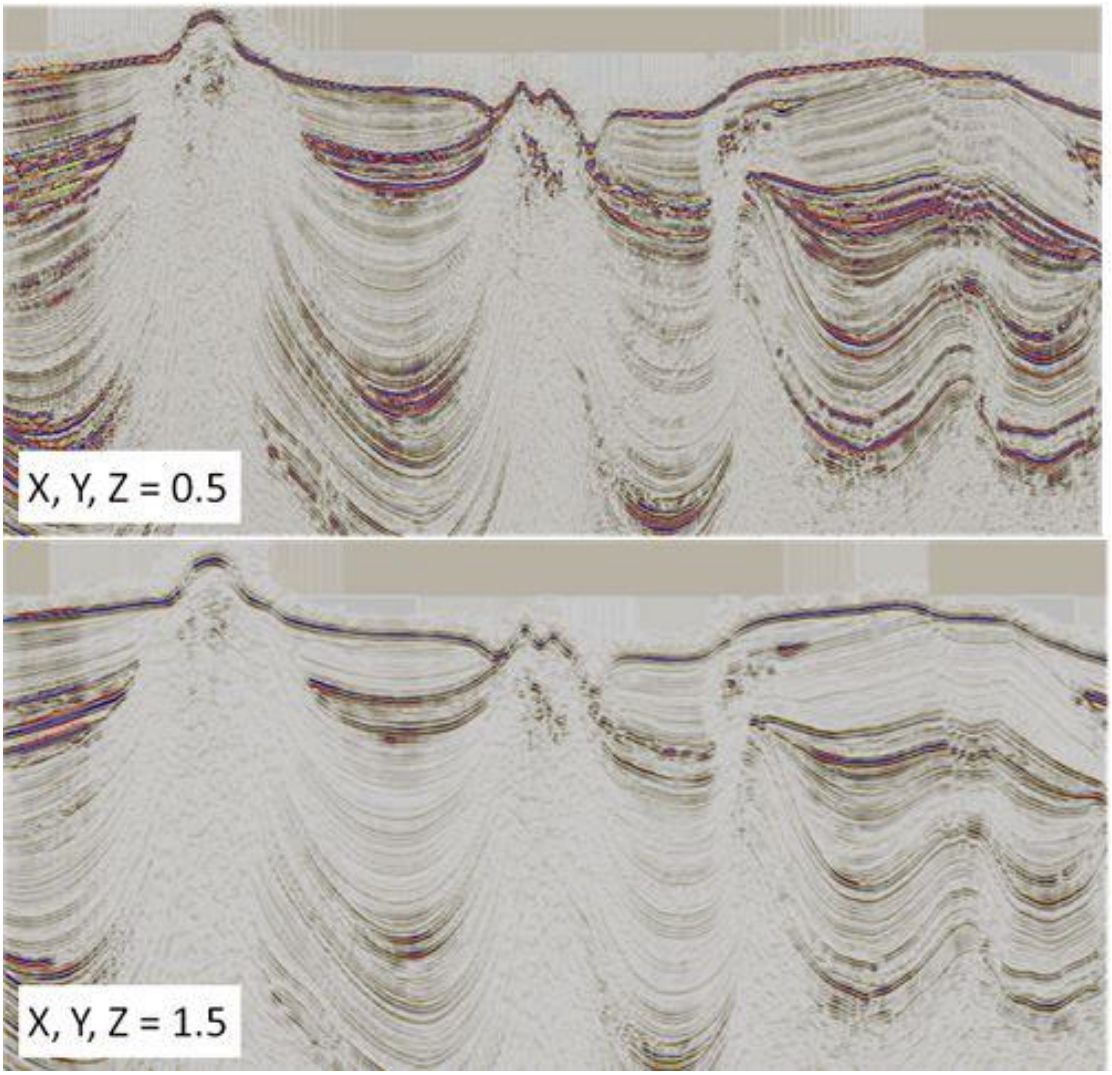

Figure 4.3 The figure shows the result of applying Structural smoothing DGEE to a data set using different filter sizes. (Petrel Workflow Tools, 2015).

given horizon should not change in principle, changes can arise if there is a picking problem, or if the layer changes laterally due to “sink-holes” or other phenomena. A very

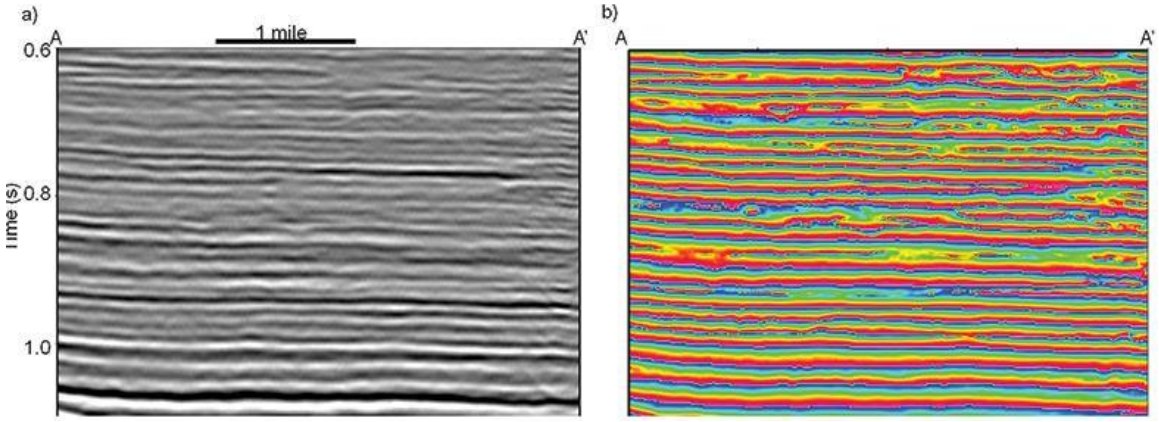

Figure 4.4. The figure shows the extracted Instantaneous attribute section to the right from the original amplitude volume on the left. The continuity and discontinuity of the reflectors is much more clear and evident in the Instantaneous attribute section (Petrel Workflow Tools, 2015).

light median filter is applied to extracted instantaneous attribute volume. The median filter is a smoothing filter that has an edge-preserving nature, and is good at removing seemingly random noise with high amplitudes (also known as salt and pepper noise) (Figure 4.5).This makes it good to use on seismic where we are concerned with preserving reflector edge information and smoothing the values in between. However, it is important to note that this filter actually filters out rapidly changing signals, which can have an unwanted effect as input to chaotic feature detection attributes such as chaos and amplitude contrast. An important thing to note here is that a median filter is a filter that enhances edges/boundaries in data. It is hence not really suitable for filtering of seismic data, as the median filter will introduce high- frequency noise (i.e. sharp edges), which does not exist naturally in band-limited data. Median filters can however be very

effective to attenuate random noise in seismic attributes (Petrel Workflow Tools, 2015). Once the noise is removed from the instantaneous attribute volume using the median

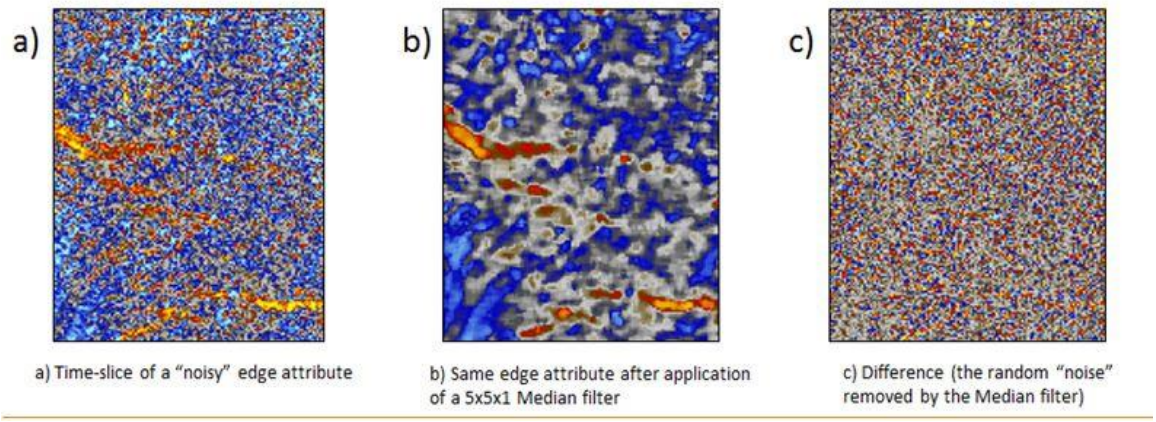

Figure 4.5 An example to demonstrate the effect of applying median filter to a dataset with a large amount of random noise (Petrel Workflow Tools, 2015).

filter, the structural smoothing filter with dip guiding and edge enhancement (Structural smoothing DgEE) is applied again to smooth out the remnant noise and enhance the structure more. A comparison between the original amplitude volume (X), structural smoothing DgEE (XS), instantaneous phase attribute volume (XSI) and the final conditioned seismic volume (XSIS) is shown in Figure 4.6. It is evident that the signal to noise ratio has been greatly improved while preserving the lateral continuity and structure in the data set.

Three conventional discontinuity detection attributes were used to test the effectiveness of these attributes in picking subtle vertical offset faults. Seismic edge-detection methods commonly measure the similarity between waveforms or traces to bring out stratigraphic and structural features expressed in seismic data (Chopra and Marfurt, 2007). Such

information provides valuable input for reservoir modeling (Chopra and Marfurt, 2007).

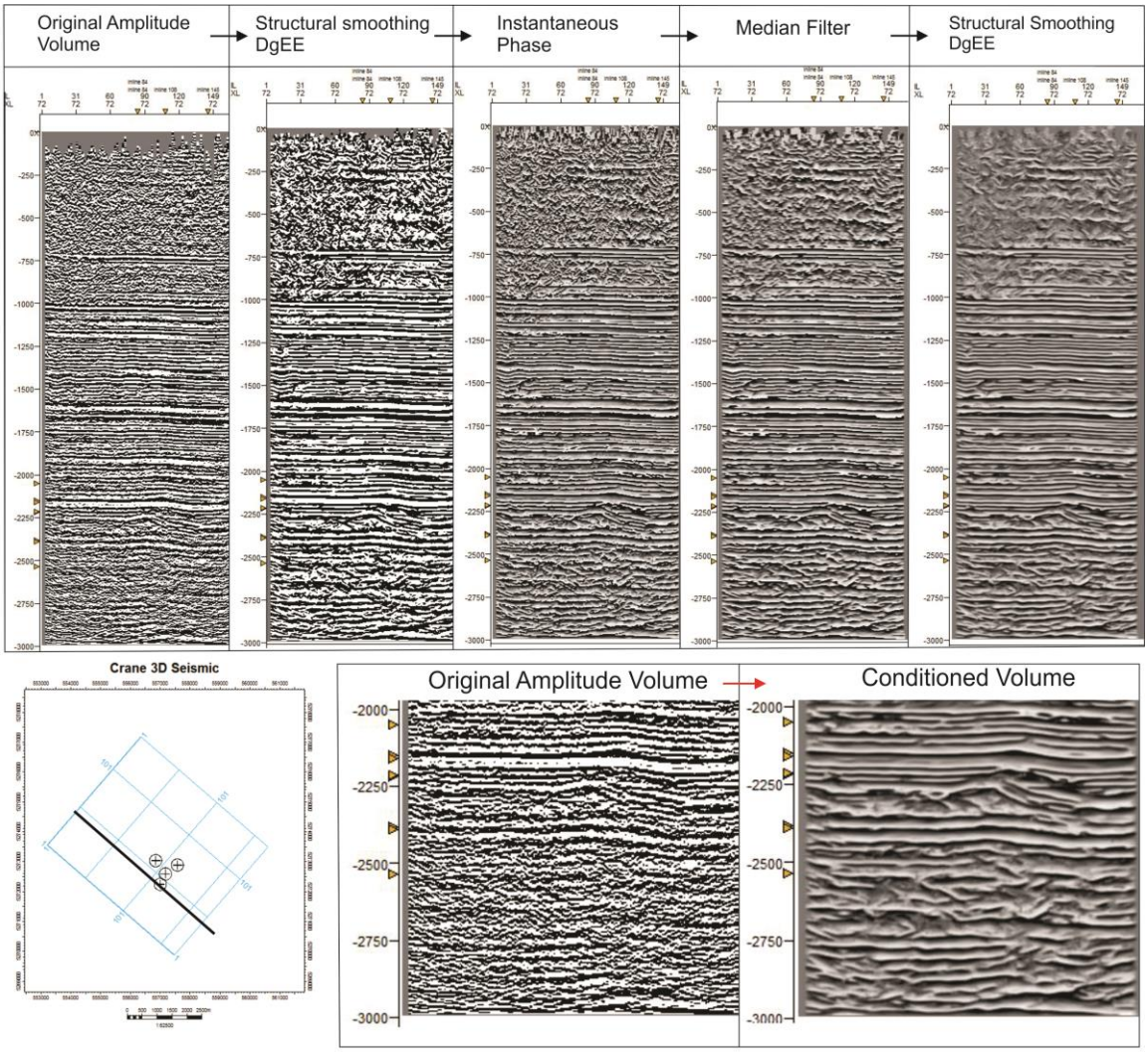

Figure 4.6 Seismic section from different 3D volumes shown here for comparison on the top of the figure. The location of the seismic section is shown in the bottom left of the figure. The area of interest from Figure 4.2 is shown here from the original amplitude volume and the final conditioned volume for comparison. Vertical Exaggeration =7.5.

The most commonly used edge-detection methods are chaos, variance, and ant tracking. A range of chaos and variance attributes was were created and evaluated for use in this study. Chaos and variance attributes show drastically different results using the same seismic data, as a result of the algorithm used by each method. The Chaos attribute is

defined as a measure of the "lack of organization" in the dip and azimuth estimation method (Petrel Workflow Tools, 2015). In other words, it searches the chaotic signal pattern contained within seismic data; therefore, chaos in the signal can be used to help clarify faults and discontinuities and to facilitate seismic classification of chaotic texture. The Chaos algorithm uses the dip/azimuth estimation approach (also referred to as the dominating orientation analysis) to extract areas of discontinuities (Randen et al., 2000). The dominating orientation is computed by the principal component analysis, which is found by aggregating the gradients (estimated during gradient estimation in the first step) into a covariance matrix, which is then decomposed into its corresponding eigenvectors and eigenvalues (Randen et al., 2000). The chaos attribute will not only enhance faults but also chaotic texture within the seismic (Randen et al., 2000). Therefore, since the vertical offsets of the faults in this study were incredibly subtle, the Variance attribute was much more useful for discontinuity detection in this data set than Chaos. The Variance attribute measures the signal unconformity using the local variance and is used to isolate discontinuities in the horizontal continuity of amplitudes (Randen et al., 2000). The variance of a slice within an unbroken reflection layer is small, whereas faults cause amplitude changes and this results in a larger variance (Randen et al., 2000). After extracting the variance attribute volume from the data set, it was used as an input attribute to generate the Ant tracking volume. Predefined "artificial ants" are placed as seeds on a seismic discontinuity volume to track and capture seismic discontinuities. Ant tracking allows the user to define six different parameters that determine how intelligent agents, "artificial ants", will behave in order to capture the events/discontinuities in seismic data. These parameters are also used to discriminate between more regional events, such as

large faults, and small scale (local) events, such as fractures. The initial ant boundary (number of voxels) defines the initial distribution of agents by putting a territorial radius around each agent; therefore, no agent is placed within the radius of another agent. For extracting large regional faults, the distribution can be coarse, such as 5-7 voxels; for detailed work and the mapping of small faults and fractures (sweet spots), the distribution can be set to 3-4 voxels. As a first step in the ant-track algorithm, each agent makes an initial estimate of the orientation for the identified local maximum within the agent's territory. The ant-track deviation (number of voxels) controls the maximum allowed deviation of each agent from a local maximum as it tracks. Each ant agent is restricted to a maximum of 15% deviation from the initial orientation. The method allows the agent to accept a local maximum of one voxel on either side of the predicted position as legal. If the maximum is outside this ant track step range, the track deviation parameter comes into play. For instance, a value of one would allow the agent to deviate by one voxel in either direction from the legal positions to search for a local maximum. If a maximum is not found, that step is recorded as an illegal step. The ant step size (number of voxels) defines the number of voxels an ant agent advances for each increment within its searching step. Increasing this value allows an ant agent to search further, but it lowers the resolution of results. The illegal steps allowed (number of voxels) parameter defines how far an agent's track can continue without finding an acceptable edge value (a local maximum). The legal steps required (number of voxels) parameter controls how "connected" a detected edge must be to help distinguish an edge from un-oriented noise. It is also expressed as the number of steps that must contain a valid edge value for the agent to continue. Illegal steps allowed and legal steps required are used in combination

with each other. For instance, if "Illegal Steps Allowed" is set to 1, that agent is only allowed to do one illegal step without finding a local maximum. Likewise, as the agent advances and encounters a valid edge, this means one legal step. If the ant advances again and finds another valid edge, this is considered second legal step. If "Legal Steps Required" is set to 2, the track is considered legitimate and recorded. If the parameter is set to 3, and on the next advance of the agent an edge is not encountered, this track will not be considered legitimate and will not be recorded. Illegal steps are only counted after legal steps have been recorded. The stop criteria refer to the percentage of illegal steps allowed throughout a single agent's life. When the accumulation of illegal steps becomes a significant portion of the agent's search area (when this value becomes too large), the search can no longer be considered legitimate fault geometry based on the stop criteria set by the user, and therefore the track is terminated (Petrel workflow tools, 2015).The Variance cube derived from the conditioned seismic volume was used to derive the final Ant Track volume. In order to be able to detect subtle discontinuities in this data set, "Aggressive Ants" mode was used with its default parameters to generate an Ant track volume. The time slices at the Bakken and Winnipeg level were extracted from the Variance volume and the Ant track volume to interpret faults.

No checkshot data was available. Therefore, in in order to continue with the interpretation of the data set, a synthetic seismogram was generated to tie the Formation tops from the well data to the seismic data. The wavelet extracted from the data set showed that the original amplitude volume is out of phase by $+32.3^0$ (Figure 4.7). Seismic data are usually processed to be zero-phase. Hence, mostly, a simple zero phase wavelet is used as input with sonic and density logs to generate the synthetic seismogram.

But, since, the seismic data used here is out of phase by +32.3^{o}, the extracted wavelet

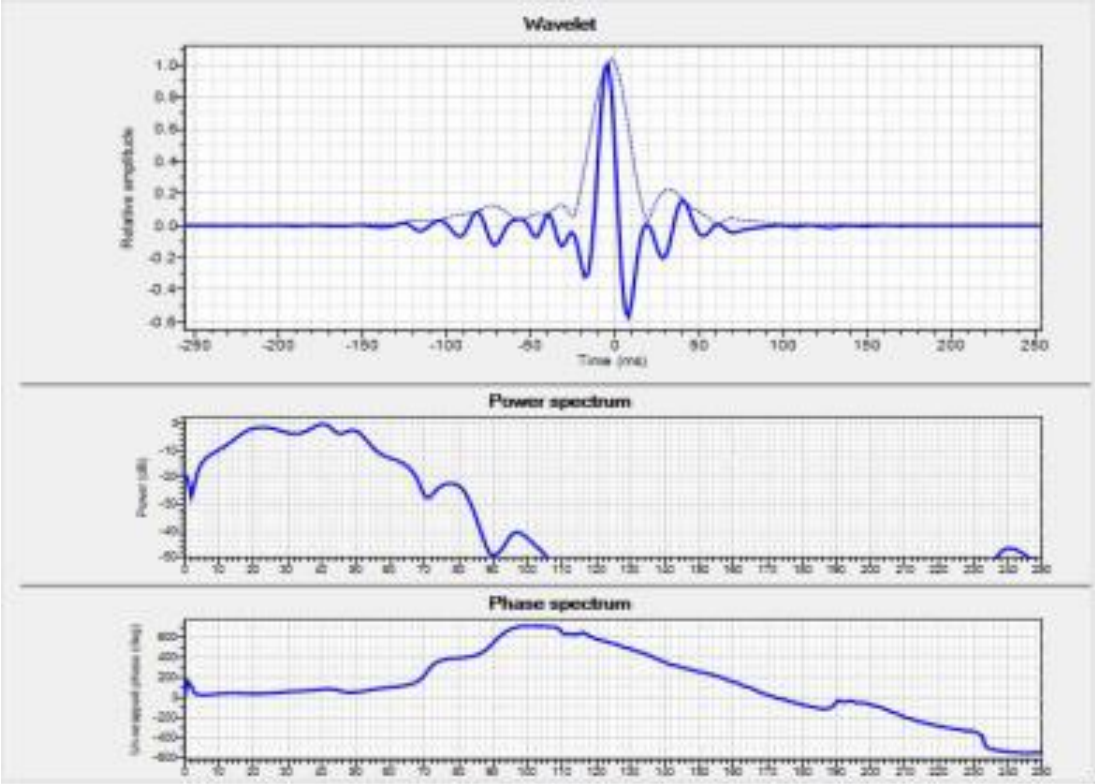

Figure 4.7 The extracted wavelet from the 3D seismic data is shown here (Petrel, 2015). This wavelet was indicated to be +32.3^{o} out of phase.

(called as Extended White) is used with the sonic and density logs to generate the synthetic seismogram shown in Figure 4.8. To confirm the accuracy of the results obtained from the synthetic seismogram, this study used a correlation of the two way times of the major unconformities obtained from the results of the synthetic seismogram with the two way times of the major unconformities obtained from the Reflection strength attribute volume (Figure 4.9). Reflection Strength has a low frequency appearance and has only positive amplitudes. It is mainly used in picking sequence boundaries, unconformities or major changes in depositional environments

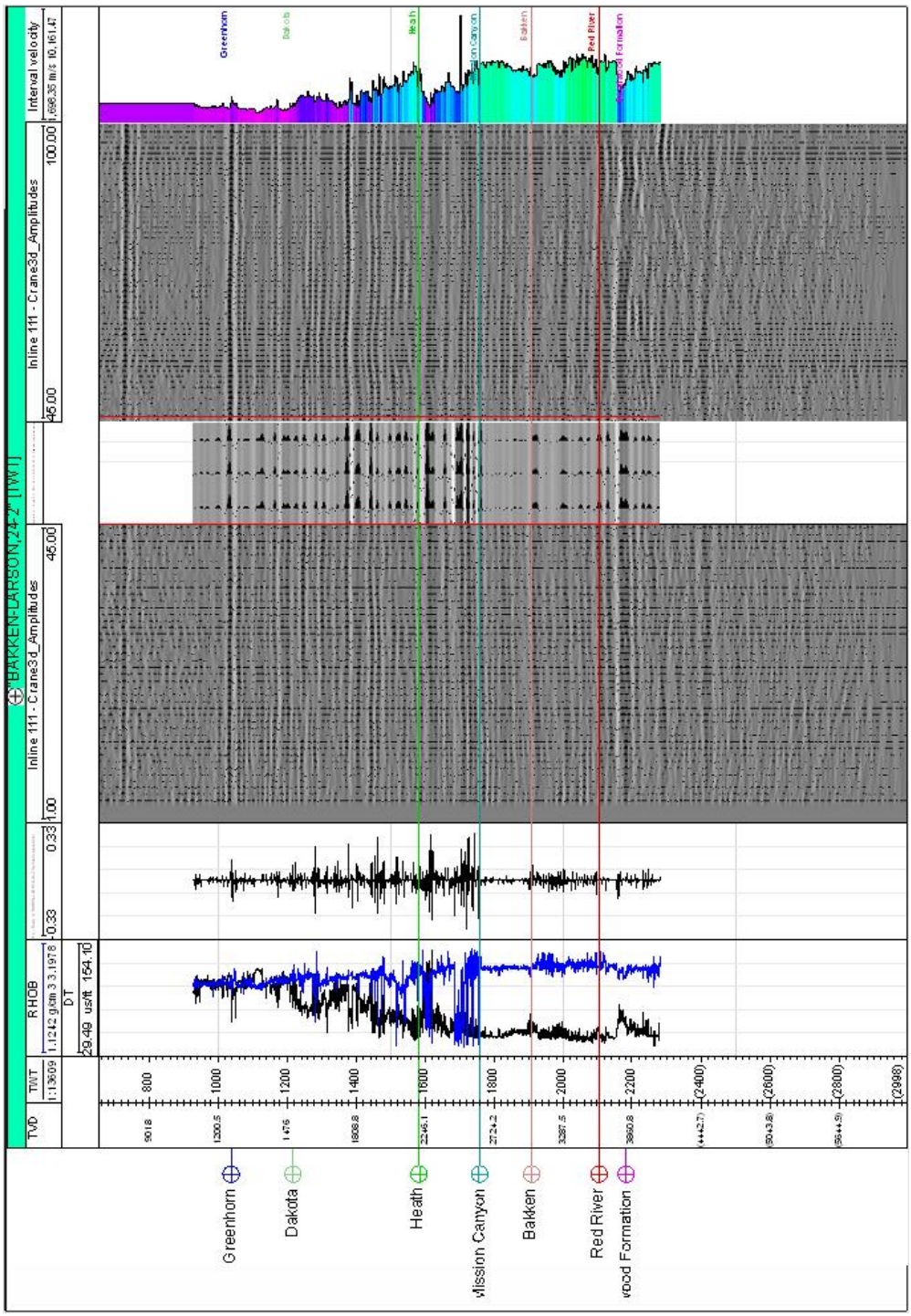

Figure 4.8 The synthetic seismogram generated using the density and sonic logs from Bakken Larsson 24-2 and the extracted wavelet (Fig. 4.7). This is the final result obtained by matching the amplitudes in the generated seismogram and seismic data (Petrel, 2015).

(Subrahmanyam and Rao, 2008). The higher values of the attribute denote the major unconformities in the dataset (Figure 4.9).

The two way time of all key horizons was derived from the seismic-well tie process as outlined above. The top of the Bakken Formation and the top of the Winnipeg Formation were selected and picked within the seismic survey. To ensure maximum confidence in the horizon interpretations, these horizons were traced using manual, 2D and 3D auto tracking techniques in combination.

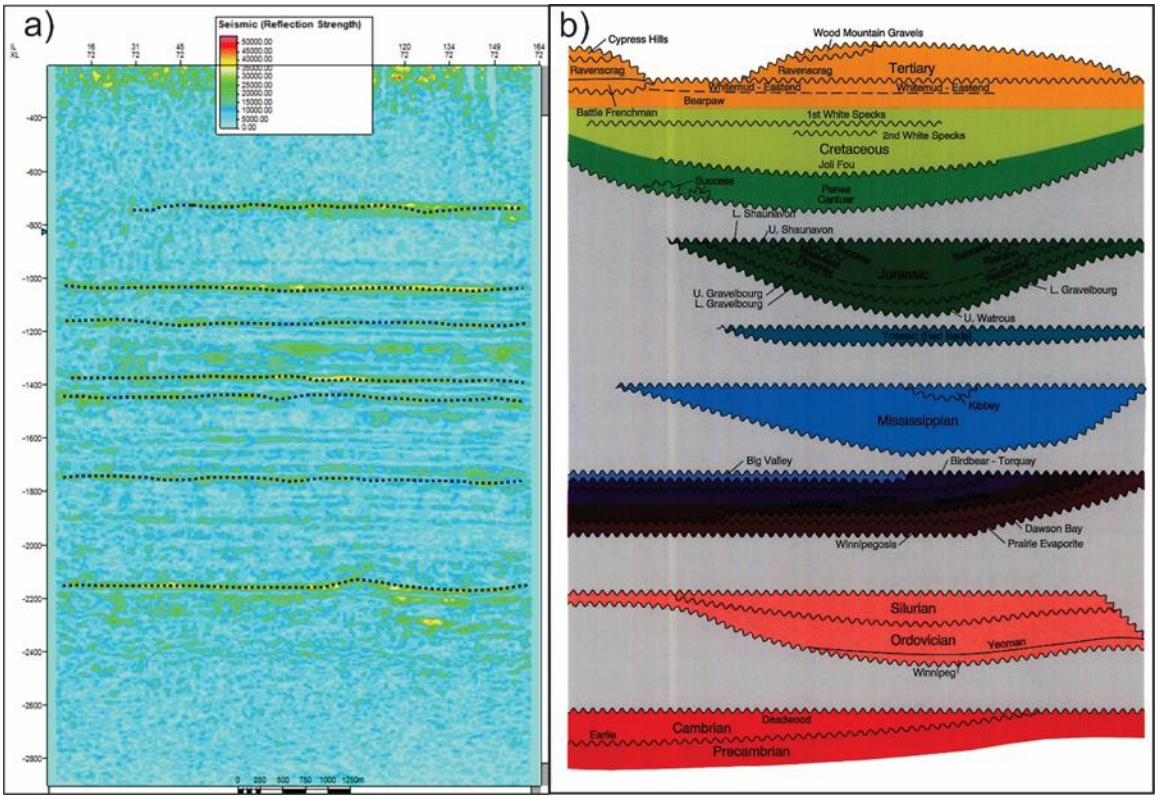

Figure 4.9 a) Seismic cross section from the Reflection Strength attribute volume. The green and yellow signal denote higher values of the attribute, which are interpreted as major unconformities in the data set (marked with dotted black lines). b) Generalized cross-section showing the major unconformities in the Williston basin and their distribution in geologic time (Anna, 2013).

4.2 Data Acquisition from Outcrop Analog

The structural model derived from the interpretation of the seismic data helped creating a conceptual fracture model with fracture orientations. But in order to get an idea of the fracture density characteristics in the Bakken Formation, the fracture network characteristics in an analog outcrop were investigated. A Field study was conducted at the Shell Canyon in the Bighorn Mountains, Wyoming (Figure 4.9). Fractures were measured in the Cottonwood Canyon Formation and the Madison group. The Cottonwood Canyon Formation is a lateral equivalent of the Bakken Formation with finer shaly upper and lower members and a coarser silty middle member (Sonnenberg and Pramudito, 2009). The fracture measurements included the orientation data and the density data. In addition, a Schmidt hammer was used to measure the elastic properties of the different members of the Cottonwood Canyon Formation for comparison with the values available for the Bakken Formation in literature. To generate a fracture model for the middle member of the Bakken Formation, it was assumed that the fracture density for the different fracture sets in the middle member of the Bakken Formation derived from the structural model was equal to the average fracture density obtained from the analog field outcrop of the Cottonwood Canyon Formation.

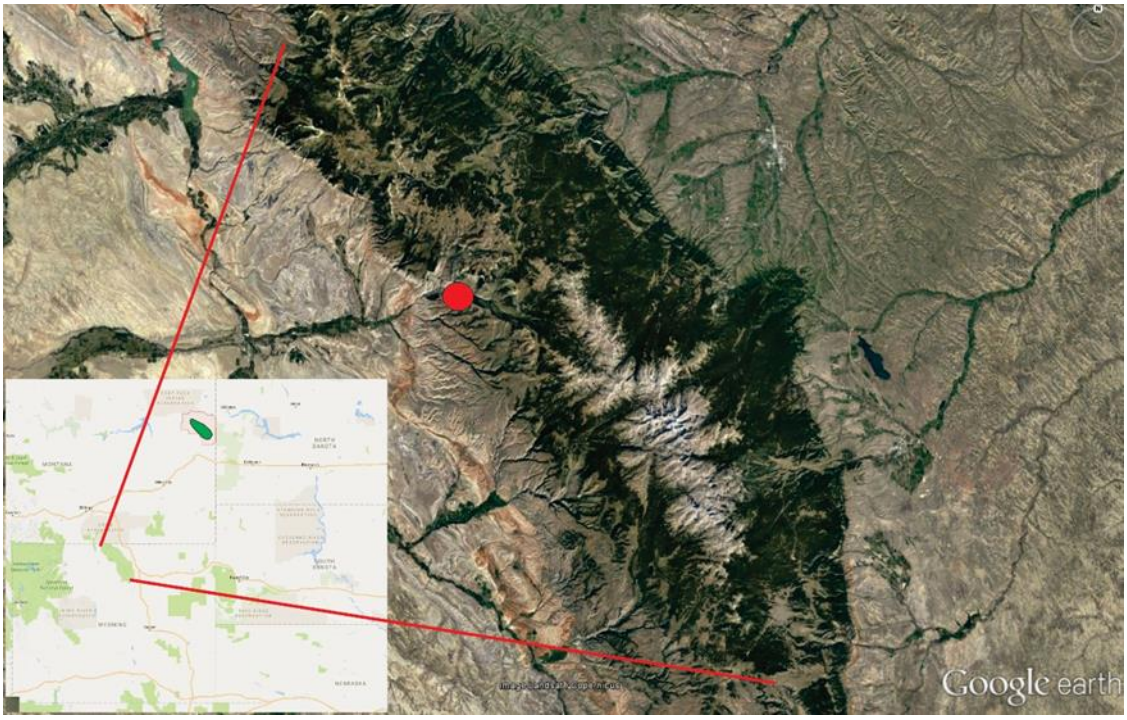

Figure 4.7 The figure shows the location of the analog outcrop in the Shell Canyon of the Bighorn Mountains in Wyoming. The dark green shaded blob in the inset map shows the location of the Elm Coulee Field in the Richland County, Montana (Google Earth).

CHAPTER 5
RESULTS

5.1 Description of the time structure maps and fault picks

The time structure maps of the Top Winnipeg Formation and Top Bakken Formation show isolated domal structures with four-way closure at both intervals (Figure 5.1a) and b)). The dome in the central portion of the seismic data set is the main focus of the study. The structural high in the western portion of the data set is a bigger dome (running parallel to the central dome), which is covered partially by the 3D seismic data set. In addition, there is a smaller dome to the north east of the central dome. Each domal structure seems to be widening laterally when traced from the Winnipeg Formation to the Bakken Formation. The central dome structure at the Top Winnipeg Formation is approximately 2500m wide in the northeast direction and 1300m wide in the northwest direction. It is approximately 400m wider along northeast and 250m wider along the northwest at the Top Bakken Formation. Contrary to this, the amplitude of the dome is lower at the top Bakken Formation compared to its amplitude at the top Winnipeg Formation. The dome structures are asymmetric and sigmoidal in shape. The investigation of the seismic sections cutting the central dome revealed a deformation zone with several faults below the dome. These faults are subtle vertical offset thrust faults rooted deep in the basement and form a positive flower structure. The time structure map of the Top Bakken Formation and Top Winnipeg Formation shows evidence of strike slip movement and rotation (Figure 5.1a) and b)).

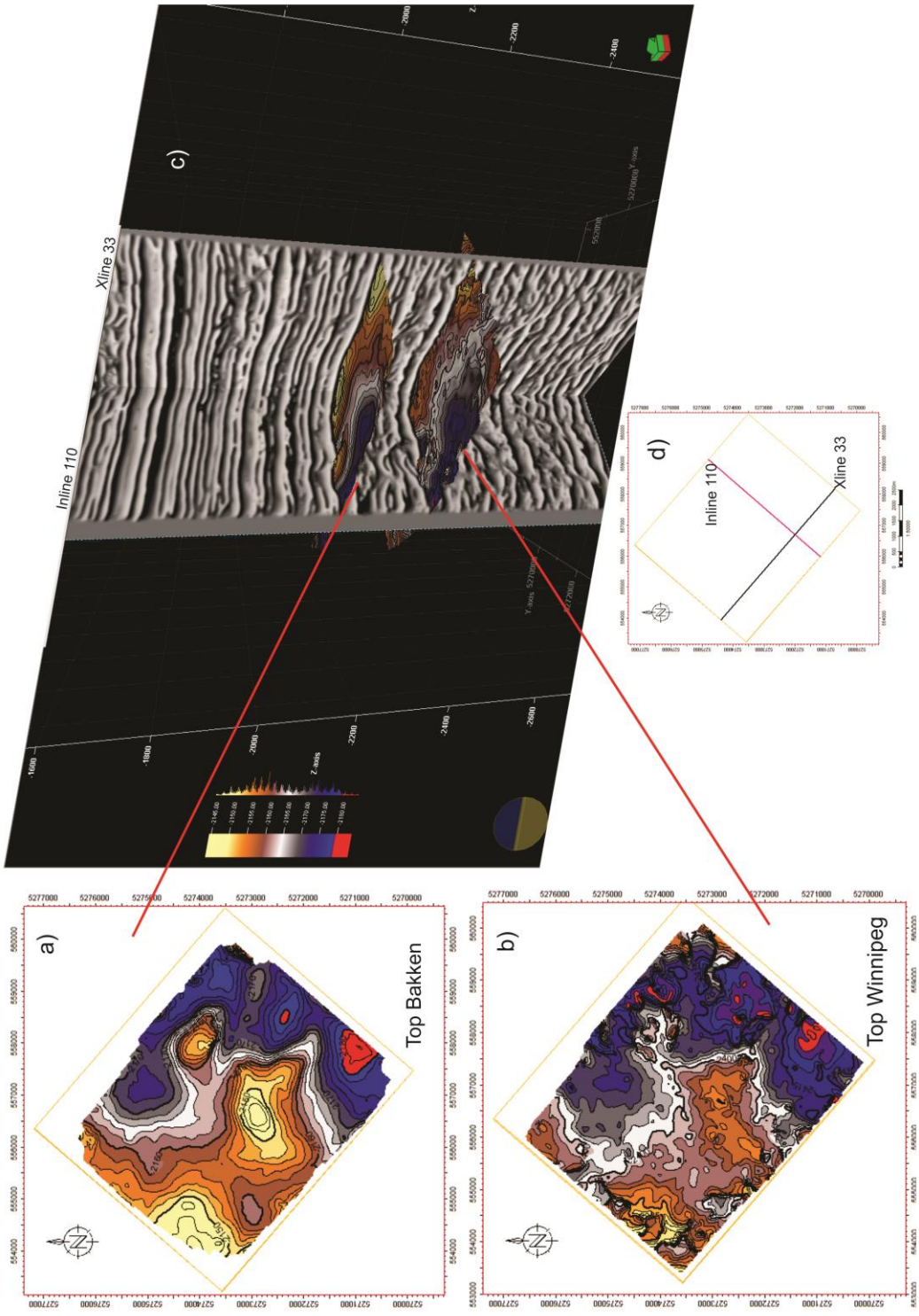

Figure 5.1 a) The time structure map of the Top Bakken is shown with warmer colors showing higher positive relief. b) The time structure map of the Top Winnipeg c) A 3D view showing the interpreted Top Bakken and Top Winnipeg. The location of the Inline and Crossline is shown in d)

5.2 Interpretation of the fault network

Since these subtle vertical offset strike slip faults were difficult to interpret in 3D without avoiding a subjective bias, a model driven approach is used to fully interpret the fault network. The central dome structure in this data set, which is the focus of this study is very similar to the pop-up structure produced by the experiment W309 in the scaled sandbox modeling study of restraining stepovers in strike-slip fault systems by McClay and Banora 2001 (Figure 5.2). This pop-up structure formed over a 150^{o} overlapping restraining stepover. The strongly sigmoidal pop-up structure is bounded by curved, oblique-slip reverse faults formed above the basement stepover (McClay and Banora, 2001). In addition, there are small displacement dextral and left lateral shears in the central regions of the pop-up structure. Also, the cross sections of the pop-up structure show a distinct asymmetry, which switches across the center of the basement stepover (McClay and Banora, 2001; Figure 5.2a)).

In the southwestern part of the pop-up structure (central dome structure), the pop-up is bounded by two oblique slip reverse faults (Figure 5.3). In addition, it can be seen in the seismic section that the southeastern part of the basement is less deformed than the northwestern part. This is similar to the cross section-45 from the analog model shown in in Figure 5.3. The bounding reverse faults are dominantly convex up. The reverse faults are rooted to a master fault deep in the basement. In the central part, the pop-up structure is symmetric (Figure 5.4). It is bounded by the same master reverse faults and there are four more oblique slip faults, which form a positive flower structure. This is similar to the cross section-32 from the analog model shown in the Figure 5.4. It can be seen that the zone of deformation is switching towards the southeast as we move to the northeastern

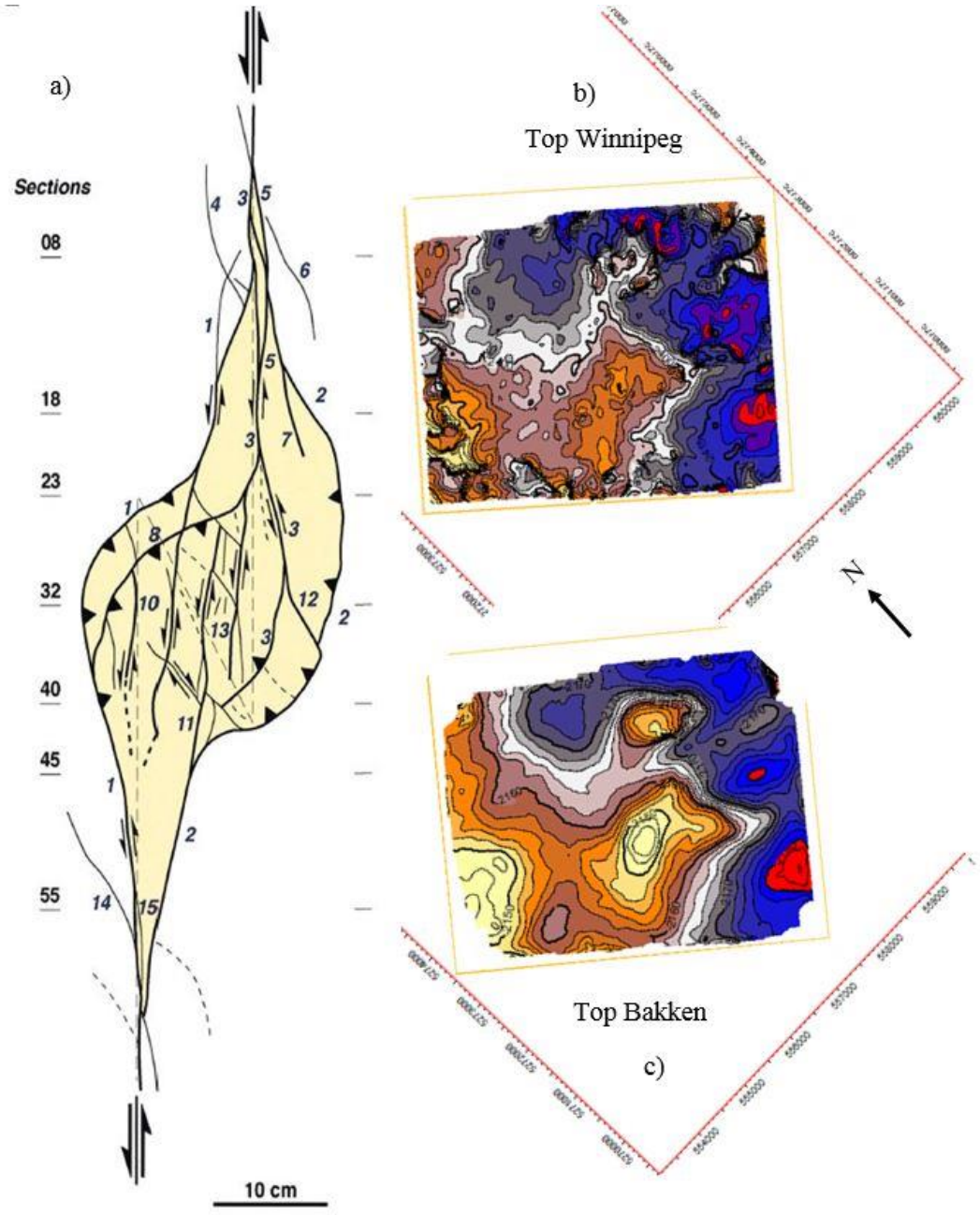

Figure 5.2 a) a line diagram of the surface of experiment W309 after 10 cm left lateral strike-slip displacement on the basement fault system (McClay and Banora, 2001). b) The time structure map of the Top Winnipeg. c) The time structure map of the Top Bakken.

parts of the pop up structure. The southeastern part is more deformed than the northwestern part as compared to the Figure 5.3.

At the northeastern end of the pop-up structure, it is still bounded by the same master oblique slip reverse faults shown in yellow and red (Figure 5.5). The pop-up has switches in asymmetry. The northwestern part of the seismic section is considerably less deformed than the southeastern part. This is similar to cross section 18 from the analog model shown in Figure 5.5. Using the model driven approach, the wrench faults were traced in 3D. The 3D fault model is shown in Figure 5.6. The faults are traced up to the Top Bakken Formation but these possibly extend above the Top Bakken Formation as well. The diverging nature of this wrench fault system can be seen in the 3D fault model (Figure 5.6 b).

The interpreted fault network is shown in Figure 5.7 on the time structure map of the Top Winnipeg Formation. The pop-up structure is bounded by two master oblique slip reverse faults shown in red and yellow. There is also a minor oblique slip reverse fault shown in green, which joins the western master fault. In addition, three left lateral strike slip faults are interpreted shown in blue, magenta and orange in the Figure 5.7. Based on the analog model, it is interpreted that this pop-up structure is a result of an obtuse angle restraining left lateral stepover in the basement (Figure 5.7). Episodic reactivation of these faults throughout the Phanerozoic leads to the evolution of the pop-up structure seen in the study area today. In addition, the results from the Ant Tracking are shown in Figure 5.8. The discontinuities are shown by shades of grey-black on the Top Bakken Formation. The implementation of aggressive parameters while extracting the Ant Track volume will detect comparatively more subtle discontinuities along with larger discontinuities as well (Figure 5.8 a)). However, the passive parameters will only extract larger discontinuities (Figure 5.8 b)). The values of the Ant track are extracted on the Top Bakken Formation

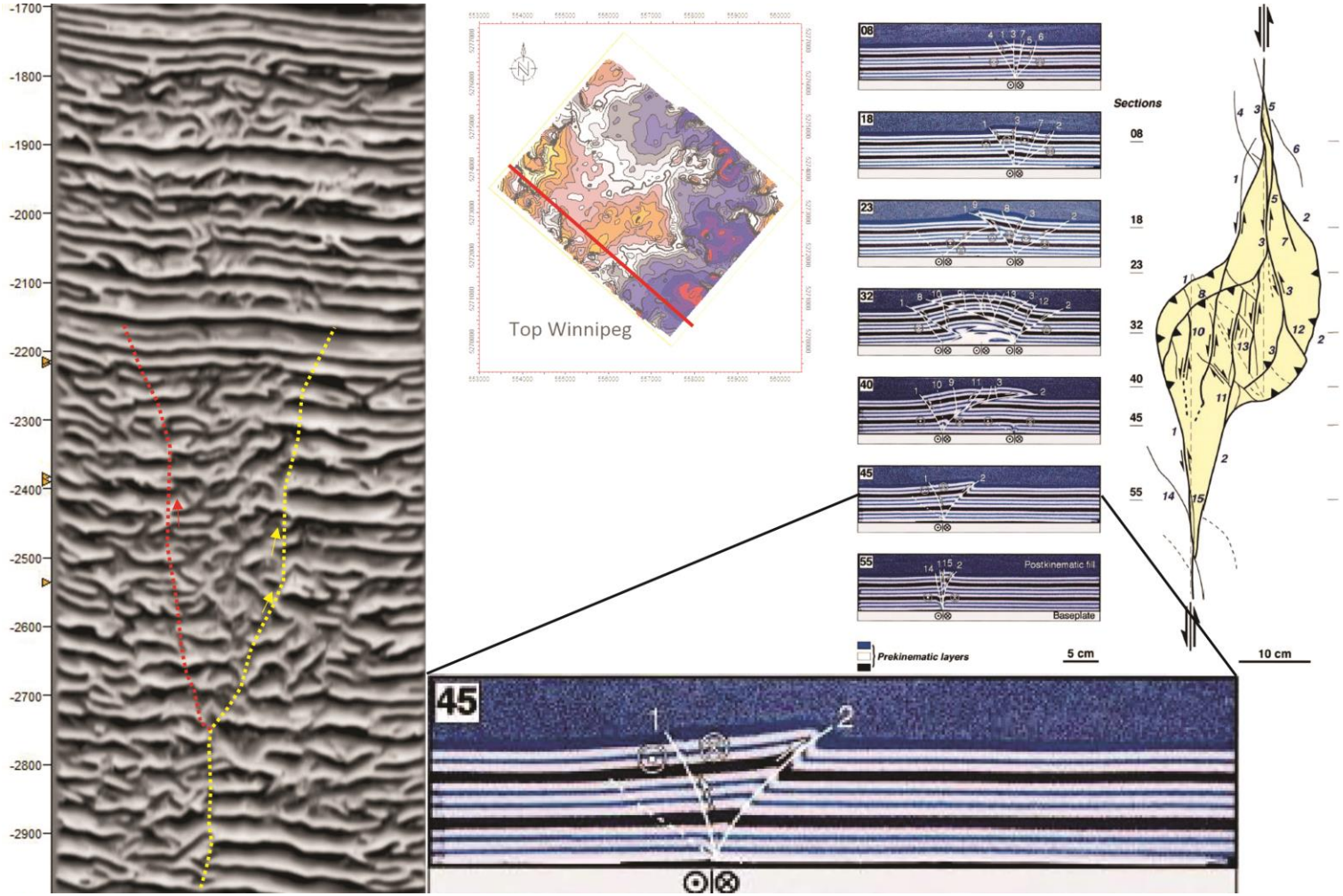

Figure 5.3 The seismic section cutting the southwestern part of the central pop up structure is shown with interpreted bounding reverse faults shown in red and yellow. Location shown with red line. The cross-section from the analog model is shown for comparison (McClay and Banora, 2001). Vertical Exaggeration =7.5

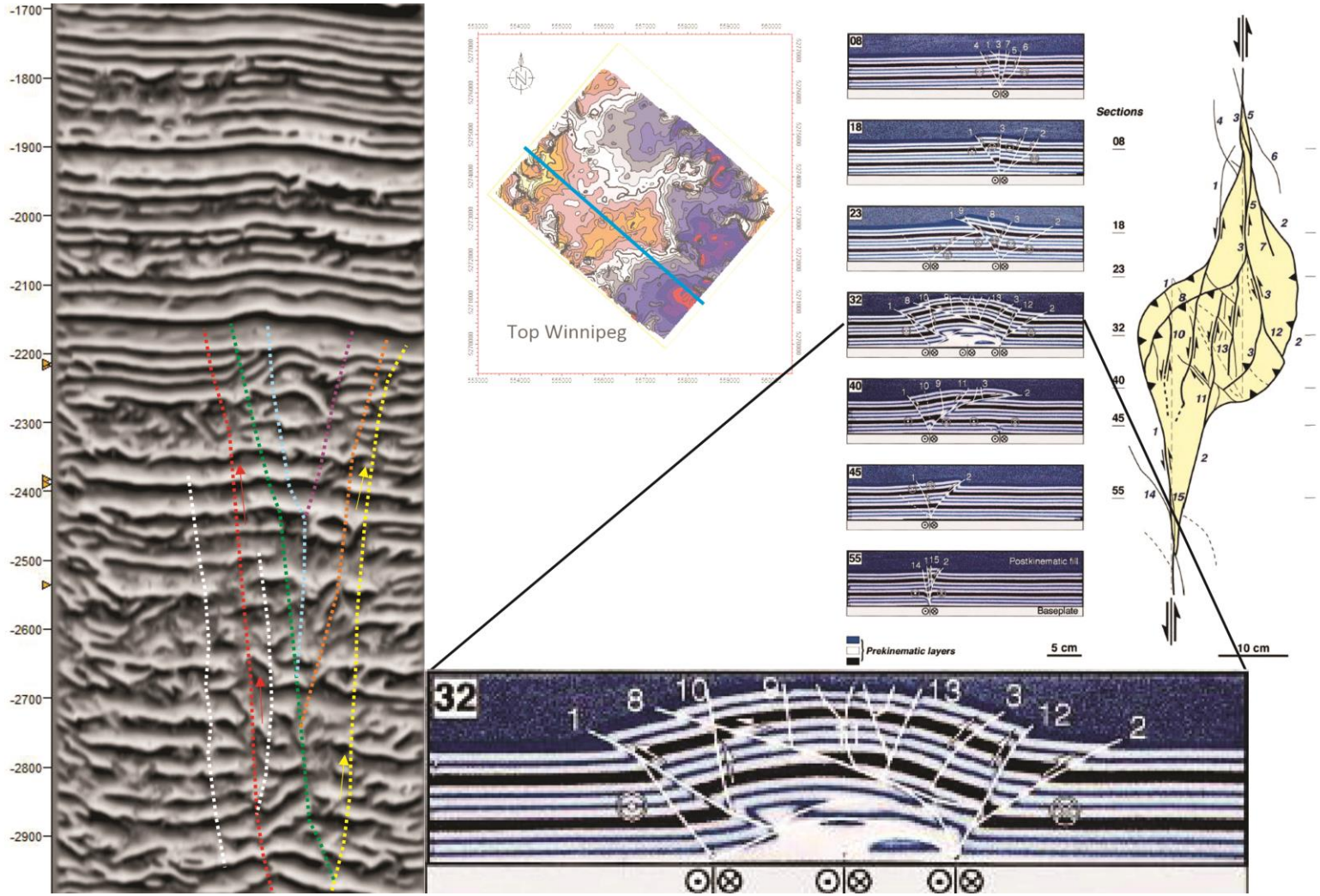

Figure 5.4. The seismic section cutting the central part of the central pop up structure is shown with interpreted bounding reverse faults shown in red and yellow. In addition, the other oblique slip faults are shown in green, orange, blue and maroon color on the seismic section. The cross-section from the analog model is shown for comparison (McClay and Banora, 2001).

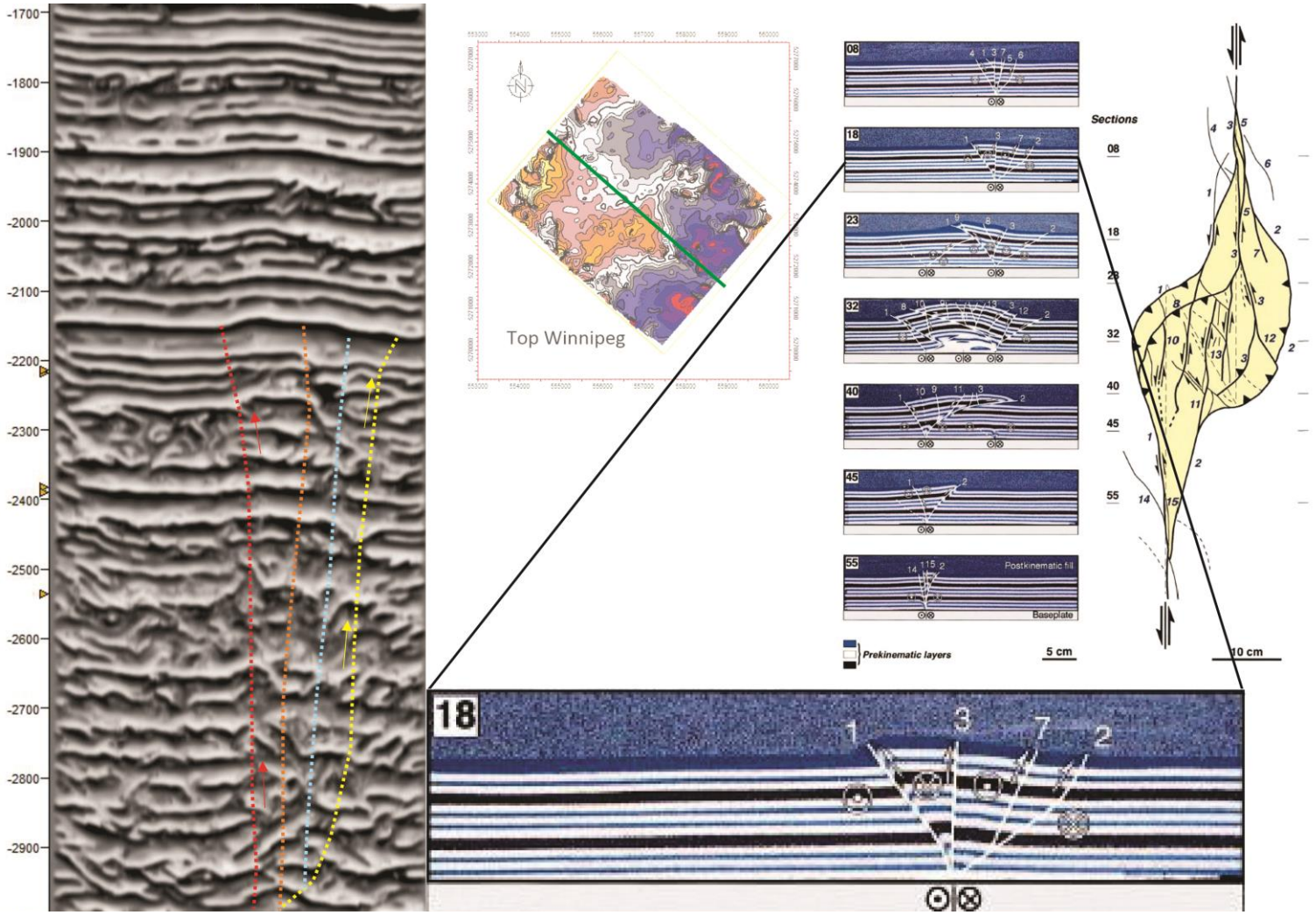

Figure 5.5. The seismic section cutting the northeastern part of the central pop up structure is shown with interpreted bounding reverse faults shown in red and yellow. In addition, the other oblique slip faults are shown in orange, and blue color on the seismic section. The cross-section from the analog model is shown for comparison (McClay and Banora, 2001).

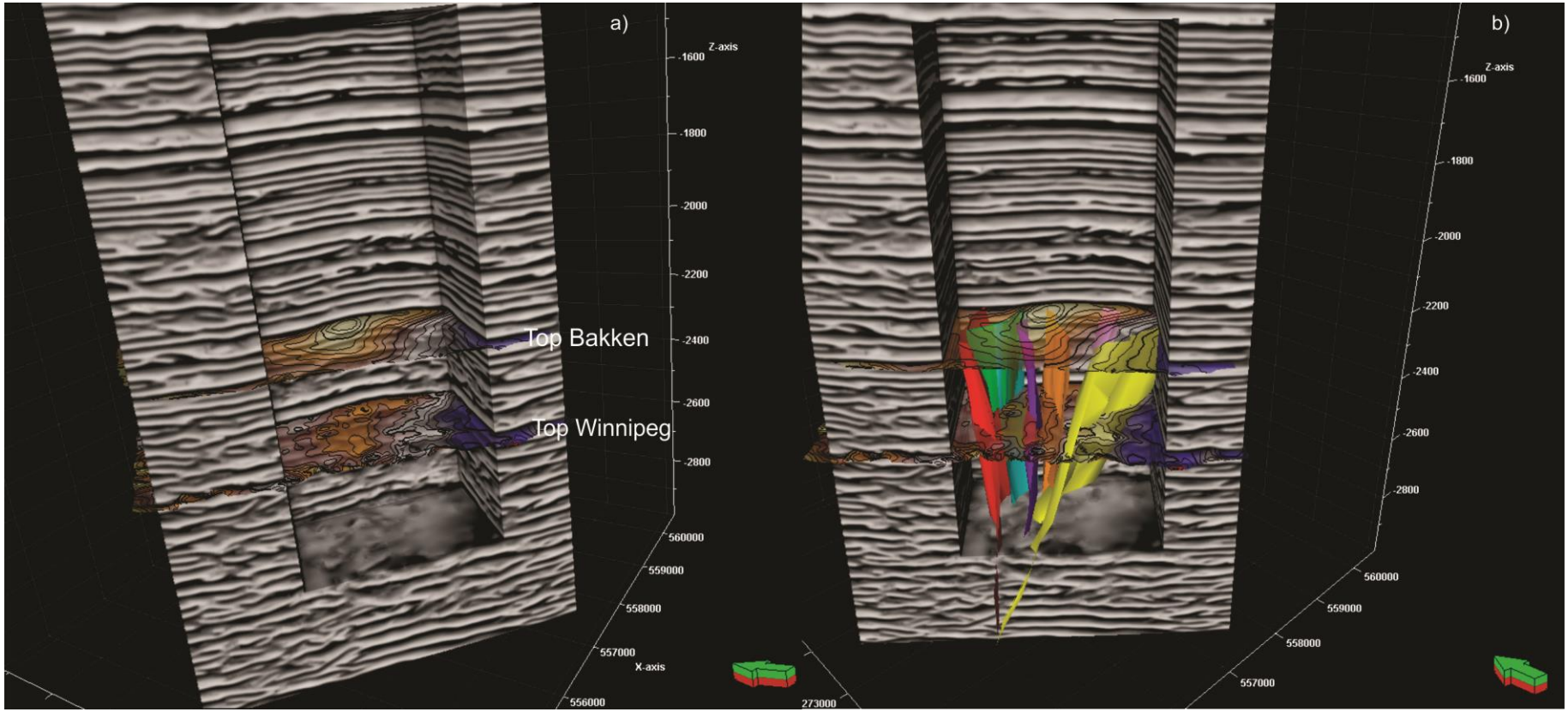

Figure 5.6 a) The un-interpreted 3D conditioned volume with the interpreted 3D surfaces (here 50% transparent): Top Bakken and Top Winnipeg. b) The 3D fault model. Faults are only interpreted up to the Top Bakken Formation. Note the diverging nature of the faults.

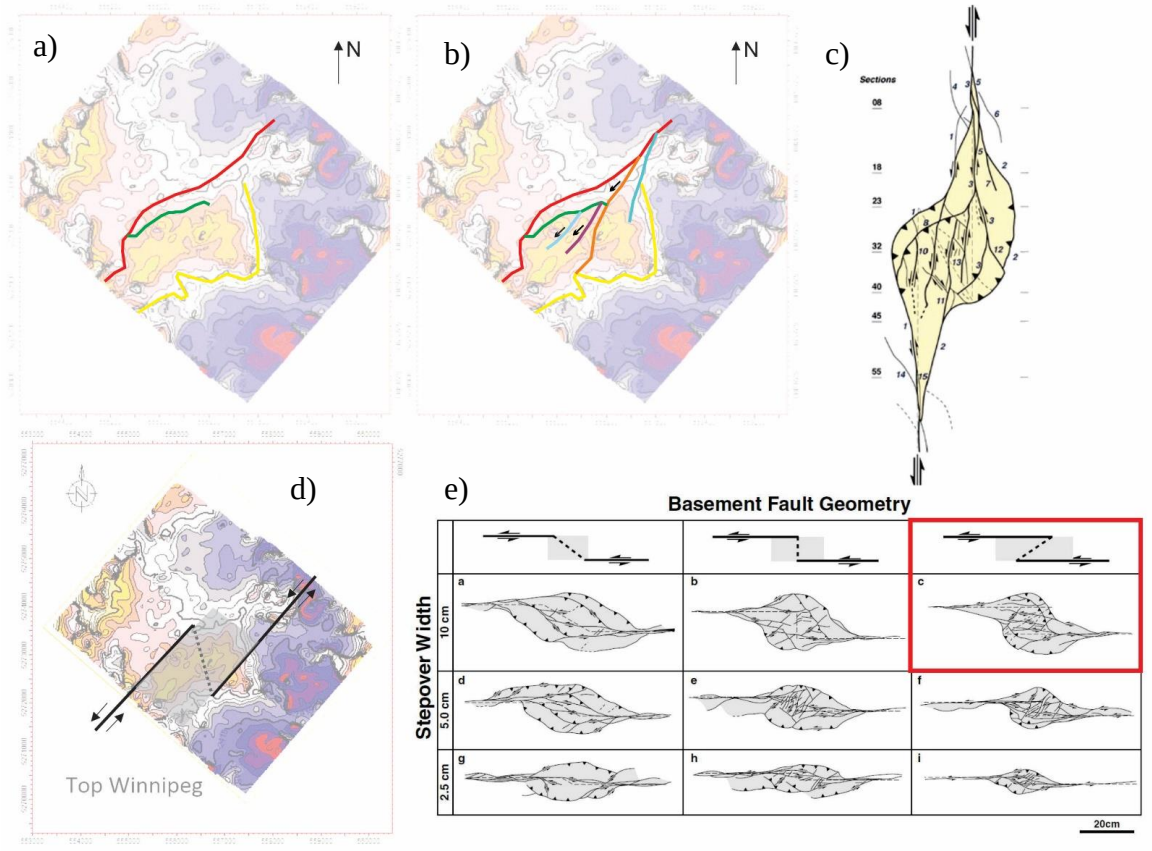

Figure 5.7 a) The major bounding thrust faults are shown with red, yellow and green color. b) The oblique slip left lateral strike slip faults are shown in blue, maroon and orange color. c) The analog pop-up structure from McClay and Banora, 2001 is shown here for comparison. d) The interpreted basement fault stepover geometry prior to the evolution of the central pop-up structure. e) Summary of the results from the McClay and Banora, 2001 for varying stepover width and basement fault geometry.

instead of a time slice to get more accurate results. This is because the Top Bakken Formation has relief across the surface but a time slice has no relief at all. The extraction is carried out using a technique called Horizon probe in Petrel 2015. The interpreted wrench fault system is overlaid onto the aggressive Ant Track Top Bakken Formation surface (Figure 5.8 c)). The Ant Track does show a lot of detected discontinuities when used with aggressive parameter. These discontinuities can't be traced in 3 dimensions

using the seismic data or the Ant Track volume. Therefore, it is suggested that most of

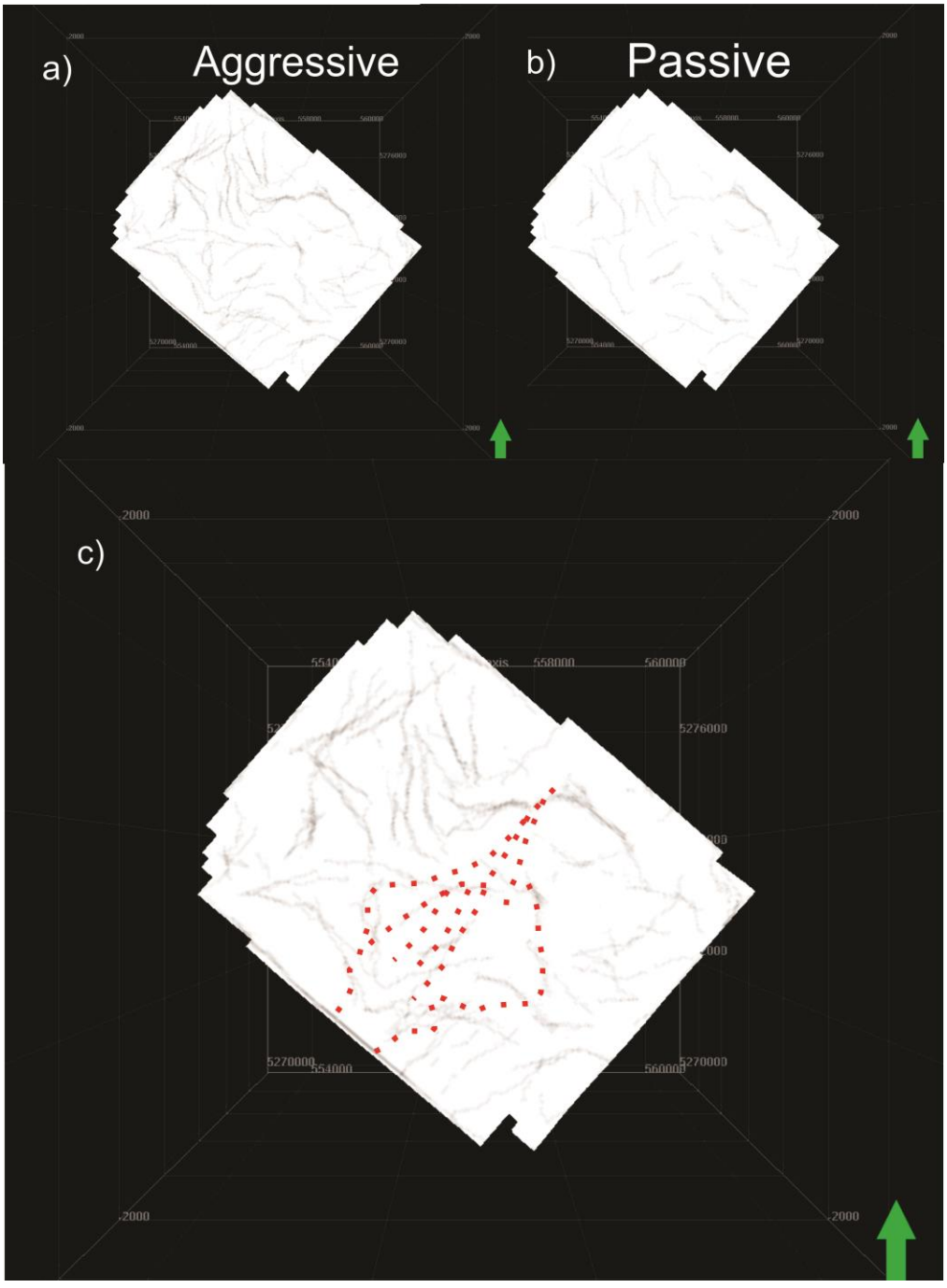

Figure 5.8 a) and b) Top Bakken Formation extracted from 3D Ant Track volume generated using aggressive parameters and passive parameters respectively. c) The faults interpreted from the seismic are shown by dotted red lines and is overlain onto a).

these discontinuities detected by the Ant Track are noises related to the low resolution of the data set. In addition, it can be seen that Ant Track (Aggressive) does detect segments of the interpreted wrench fault system. But it is not possible to make interpretations solely on the basis of the Ant Tracking since the vertical offsets along a single fault might change along its length and become lesser than the seismic resolution. Therefore, making it impossible to be traced in seismic. Therefore, a model driven approach is necessary to interpret such fault systems in 3D seismic data.

5.3 Conceptual Fracture Model

The localized stresses exert a much greater control on the fracture network characteristics than the far field regional stresses. The structural model was used to derive the conceptual 3D fracture model (Figure 5.9 a)). A cartoon of the Bakken formation with the interpreted faults is shown. The fracture planes in the cross section are shown with red. The fracture orientations within the pop-up structure are shown, on the contact of the upper shale member and middle member of the Bakken Formation, with red and green lines (Figure 5.9 a)). An oblique slip reverse fault leads to extension perpendicular to the trend of the fault and oblique to the trend of the fault. Hence, a northeast left lateral oblique slip fault will generate extension fractures in northeast direction and north northwest direction (Figure 5.9 b), a), and c)). In addition, the density of fractures will be considerably higher closer to the intersection of two faults due to increased local stresses.

The conceptual 2D fracture model is shown with the interpreted faults in Figure 5.9 c).

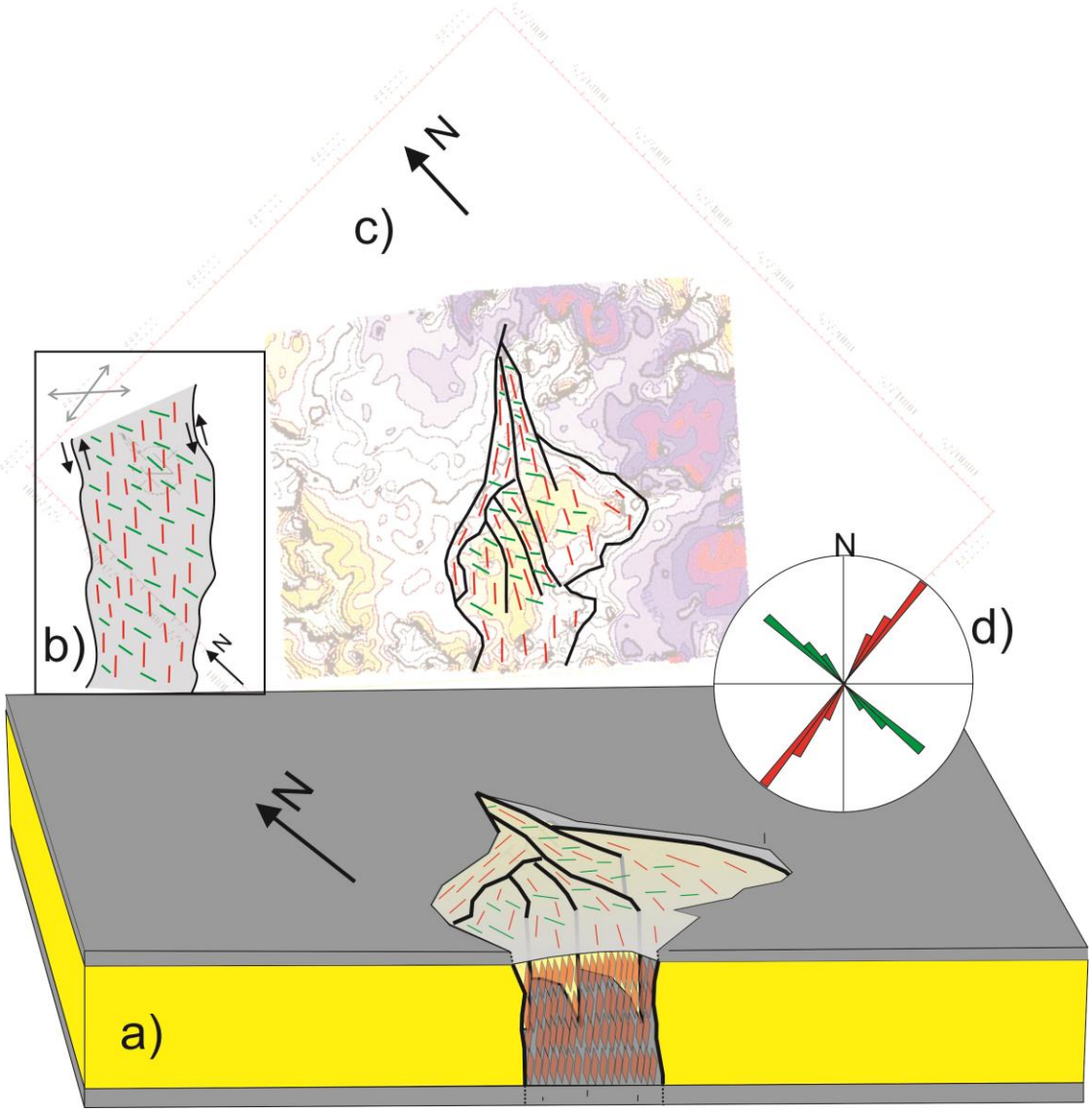

Figure 5.9 a) The conceptual 3D fracture model. The layers in grey are the marine shale members and the layer in yellow is the middle member of the Bakken Formation. The fracture planes are shown with red in the cross section. Faults are shown with heavier black lines. b) An oblique slip left lateral strike slip system causes extension in the directions shown by grey arrows leading to fracture sets in two directions shown by green and red. c) The conceptual 2D fracture model shown on the time structure map with faults shown by black lines and fracture sets shown by red and green. d) A hypothesized approximate expected rose diagram of the fractures in the pop-up structure.

There are two prominent fracture orientations: NE-SW (shown in red) and NW-SE (shown in green) (Figure 5.9 d)).

The estimation of rock properties using seismic data and derived attributes has always been a very important task. There are several methods for achieving this goal, including Genetic Inversion. This method is used here to derive a 3 dimensional Density and Sonic Velocity volume, which contains the density and sonic velocity information of the rocks. In this technique, multi-layer neural networks as well as genetic algorithm are combined in order to provide a robust and straight forward seismic inversion. The time slice from the density cube and sonic velocity cube at the Top Bakken Formation shows lower density and higher P-sonic (μs/ft) around the pop-up structure (Figure 5.10 a) and b) respectively). This is indicative of higher porosity. The density time slice shows linear trends in lower density (Figure 5.10 c)), which are interpreted to be fracture networks (Figure 5.10 d)). The fracture trends traced on the Density time slice (Figure 5.10 e)) are very similar to the fracture trends obtained from the conceptual fracture model derived from the structural model (Figure 5.10 f) and Figure 5.9 d)). This is very reassuring.

The results from the analog field outcrop study were used to give approximate measurement of the fracture density in the middle member of the Bakken Formation at the study area. The Cottonwood Canyon Formation (Figure 5.11) outcrops in the Shell Canyon at the Bighorn Mountains, Wyoming. The middle member of the Cottonwood Canyon Formation (shaded in yellow, Figure 5.11) is heavily fractured by dominantly two roughly orthogonal fracture sets. There are three to four fracture sets are observed at the outcrop. For the purpose of measuring the average density of the fractures in the Cottonwood Canyon Formation, only two dominant fracture sets are used. The fracture

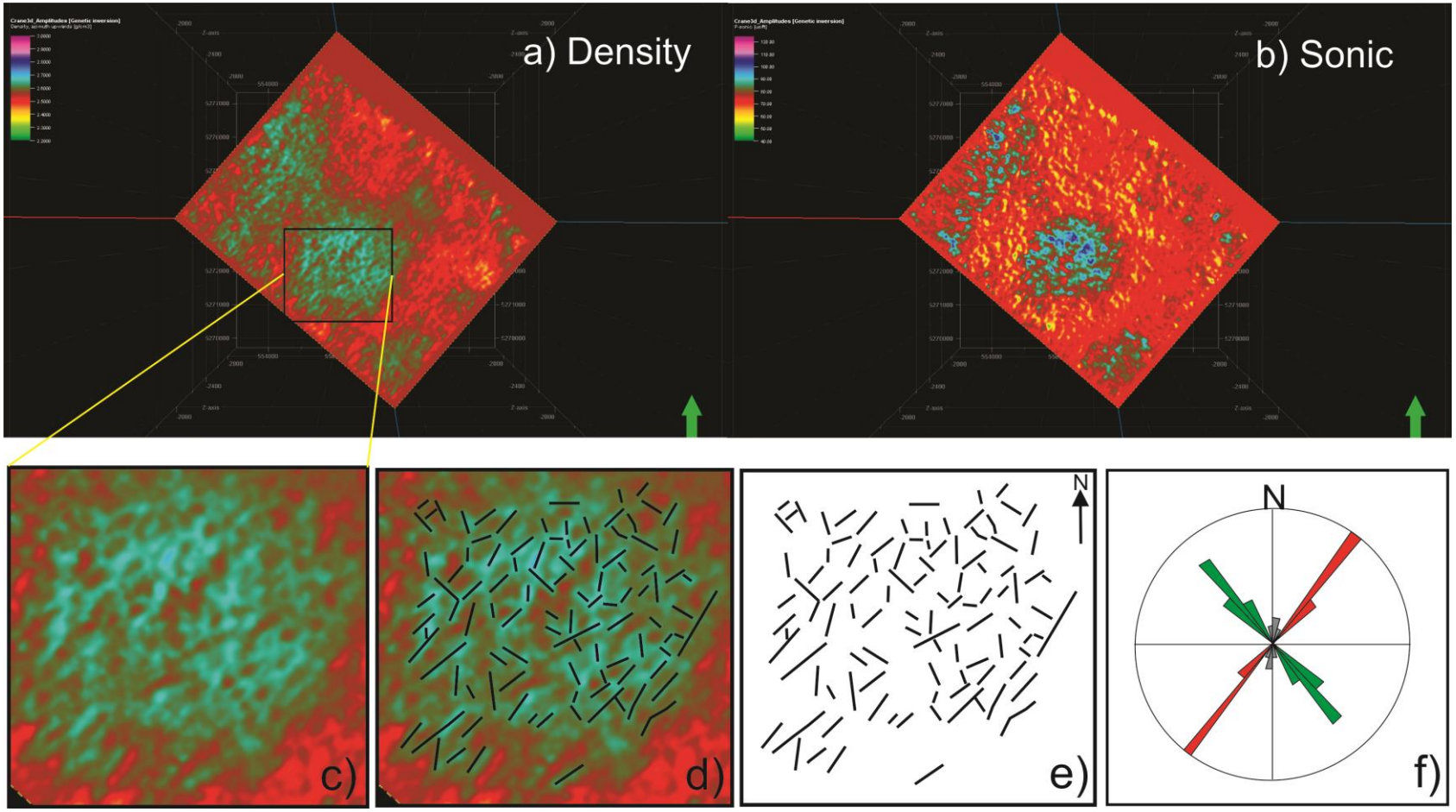

Figure 5.10 a) The Density time slice and b) The Sonic time slice at Top Bakken Formation. Lower density values are shown by green color and blue shows higher values of P-Sonic (µs/ft). c) A zoomed in snapshot of the lower density trends over the location of the pop-up structure d) Interpreted trends on the density time slice e) Interpreted fractures from the density trends f) Rose diagram for the fracture network in part e. rose diagram of the fractures shown in e).

sets used, trend North East (average N 55^0) and North West (N 308) as seen in the rose diagram in Figure 5.11. The fracture density in the middle member of the Cottonwood Formation was observed to be 22.8 fractures per meter. Very few fractures penetrated the overlying shale member of the Cottonwood Canyon Formation. The fracture density in the overlying Madison limestone (shaded in blue, Figure 5.11) was 2.3 fractures per meter.

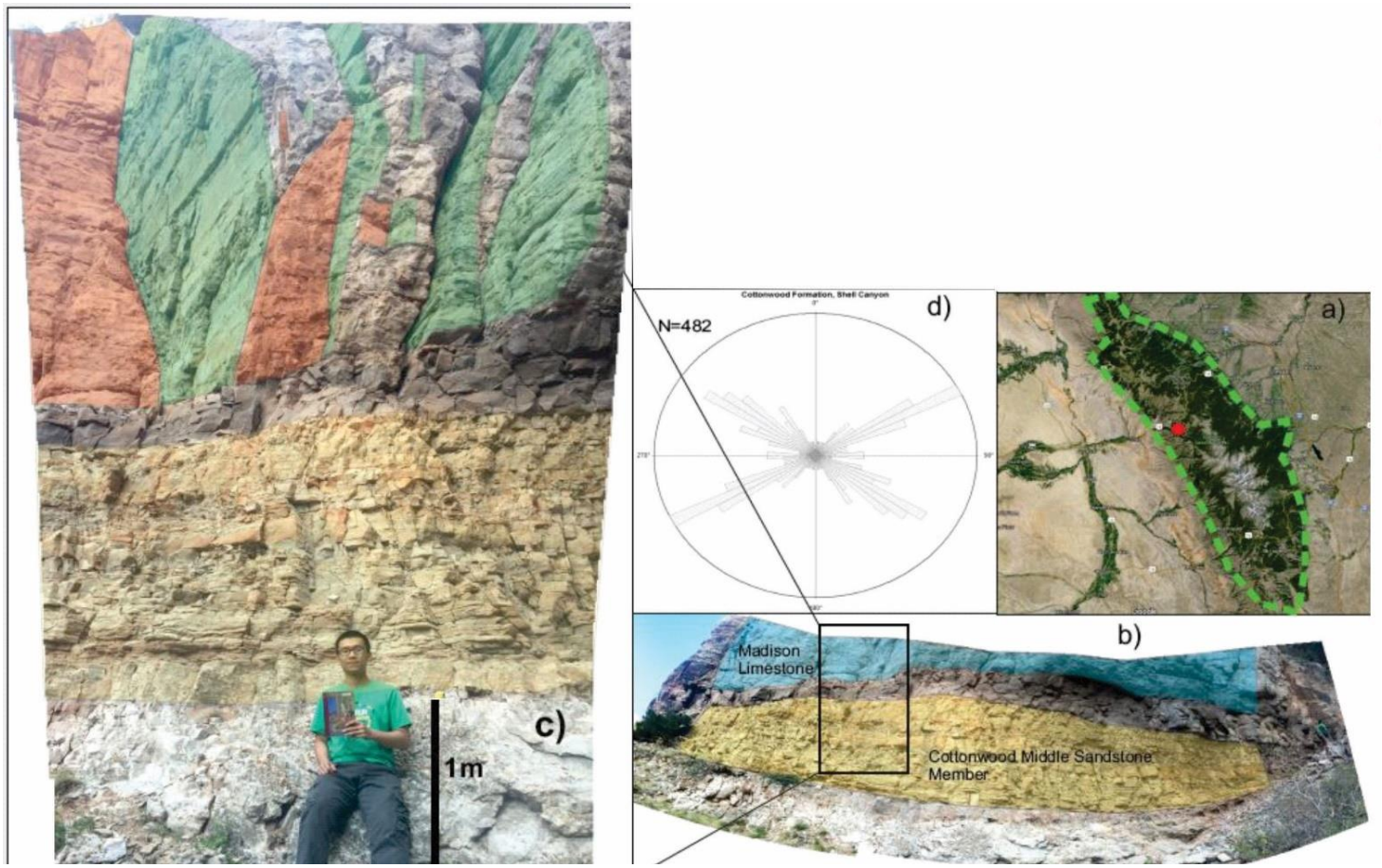

Figure 5.11 a) The location of the outcrop (Latitude: 44°34'25.32"N, and Longitude: 107°41'49.95"W) - Shell Canyon, Bighorn Mountains, Wyoming, US. b) a panoramic image of the outcrop with Cottonwood Canyon Formation shaded in yellow and the overlying Madison Limestone shaded in blue. c) A zoomed in portion from the panoramic image of the outcrop showing the fracture sets in the Cottonwood Canyon Formation. The big fractures in the overlying Madison Limestone are shaded in green and red. The fractures in thicker Madison Limestone are considerably larger and less dense than the fractures in thinner Cottonwood Canyon Formation. d) A rose diagram showing the fracture orientations of 482 measured fractures in the Cottonwood Canyon Formation.

CHAPTER 6
DISCUSSION

This study used a 3D seismic data set from the Crane Field to investigate the impact of structure on the fracture network characteristics in the middle member of the Bakken Formation. A workflow was used to improve the signal to noise ratio in the seismic data to facilitate accurate interpretation of the basement structure. Further investigation revealed the presence of a pop-up structure in the central portion overlying a zone of basement deformation. This zone of deformation was interpreted to be composed of a left lateral wrench faulting system based on a model-driven approach. In addition, the presence of this left lateral wrench fault network is interpreted to be related to a regional left lateral strike slip system – the Brockton Froid Fault Zone. The fracture network characteristics in the middle member of the Bakken Formation are directly related to the local stresses generated by the interpreted left lateral wrench fault system in the study. There are two fracture sets- NE-SW and NW-SE. The density of each fracture set is assumed to be equal to the average density of fractures in the analogous middle member of the Cottonwood Canyon Formation.

This study builds upon the recent works that investigated the structure of the Elm Coulee Field in order to explain the presence of anomalous sweet spots demonstrated by the EURs of horizontal wells in the area. A detailed three-dimensional mapping of the faults in the Elm Coulee Field has been lacking. Almanza (2011) used the sweet spots in the first year production data to derive a fracture model. In contrast, this study uses structural interpretations to explain the presence of the ovoid shape sweet spots. Honsberger (2013)

used surface mapping of lineaments at the Top Bakken Formation interval and Top Winnipeg Formation interval to interpret faults and loosely related the interpreted lineaments to a basement-driven northeast-oriented left lateral strike slip system. This study goes on further to map the structure and faults in 3 dimensions using a model driven approach, which reveals that the central pop-up structure evolved from an obtuse angle left lateral step over system in the basement. Additionally, this study establishes that the Ant tracking attribute volume does show some segments of the major faults, which were interpreted through the model driven approach but the interpretation of the fault system solely on the basis of the Ant Track attribute volume is impossible (Fig 5.8) as suggested in Eidsnes (2014).

A significant result of this thesis is to establish a workflow for 3D mapping of the subtle vertical offset wrench faults objectively in 3D seismic data. It is difficult to manually map wrench fault networks in 3D seismic due to very subtle vertical offsets and abrupt changes in the trend and dip of the fault over a short distance. Additionally, the conventional discontinuity detection attributes are unsuccessful in mapping such fault networks. The study demonstrates the importance of using model driven approach in mapping subtle vertical offset wrench faulting networks, which lead to formation of pop-up structures. This workflow can be used in mapping faults in other analogous oil fields in which the reservoirs show pop-up structures associated with a wrench fault system. Additionally, it can be used for mapping the wrench fault networks elsewhere in the Elm Coulee Field.

In addition, this study has used a workflow successfully for conditioning the 3D seismic data in order to increase the signal to noise ratio in the deeper intervals of the data set so

that the basement structure can be studied with precision. It is interpreted that the pop up structure has evolved from repeated movements on an obtuse angle left lateral strike slip stepover (Fig. 5.7 d). This strike slip step over system may be secondary to the regional left lateral strike slip fault- Brockton Froid Fault zone (Precambrian), which lies in close proximity to the study area to the north. Although the Ancient Rocky Mountain and Antler orogenies must have caused reactivation and wrench faulting motion on this strike slip stepover system, most of the movement must have occurred during the Laramide orogeny due to favorable stress orientation and thick-skinned nature of the Laramide orogeny.

The natural fracture networks in the study are controlled by localized stresses rather than the far field regional stresses. The presence of natural fractures enhances the productivity of an unconventional reservoir exponentially. The generation of oil in the middle member of the Bakken Formation takes place in Late Cretaceous. The central pop-up structure must have fully evolved or should be in the final stages by this time (Figure 6.1 b)). This is because Laramide Orogeny is the youngest event that could have caused reactivation on the basement structure. The structure seen in the study area was already in place when the oil was being generated from the lower and upper members of the Bakken Formation. The middle member of the Bakken Formation forms a continuous oil accumulation. The oil from the upper and lower members of the Bakken Formation would preferentially flow into the deformation zones below the pop-up structure (Figure 6.1 c)). These

deformation zones, due to their higher natural porosity and permeability, will have

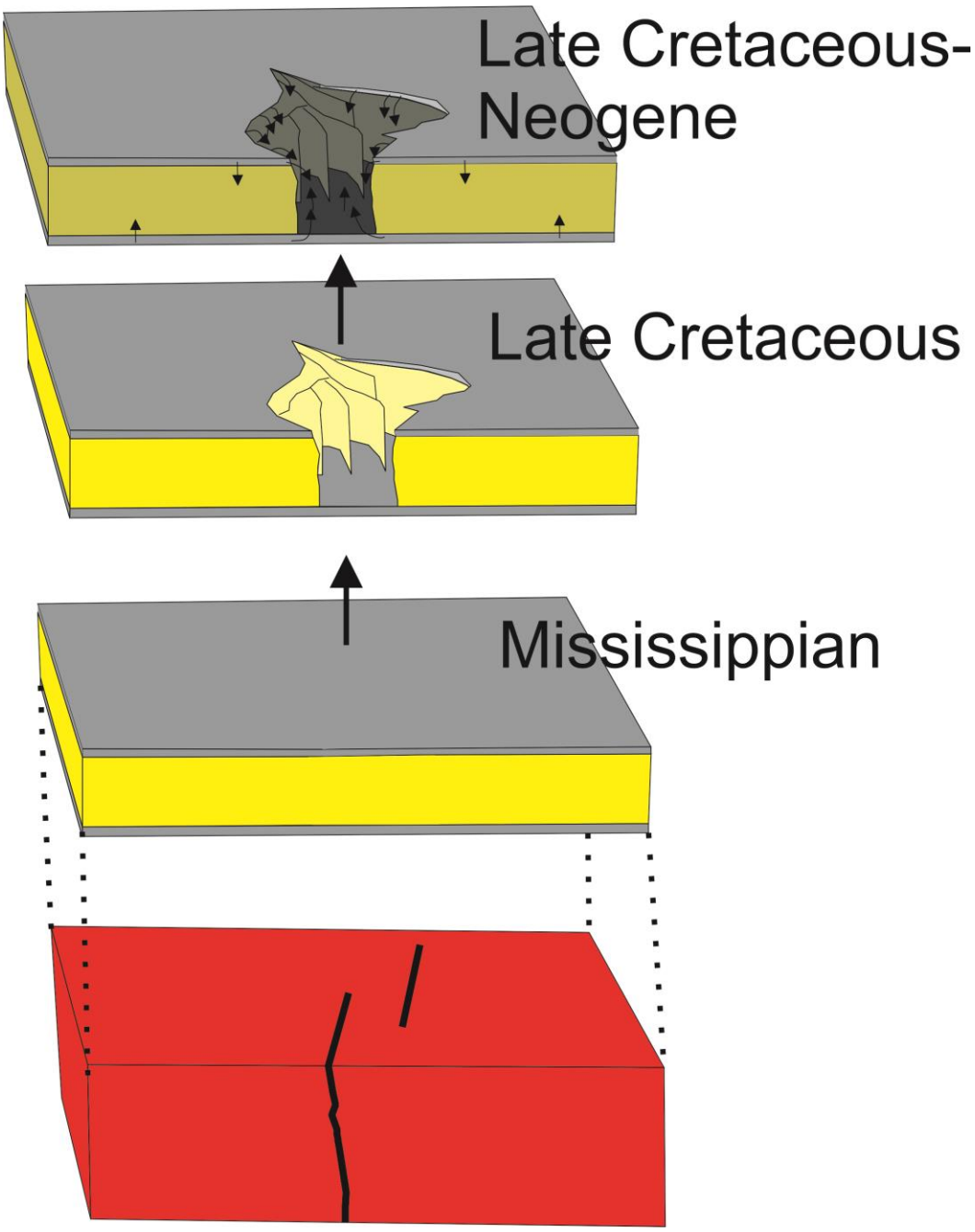

Figure 6.1 A schematic diagram showing the evolution of the system from its formation to the modern day. The step over fault system in the basement starts affecting the structure of the Bakken Formation after its formation in the Devonian-Mississippian time. The pop-up structure has evolved by the time oil is being generated in the Late Cretaceous. The oil from the upper and lower members preferentially flow into the deformed zone in the middle member of the Bakken formation, with higher secondary porosity and permeability.

exponentially higher production compared to the surrounding region (Figure 6.2). Hence, the 3D mapping of structure of the entire Elm Coulee Field is necessary to investigate the fracture network characteristics in middle member of the Bakken Formation in the area.

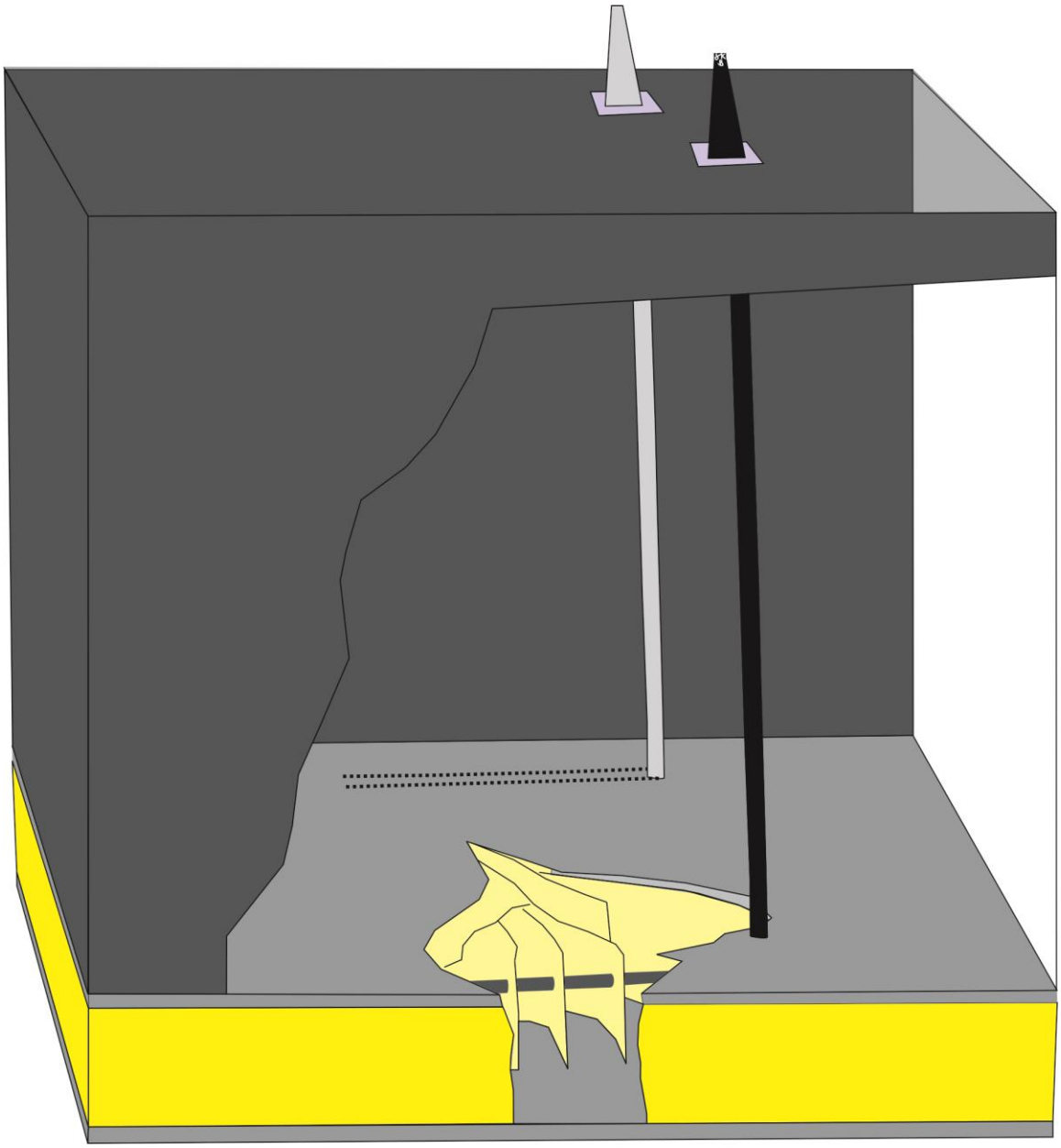

Figure 6.2 The well shown in black, which penetrates the deformed zone with wrench fault system, produces much more efficiently compared to the well shown in light gray color. This is due to higher natural fracture density in the deformed zone of the pop-up structure.

This will aid in delineating sweet spots across the Field. Additionally, the ovoid shaped sweet spots identified in Almanza (2011) (Figure 1.2 b) and Figure 6.3 c)) might be representative of the pop-up structures similar to the pop-up structure investigated in this study. Hence, it is hypothesized that there are parallel left lateral strike slip step overs with varying step over angle leading to varying pop up geometries in the Elm Coulee Field (Figure 6.3 d)). In addition, s seismic section from Eidsnes's study when vertically exaggerated also shows a probable domal structure with a zone of deformation beneath it (Figure 6.4). The seismic section is from the Vaux seismic survey which lies north of the study area in the Elm Coulee Field. The analog models from McClay and Banora 2001 can be used to aid interpretation of such pop up structures through-out the Elm Coulee Field. Increased fracturing in the deformation zones underlying pop-up structures lead to Formation of sweet spots at the location of the pop-up structures (Figure 6.1 and Figure 6.2). The structure and fracture network characteristics help explain the presence of regions of anomalously high EUR values in the Elm Coulee Field. The region of anomalously EURs in the Elm Coulee Field may be regions where the middle member of the Bakken Formation has increased natural fracturing related to the local stresses induced by left-lateral oblique slip strike slip faults.

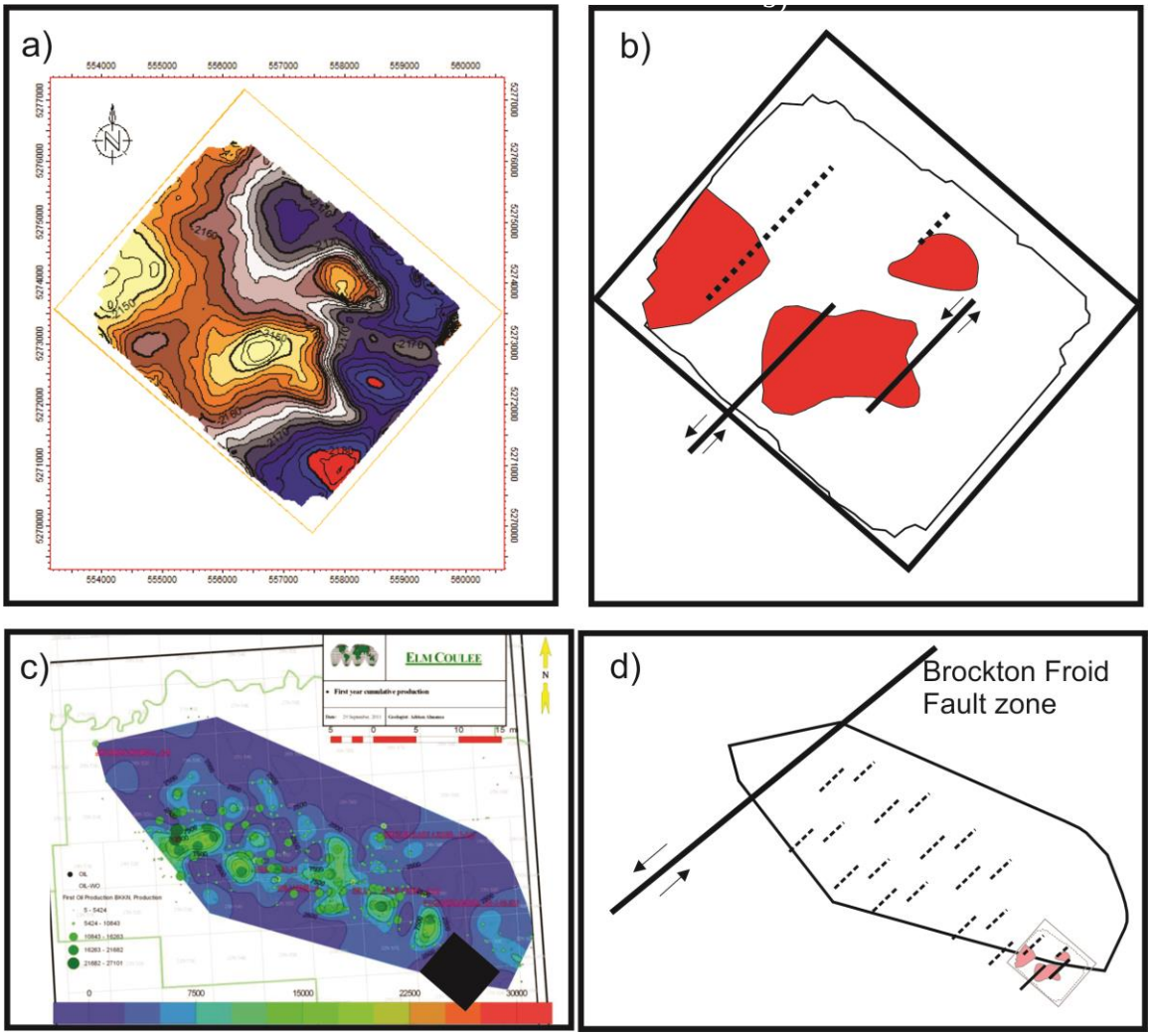

Figure 6.3 a) The time structure of the Top Bakken Formation b) The interpreted basement step over system for the central pop-up structure relative to the location of the pop-up structure in the basement. The black lines show interpreted step over system. c) First year cumulative production data showing ovoid shaped sweet spots in the Elm Coulee Field with anomalously high production (Almanza, 2011). d) The dotted lines show hypothesized stepovers throughout the Elm Coulee Field. The associated of these hypothesized stepovers with the regional Brockton Froid Fault zone is shown as well.

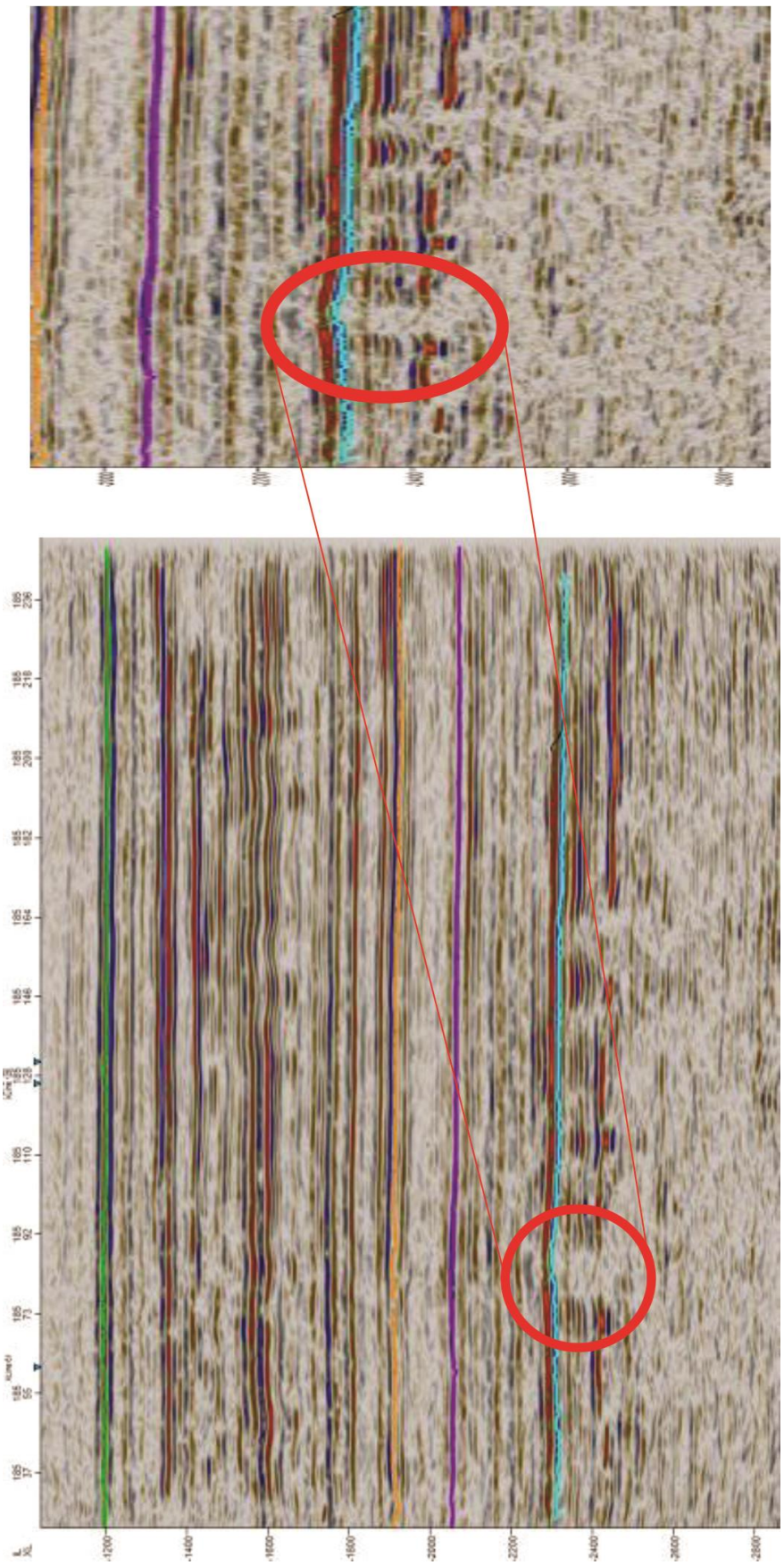

Figure 6.4 Inline 185: Vaux Survey (Eidsnes, 2014). The vertically exaggerated zoomed in version on the right shows the dome structure, which might be similar to the one investigated in this study.

CHAPTER 7
CONCLUSION

This study has built a structural model, which can help explain the presence of regions of anomalously high production (high EUR) in the Elm Coulee Field. There are pop-up structures overlying zones of deformation. The central pop-up structure overlies a system of left lateral oblique slip northeast-oriented faults. This pop-up structure and fault system evolved from an obtuse angle left lateral basement step over. This strike slip step over system may be secondary to the regional left lateral strike skip fault, Brockton Froid Fault zone (Precambrian), which lies in close proximity to the study area to the north. Although the Ancestral Rocky Mountain and Antler orogenies must have caused reactivation and wrench faulting motion on this strike slip stepover system, most of the movement must have occurred during the Laramide orogeny due to favorable stress orientation and thick-skinned nature of the Laramide orogeny. The fracture network characteristics in the pop-up structure will be controlled by the local stresses rather than the far field stresses. These deformation zones, due to their higher natural porosity and permeability, will have exponentially higher production compared to the surrounding region. This will aid in delineating sweet spots across the Field. Additionally, it is hypothesized that there are parallel left lateral strike slip step overs with varying step over angle leading to varying pop up geometries in the Elm Coulee Field. The analog models from McClay and Banora 2001 can be used to aid interpretation of such pop up structures through-out the Elm Coulee Field. The structure and fracture network characteristics help

explain the presence of regions of anomalously high EUR values in the Elm Coulee Field.

It is difficult to manually map wrench fault networks in 3D seismic due to very subtle vertical offsets and abrupt changes in the trend and dip of the fault over a short distance. Additionally, the conventional discontinuity detection attributes are unsuccessful in mapping such fault networks. A model driven approach can be used in mapping subtle vertical offset wrench faulting networks, which lead to formation of pop-up structures. This workflow can be used for mapping the fault networks elsewhere in the Elm Coulee Field. In addition, it can be used in mapping faults in other analogous Fields in which the reservoirs are affected by Wrench faults.

REFERENCES

Ahern, J., and Mrkvicka, S., 1984, A mechanical and thermal model for the evolution of the Williston Basin: Tectonics, v. 3, p. 79-102.

Almanza, A., 2011, Integrated 3D Geological Model of the Mississippian Devonian Bakken Formation, Elm Coulee, Williston Basin: Richland County, Montana: Master's thesis, Colorado School of Mines, Golden, Colorado.

Angulo, S., Buatois, L. and Halabura, S., 2008. Paleoenvironmental and sequence-stratigraphic reinterpretation of the Upper Devonian-lower Mississippian Bakken Formation of subsurface Saskatchewan integrating sedimentological and ichnological data. Summary of Investigations, 1, pp.2008-4

Anna, L.O., 2013, Geologic assessment of undiscovered oil and gas in the Williston Basin Province, Montana, North Dakota, and South Dakota, *in* United States Geological Survey, 2013, DDS 69–W, Chap. 3

Brown, D.L., and Brown, D.L., 1987, Wrench-style deformation and paleostructural influence on sedimentation in and around a cratonic basin. In: Williston Basin: Anatomy of a Cratonic Oil Province, Denver, Colorado, Rocky Mountain Association of Geologists, p. 57-70

Chopra, S., and Marfurt, K.J., 2007, Seismic attributes for fault/fracture characterization, *in* SEG Technical Program Expanded Abstracts 2007: Society of Exploration Geophysicists, p. 1520-1524.

Christie-Blick, N., and Biddle, K.T., 1985, Deformation and basin formation along strike-slip faults: Strike-slip deformation, basin formation, and sedimentation, p. 1-34.

Clement, J.H., 1987, Cedar Creek: A significant paleotectonic feature of the Williston Basin: M. W. Longman, ed., Williston basin: anatomy of a cratonic oil province: Rocky Mountain Association of Geologists, p. 323–336

Eidsnes, H.V.H., 2014, Structural and stratigraphic factors influencing hydrocarbon accumulations in the Bakken Petroleum System in the Elm Coulee field, Williston Basin, Montana: Master's Thesis, Colorado School of Mines, Golden, Colorado.

Gaswirth, S.B., Marra, K.R., Cook, T.A., Charpentier, R.R., Gautier, D.L., Higley, D.K., Klett, T.R., Lewan, M.D., Lillis, P.G., and Schenk, C.J., 2013, Assessment of Undiscovered Oil Resources in the Bakken and Three Forks Formations, Williston Basin Province, Montana, North Dakota, and South Dakota, 2013, .

Gerhard, L., and Anderson, S., 1988, Geology of the Williston basin (United States portion): Sedimentary Cover; North American Craton; US Geological Society of America, the Geology of North America, v. 2, p. 221-241.

Gerhard, L., Anderson, S., and LeFever, J., 1987, Structural history of the Nesson anticline, in Longman, M.W., ed., Williston Basin: Anatomy of a cratonic oil province: Rocky Mountain Association of Geologists, p. 337–353..

Gerhard, L.C., Anderson, S.B., and Fischer, D.W., 1990, Petroleum geology of the Williston Basin: Interior Cratonic Basins: AAPG Memoir, v. 51, p. 507-559.

Gerhard, L.C., Anderson, S.B., Lefever, J.A., and Carlson, C.G., 1982, Geological development, origin, and energy mineral resources of Williston Basin, North Dakota: AAPG Bulletin, v. 66, p. 989-1020.

Green, A., Weber, W., and Hajnal, Z., 1985, Evolution of Proterozoic terrains beneath the Williston Basin: Geology, v. 13, p. 624-628.

Honsberger, 2013, Geophysical Insights into the Bakken: Secrets from a Sleeping Giant, Elm Coulee Bakken Field (Sleeping Giant), Montana USA: Search and Discovery Article #20187, p. 7.

Jansen, K., 2005, Seismic Investigation of Wrench Faulting and Fracturing at Rulison Field, Colorado: Master's Thesis, Colorado School of Mines, Golden, CO, USA

Kuhn, P.P., di Primio, R., Hill, R., Lawrence, J.R., and Horsfield, B., 2012, Three-dimensional modeling study of the low-permeability petroleum system of the Bakken Formation: AAPG Bulletin, v. 96, p. 1867-1897.

Lefever, J.A., Martinuik, C.D., Dancsok, E.F., and Mahnic, P.A., 1991, Petroleum potential of the middle member, Bakken Formation, Williston Basin, *:*

Christopher, J. E. and Haidl, eds., Sixth International Williston Basin Symposium, Saskatchewan Geological Society Special Publication 11, Saskatchewan

McClay, K., and Banora, M., 2001, Analog models of restraining stepovers in strike-slip fault systems: AAPG Bulletin, v. 85, p. 233-260.

Meissner, F.F., 1991, Petroleum geology of the Bakken Formation, Williston Basin, North Dakota and Montana, in 1978 Williston Basin Symposium, edited by D. Rehrig, Montana Geological Society, Billings, Montana, p. 207-227

Petrel Workflow Tools. (Version 2015): Schlumberger Information Solutions.

Pitman, J. K., L. C. Price, and J. A. LeFever, 2001, Diagenesis and fracture development in the Bakken Formation, Williston Basin: Implications for reservoir quality in the middle member: U.S. Geological Survey Professional Paper 1653, 19 p

Price, L., and LeFever, J., 1992, Does horizontal Bakken drilling imply a huge oil-resource in fractured shales: Geological Studies Relevant to Horizontal Drilling: Examples from Western North America: Denver, Colorado, Rocky Mountain Association of Geologists, p. 199-224.

Randen, T., Monsen, E., Signer, C., Abrahamsen, A., Hansen, J.O., Sæter, T., and Schlaf, J., 2000, Three-dimensional texture attributes for seismic data analysis, *in* SEG Technical Program Expanded Abstracts 2000: Society of Exploration Geophysicists, p. 668-671.

Shepard, W., 1990, Tectonics and thermal maturation of the Bakken Formation of the Williston Basin, with comments on Landsat analysis applications: Montana Geological Society Bakken Workshop: Billings, Montana, p. 167-177.

Sloss, L., 1963, Sequences in the cratonic interior of North America: Geological Society of America Bulletin, v. 74, p. 93-114.

Sonnenberg, S.A., LeFever, J.A., and Hill, R.J., 2011, , Fracturing in the Bakken Petroleum System, Williston Basin: in J. W. Robinson, J. A. LeFever, S. B. Gaswirth, eds., The Bakken-Three Forks Petroleum System in the Williston Basin: Rocky Mountain Association of Geologists, 2011, p. 393-417.

Sonnenberg, S.A., and Pramudito, A., 2009, Petroleum geology of the giant Elm Coulee field, Williston Basin: AAPG Bulletin, v. 93, p. 1127-1153.

Subrahmanyam, D., and Rao, P., Seismic attributes–A review, *in* 7th International Conference & Exposition on Petroleum Geophysics, Hyderabad, p. 398-404.

Thomas, G.E., 1974, Lineament-block tectonics: Williston-Blood Creek Basin: AAPG Bulletin, v. 58, p. 1305-1322.

Webster, R.L., 1984, Petroleum source rocks and stratigraphy of the Bakken Formation in North Dakota. In Woodward, J., F.F. Meissner, and J.L. Clayton (Eds.), Hydrocarbon Source Rocks of the Greater Rocky Mountain Region, Rocky Mountain Association of Geologists, p. 57-82.

Williams, H., Hoffman, P.F., Lewry, J.F., Monger, J.W., and Rivers, T., 1991, Anatomy of North America: thematic geologic portrayals of the continent: Tectonophysics, v. 187, p. 117-134.

APPENDIX

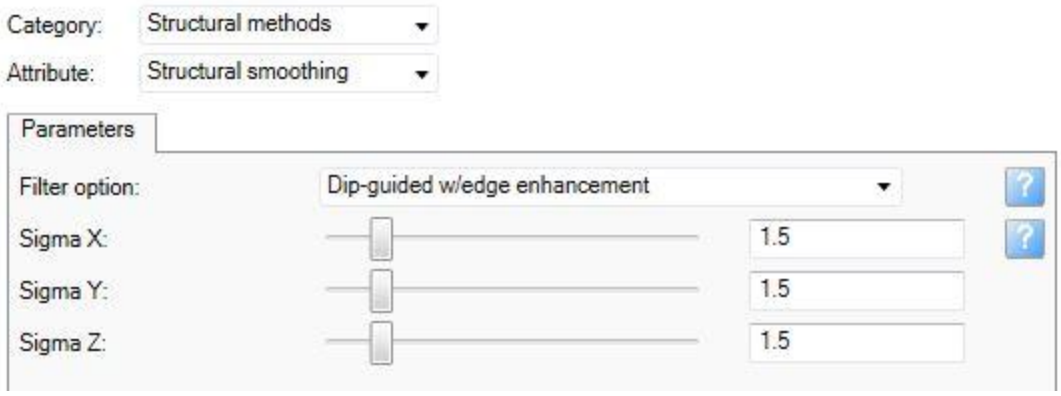

Parameters used for Structural smoothing DGEE (Figure 4.2).

Parameters used for extraction of Instantaneous Phase attribute (Figure 4.2).

Parameters used for Median Filter (Figure 4.2).

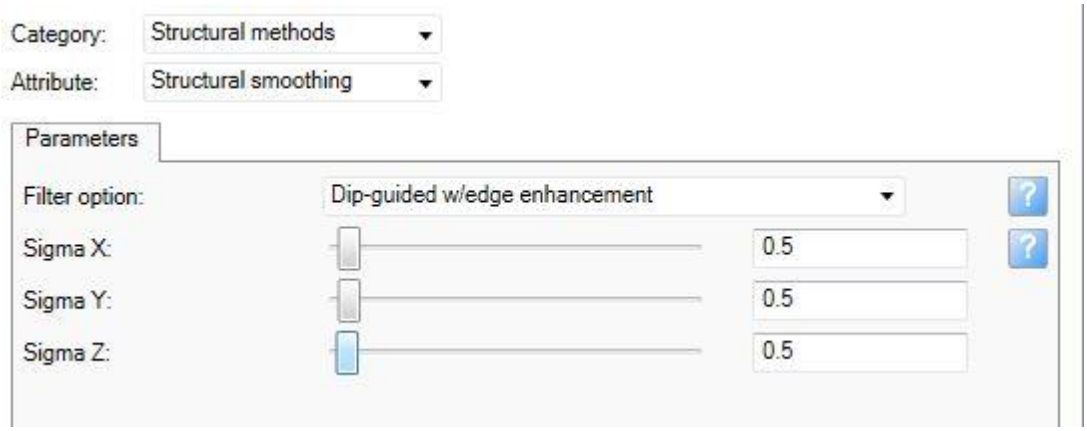

Parameters used for final Structural smoothing DGEE after the application of Median filter (Figure 4.2).

Parameters used for extraction of Passive and Aggressive Ant Track volumes (Figure 4.2, Figure 5.8).